Neurogenesis in the Olfactory System: The Functional Activity of Immature Olfactory Sensory Neurons and Postnatal-Born Granule Cells

by

Szu Wei (Jane) Huang

B.A., Colgate University, 2012

Submitted to the Graduate Faculty of the

School of Medicine in partial fulfillment

of the requirements for the degree of

Doctor of Philosophy

University of Pittsburgh

2022

UNIVERSITY OF PITTSBURGH

SCHOOL OF MEDICINE

This dissertation was presented

by

Szu Wei (Jane) Huang

It was defended on

August 8, 2022

and approved by

Dr. Stephen D. Meriney, Professor and Chair, Departments of Neuroscience and Psychiatry, University of Pittsburgh

Dr. Brian M. Davis, Professor, Department of Neurobiology, University of Pittsburgh

Dr. Anne-Marie Oswald, Associate Professor, Department of Neurobiology, University of Chicago

Dr. Rebecca P. Seal, PhD, Associate Professor, Department of Neurobiology, University of Pittsburgh

Dissertation Co-Director: Dr. Claire E. Cheetham, Assistant Professor, Department of Neurobiology, University of Pittsburgh

Dissertation Co-Director: Dr. Nathaniel N. Urban, Professor and Provost, Department of Biological Sciences, Lehigh University

Neurogenesis in the Olfactory System: The Functional Activity of Immature Olfactory Sensory Neurons and Postnatal-Born Granule Cells

Szu Wei (Jane) Huang, PhD

University of Pittsburgh, 2022

Adult neurogenesis in the rodent olfactory system provides a continuous source of olfactory sensory neurons (OSNs) in the olfactory epithelium (OE) and granule cells (GCs) in the olfactory bulb (OB). These new neurons must integrate into established circuitry without disrupting pre-existing functions. In the OE, OSNs project their axons to the glomerular layer of the OB, where they synapse with the neurons of the OB. Immature OSNs express the olfactory receptors and proteins required for signal transduction, but it is unknown whether they form functional synapses with OB neurons and contribute to odor processing. Here, I show that immature OSNs make monosynaptic connections with superficial tufted cells in the OB, and that these connections were formed within five days after terminal cell division. This data suggest that immature OSNs may play a previously unappreciated role in odor processing alongside their mature counterparts.

In the OB, the somata of early postnatal-born GCs are found in the superficial granule cell layer (GCL), and their dendrites occupy the superficial external plexiform layer (EPL), whereas the somata of late postnatal-born GCs are found in the deep GCL, and their dendrites are found in the deeper EPL. The lateral dendrites of mitral cells (MCs) and tufted cells (TCs), the primary output neurons of the OB, are also segregated in the EPL, where they form dendrodendritic synapses with GCs. In this dissertation, I tested whether birth date related anatomical differences between subpopulations of GCs could lead to differential connectivity with MCs and TCs. By

selectively photoactivating either an early or late postnatal-born population of GCs, I found that the overall population of MCs receive greater inhibition from both early and late postnatal-born GCs compared to TCs. The difference in inhibition was more pronounced following activation of late postnatal-born GCs, which may be explained by a trend for late postnatal-born GCs to preferentially connect with MCs. Together, these data provide evidence for functional differences in connectivity resulting from anatomical differences between subpopulations of postnatal-born GCs, which may in turn differentially modulate the parallel odor processing streams formed by MC and TC output.

Table of Contents

List of Tables

List of Figures

Preface

None of the work presented in this dissertation would have been possible without the support of many individuals. First, I would like to thank my mentors, Drs. Nathan Urban and Claire Cheetham. Their patience, compassion, and encouragement uplifted me when I was downtrodden, and their breadth of knowledge and intellectual rigor are a continuous source of inspiration. I also thank the members of my committee: Drs. Brian Davis, Becky Seal, Steve Meriney, who served as the chair of my committee, and Anne-Marie Oswald, who continued to lend me her olfaction expertise as my outside examiner despite having relocated to Chicago. I am grateful for their guidance throughout my graduate training.

Past members of the Urban lab have also contributed to the success of this project. I thank former postdocs Drs. Nate Glasgow and Matt Rannals for their mentorship during my first forays into slice electrophysiology and for their commiseration whenever experiments failed because of unknown ephys voodoo. Special thanks to Dr. Shawn Burton, who has provided invaluable feedback and insight into my projects and whose immense depth of knowledge in all things olfaction is awe-inspiring. I thank Greg LaRocca, whose immaculate organizational skills as a lab manager was indispensable. I thank the past and current members of the Cheetham lab: Taryn Brechbill, Jordan Gregory, Tenzin Kunkhyen, Alyssa Lauer, and Alex Rangel; they've adopted me into the lab and have all made significant contributions to the olfactory sensory neuron project.

Finally, I thank all my friends who have kept me sane on this journey. I thank my family, who have always trusted and supported whatever endeavor I attempted. Most of all, I thank Nate Taylor, for his endless love, support, and willingness to buy me ice cream.

1.0 Introduction

Most brain regions in vertebrates do not display adult neurogenesis (Gould, 2007). Two key regions in the adult mammalian brain—the olfactory bulb and the hippocampus, areas responsible for olfactory processing and learning and memory, respectively— are the exception and continue to generate new neurons into adulthood (Altman, 1969; Altman and Das, 1965). Each new adult-born neuron must integrate into established circuitry without disrupting pre-existing functions. Sensory experience and activity modulate the survival and integration of these new neurons, which in turn may shape the neural representation of external sensory stimuli (Alonso et al., 2006; Lemasson et al., 2005; Santoro and Dulac, 2012; Watt et al., 2004).

Here, I leverage the well-defined functional organization of the mouse olfactory system to study how adult neurogenesis contributes to the processing of sensory stimuli. The peripheral olfactory system also exhibits adult neurogenesis in the continuous generation of olfactory sensory neurons. These neurons perform the first step in olfactory processing by binding odorant molecules and transducing the information about chemicals in the environment to patterns of activity in olfactory sensory neurons (Caggiano et al., 1994; Graziadei and Graziadei, 1979).

I first examine whether immature olfactory sensory neurons generated via adult neurogenesis in the olfactory epithelium are capable of transducing odor stimuli and providing input to olfactory bulb neurons. This knowledge will be important for understanding how these new neurons establish appropriate functional connections and how function is maintained during the turnover of these neurons that occurs throughout life. Next, I investigate how adult-born olfactory bulb granule cells form connections with the two principal neuron types of the olfactory bulb—mitral and tufted cells. Specifically, I test whether known birth date related anatomical

differences in postnatal-born granule cells lead to differences in functional connectivity with the principal neurons of the olfactory bulb. Understanding the contribution of adult neurogenesis to sensory processing bears implications for both experience-dependent plasticity in the healthy brain and regeneration following disease or injury.

1.1 Overview of olfaction

Olfaction, or the sense of smell, allows an animal to gather and discriminate between signals originating from chemical substances in its environment. The olfactory system transforms the odor information into meaningful neural representations that help guide behavior and survival in the world. In terms of evolution, olfaction is the oldest sensory system and is vital for sensing, engaging with, and adapting to the outside world. Animals use olfaction for a wide range of behaviors critical for survival, including food-gathering, breeding, and predator avoidance (Ache and Young, 2005; Capaldi et al., 2004; Coopersmith and Leon, 1984; Levy et al., 2004; Sarafoleanu et al., 2009).

It is difficult for humans, who rely heavily on the visual system, to fully appreciate the importance of olfaction. The common belief that human olfaction is impoverished and inconsequential to daily life originates from Brocca's work in the 1800s, in which he noted the relatively small size of the human olfactory bulb compared to the rest of the brain (McGann, 2017). Humans have about 400 olfactory receptor genes—a number that, although small compared to the ~1200 olfactory receptor genes found in mice, is still quite large (Glusman et al., 2001; Godfrey et al., 2004; Malnic et al., 2004; Young et al., 2002; Zhang and Firestein, 2002). In 2014, Keller and colleagues tested human subjects on panels of odorant mixtures and estimated that humans

can discriminate between an astonishing number of 1 trillion olfactory stimuli (Bushdid et al., 2014). However, a follow-up study by Gerkin and Castro disputes this claim and argues that the results presented by Bushdid and colleagues are skewed by problematic experimental parameters and analysis frameworks (Gerkin and Castro, 2015). Although the exact number of smells a human can distinguish has yet to be conclusively determined, recent studies suggest that human olfaction is far more powerful than originally assumed (Shepherd, 2004a).

It is an indisputable fact that a healthy olfactory system is necessary to a satisfactory quality of life in humans. Odors—whether pleasant or aversive, familiar or unfamiliar—can influence autonomic nervous system responses, heighten stress levels, and provoke involuntary facial expressions or avoidance behavior (He et al., 2014; Joussain et al., 2014; Smeets and Dijksterhuis, 2014). There are also studies linking an individual's unique human leukocyte antigen (HLA) expression with the specific odor the person produces (Secundo et al., 2015), which some have dubbed a person's "body odorcocktail" (Lundström and Olsson, 2010; McGann, 2017; Milinski et al., 2013). Perception of other people's body odorcocktail has been linked to mate choice and processing of social signals such as aggression and stress in humans (Lübke and Pause, 2015; Pause, 2012; Roberts and Roiser, 2010).

Olfactory dysfunction is also present in many diseases. Millions of people suffer from olfactory deficits and anosmia in their lifetimes, and the prevalence of these disorders are increased in the aged populations or patients with neurodegenerative diseases (Boesveldt and Parma, 2021). Especially relevant is the ongoing pandemic and the common COVID-related symptom of anosmia; likely tens of millions of people around the world have experienced olfactory loss in the past two years (Butowt and von Bartheld, 2021). Patients with olfactory disorders suffer from a severely reduced quality of life along with increased emotional and social distress (Neuland et al.,

2011). Although the work described in this dissertation specifically focuses on the role of adult neurogenesis in the olfactory circuitry, understanding how newly generated neurons integrate into pre-existing circuitry in the olfactory system may provide insights into potential therapeutic targets for repair following disease outside the olfactory system (Durante et al., 2020).

1.2 Organization of the olfactory system

Olfactory processing in the mammalian system begins in the nasal turbinates of the nose when odorant molecules bind to olfactory sensory neurons (OSNs) that reside in the olfactory epithelium (OE). The OSNs then relay this information to the olfactory bulb (OB); neurons in the OB further process the odor information before transmitting it to higher cortical regions (Igarashi et al., 2012; Nagayama et al., 2010). The following sections describe the olfactory components involved in odor transduction from the nose to the OB.

1.2.1 Olfactory sensory neurons

OSNs are bipolar neurons found in the OE. On the apical side, they extend dendrites to the epithelial surface. Each dendrite that protrudes into the nasal cavity has 10-30 cilia that express olfactory receptors (ORs), which allow them to bind odorant molecules carried into the nose (Falk et al., 2015). On the basal side, OSNs extend an axon that travels through the cribriform plate to the OB (Buck, 1996). The axons of OSNs terminate in spherical regions of neuropil called glomeruli (Vassar et al., 1994), and axons expressing the same OR converge onto the same glomerulus (Ressler et al., 1994; Serizawa et al., 2000). One study using C57BL/6J mice estimated

that each OR gene is expressed by a median number of 5,983 OSNs, for a total of ~6.6 million OSNs expressing ~1,100 total OR genes in the murine genome (Bressel et al., 2016).

ORs are G-protein coupled receptors, and the binding of odorant molecules initiates a signaling cascade that leads to the production of cAMP (Connelly et al., 2015; Kato and Touhara, 2009). cAMP opens cyclic nucleotide-gated (CNG) channels, allowing Ca^{2+} and Na^{+} influx and subsequent Cl^{-} efflux through Ca^{2+}-activated chloride channels. The movement of these ions leads to the depolarization of the membrane potentials of OSNs and generation of action potentials (APs). About 1,100 OR genes are found in the murine genome. One OR can recognize multiple odorants, and multiple ORs can detect the same odorant (Adipietro et al., 2012; Buck and Axel, 1991; Nei et al., 2008). ORs also function in a combinatorial manner such that different combinations of ORs detect different odorants or odorant mixtures (Malnic et al., 1999).

1.2.2 The olfactory bulb: the glomerular layer

The OB is composed of multiple well-defined lamina, with distinct neuronal cell types occupying each lamina (Figure 1) (Price and Powell, 1970a). Following odorant binding by OSNs, the next step in olfactory processing occurs in the glomerular layer (GL) of the OB, in which OSN afferents are organized into glomeruli. Each mouse brain is thought to contain four glomeruli for each OR, with two glomeruli in each bulb. The exact total number of glomeruli in the brain is disputed, though estimates range from 1,800 to 3,600 (Richard et al., 2010; Royet et al., 1988; Zapiec and Mombaerts, 2015). The locations of glomeruli are also stereotyped and conserved both between animals and across species (rat and mouse) (Soucy et al., 2009).

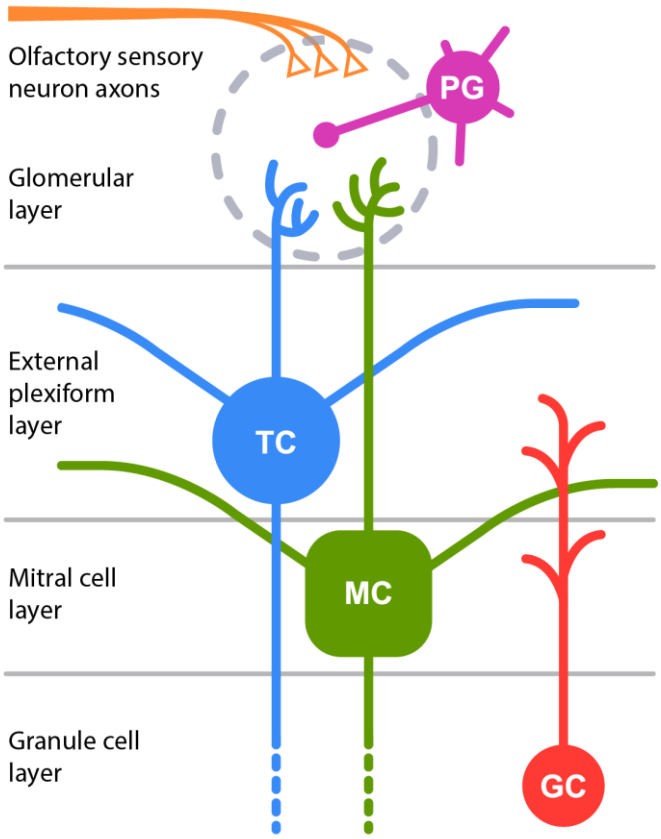

Figure 1. Schematic of olfactory bulb circuitry

Due to the OSNs' ability to bind and respond to multiple ligands, the binding of an odorant molecule is transduced into a stereotyped map of activated glomeruli in the OB (Vassar et al., 1994). Odor information is thus represented by the pattern of glomerular activation (Rubin and Katz, 1999). Aside from OSN afferents, each glomerulus also consists of the processes of local juxtaglomerular cell types and the apical dendrites of mitral cells (MCs) and tufted cells (TCs), the principal output neurons of the OB (Mombaerts, 1996; Mombaerts et al., 1996). Each glomerulus functions as a microcircuit where both the OSN axons and the input received by MCs and TCs are modulated by the surrounding juxtaglomerular neurons, a broad umbrella term for cell types found around glomeruli in the GL.

Juxtaglomerular neurons include periglomerular cells (PGCs), superficial short-axon cells (sSACs), and external tufted cells (ETCs) (Pinching and Powell, 1971a). The vast majority of juxtaglomerular neurons are GABAergic (Kiyokage et al., 2010; Parrish-Aungst et al., 2007), the most numerous type of which are the PGCs, representing 60% of all cells in the GL (Parrish-Aungst et al., 2007). PGCs possess a short dendrite that usually only innervates one glomerulus and has a more limited range compared to the dendrites of ETCs; PGC dendrites mainly mediate intraglomerular connections (Pinching and Powell, 1971a).

sSACs, unlike PGCs, are sparser in number and send extensive processes to neighboring glomeruli. About 80% of sSACs express GAD67, and the remaining only express GAD65 or co-express GAD65 and Gad67 (Parrish-Aungst et al., 2007). They release both dopamine and GABA onto ETCs and form weak connections with MCs and TCs (Burton, 2017; Liu et al., 2013; Vaaga et al., 2017). sSACs are unique in that they mediate both excitatory and inhibitory input onto ETCs, MCs, and TCs through separate signaling pathways (Liu et al., 2013; Liu et al., 2016; Vaaga et al., 2017).

ETCs are a glutamatergic cell type characterized by a lack of lateral dendrites (Hayar et al., 2004a; Hayar et al., 2004b); they receive strong monosynaptic input from OSNs and in turn provide input onto both MCs and TCs (De Saint Jan et al., 2009; Najac et al., 2011). A study has also suggested that the majority of excitatory OSN input received by MCs is actually via a disynaptic signaling pathway mediated by ETCs (Gire et al., 2012).

1.2.3 The olfactory bulb: the external plexiform and mitral cell layers

The external plexiform layer (EPL) lies beneath the GL, and the much narrower mitral cell layer (MCL) lies below the EPL. STCs are found at the border between the GL and the EPL (Mori

et al., 1983; Orona et al., 1984). Like ETCs, STCs receive direct monosynaptic input from OSNs (Sun et al., 2020), but unlike ETCs, they possess long lateral dendrites in the EPL and exhibit non-bursting spike patterns without a depolarizing envelope (Antal et al., 2006; De Saint Jan et al., 2009; Hayar et al., 2004b; Jones et al., 2020; Liu et al., 2012; Liu and Shipley, 2008).

TCs, whose cell bodies are scattered throughout the EPL, and MCs, which are found tightly packed in a single layer in the mitral cell layer (MCL), share a number of similarities (Mori et al., 1983; Orona et al., 1984). Both MCs and TCs are large projection neurons with a primary dendrite that extends to a single glomerulus in the GL and lateral or secondary dendrites that extend horizontally in the EPL (Mombaerts, 1996; Mombaerts et al., 1996; Shepherd, 2004b). "Sister" cells with apical dendrites projecting to the same glomerulus share correlated responses to odors (Dhawale et al., 2010). Additionally, both MCs and TCs provide glutamatergic input onto granule cells (GCs) and receive inhibition in turn via dendrodendritic synapses (Christie et al., 2001; Schoppa et al., 1998).

The morphology of TCs is diverse, and TCs can be further divided into subtypes based on either the location of their somata in the EPL or their dendritic morphology. As described previously, ETCs are found in the GL, whereas STCs reside at the border between the GL and the EPL. The TCs described in this section are found throughout the EPL and are sometimes known as middle TCs; we refer to them simply as TCs in this dissertation. A small number of TCs are also found in close proximity to the MCL; their large size and physiological similarity to MCs have led some to label them as "displaced" MCs (Belluscio et al., 2002; Nagayama et al., 2014; Orona et al., 1984; Pinching and Powell, 1971b; Shepherd, 2004b).

The dendrites and axonal projections of MCs and TCs are also spatially segregated like their somata. MC lateral dendrites are mostly found in the deeper section of the EPL, whereas TC

dendrites course along the superficial and middle regions of the EPL (Mori et al., 1983; Orona et al., 1984). TCs project their axons to the anterior olfactory nucleus and anterior piriform cortex, whereas MC projections are more distributed and target all areas of the olfactory cortex (Igarashi et al., 2012; Nagayama et al., 2010).

Aside from anatomical differences, MCs and TCs differ in their physiology and responses to odor stimuli. TCs have lower odorant response thresholds and increased spiking activity in response to odorant input compared to MCs, possibly due to receiving weaker lateral inhibition than MCs (Christie et al., 2001; Geramita et al., 2016; Nagayama et al., 2014; Nagayama et al., 2004). Compared to MCs, TCs also receive stronger direct OSN input, fire earlier in the sniff cycle, have a shorter onset latency, and respond to a wider range of odor concentrations (Fukunaga et al., 2012; Gire et al., 2012; Igarashi et al., 2012). These differences suggest that MC and TC outputs represent two parallel streams of olfactory processing (Geramita et al., 2016).

1.2.4 The olfactory bulb: the granule cell layer

GCs are small GABAergic interneurons that make up the majority of the cells in the granule cell layer (GCL) and are found in clusters of 2-10 cells (Price and Powell, 1970b). They outnumber MCs by a factor of 50-100; the much larger number of inhibitory vs. excitatory neurons is the inverse of the proportions observed in the cortex and hippocampus (Shepherd, 2004b). GCs are biochemically diverse; subtypes expressing different markers such as calretinin, CaMKIIα, and 5T4 occupy different regions of the GCL and may be generated at different times in the animal's life (Hardy et al., 2018; Imamura et al., 2006; Malvaut et al., 2017; Takahashi et al., 2016).

The dendrites of GCs may be found in the superficial or deep regions of the EPL, depending on the location of the GC somata in the GCL. The dendrites of superficial GCs occupy the

superficial regions of the EPL, and the dendrites of deeper GCs occupy the deeper regions of the EPL. (Mori et al., 1983; Orona et al., 1983). Although GCs do not have axons, they receive glutamatergic input from and provide GABAergic output onto MCs and TCs via dendrodendritic synapses with the lateral dendrites of the output neurons (Egger and Urban, 2006; Price and Powell, 1970b). GCs also receive excitatory input in their proximal apical and basal domains, mediated by axodendritic synapses formed with the axon collaterals of MCs and TCs. Excitation of GCs at axodendritic synapses is fast and mediated by AMPA receptors (Balu et al., 2007; Isaacson, 2001; Isaacson and Strowbridge, 1998). Although GCs do not have axons, they are capable of firing sparse APs with long latencies in response to stimulation, and these APs are triggered more readily by excitatory inputs at axodendritic synapses than at dendrodendritic synapses (Burton, 2017; Burton and Urban, 2015; Halabisky and Strowbridge, 2003).

Current evidence suggests that GC-mediated inhibition can occur independently of APs by two mechanisms (Wienisch and Murthy, 2016). First, each spine on the dendrite acts as a mini-neuron capable of GABA release following local spine depolarization (Egger and Urban, 2006). Ca^{2+} influx through voltage-dependent Ca^{2+} channels and NMDA receptors leads to neurotransmitter release onto MCs and TCs, resulting in lateral or recurrent inhibition (Egger et al., 2005; Isaacson and Strowbridge, 1998; Lage-Rupprecht et al., 2020; Schoppa et al., 1998). Second, each dendritic branch can also function as an independent unit by generating local spikelets mediated by Na_v channels, leading to Ca^{2+} entry through high-voltage-activated Ca^{2+} channels and GABA release (Burton and Urban, 2015; Bywalez et al., 2015; Egger et al., 2005). Global release resulting from sodium APs generated by glomerular inputs has also been observed. Here, AP generation leads to a long-lasting depolarization involving NMDA receptors,

nonselective cation conductance I_{can} channels, and transient receptor potential (canonical) (TRPC) channels, followed by Ca^{2+} entry through T-type Ca_v channels (Egger, 2008; Stroh et al., 2012).

GC-mediated inhibition has both a fast and a slow component, resulting in prolonged inhibition of MCs and TCs and asynchronous release of GABA (Isaacson and Strowbridge, 1998; Schoppa and Westbrook, 1999). There are two forms of GC-mediated inhibition of MCs and TCs: recurrent inhibition and lateral inhibition. In recurrent inhibition, MC or TC excitation of a GC causes the GC to release GABA back onto the original MC or TC; in lateral inhibition, MC or TC excitation of a GC causes the GC to inhibit MCs and TCs of neighboring glomeruli (Egger and Kuner, 2021; Margrie et al., 2001). Lateral inhibition modulates MC and TC activity by decorrelating their odor responses, which sharpens the patterning of unique glomerular responses to odor stimuli and improves odor discrimination (Arevian et al., 2008; Gschwend et al., 2015; Urban and Sakmann, 2002; Yokoi et al., 1995).

The bulk of feedback projections in the OB originating from the cortex targets GCs. Excitatory feedback from the piriform cortex drives inhibition of odor-evoked MC and TC activity (Boyd et al., 2015; Boyd et al., 2012; Wu et al., 2020). GCs also receive glutamatergic feedback from anterior olfactory nucleus axons along with direct projections from the hippocampus and entorhinal cortex (Markopoulos et al., 2012; Padmanabhan et al., 2019). Additionally, GABAergic feedback originating from the forebrain modulates local oscillations in the OB (Gracia-Llanes et al., 2010; Villar et al., 2021).

1.3 Adult neurogenesis

The dominant dogma for over a century has been that mammalian neurogenesis only occurs during the embryonic stage in the central nervous system (Cajal, 1913). In recent decades, however, this dogma has been overturned starting with work by Joseph Altman, who demonstrated evidence for newly generated GCs in the postnatal rat hippocampus and OB (Altman, 1969; Altman and Das, 1965). The development of bromodeoxyuridine (BrdU), a thymidine analogue that labels dividing precursor cells (Kuhn et al., 1996), revolutionized the field of adult neurogenesis. It is now widely accepted that adult neurogenesis in mammals occurs in two neurogenesis zones: the subgranular zone (SGZ) and the subventricular zone (SVZ). In non-primate mammals, the SGZ generates the dentate granule cells of the hippocampus, and the SVZ generates the interneurons of the OB (Ming and Song, 2011; Paredes et al., 2016). In this process, newly generated neurons become functionally mature and integrate into pre-existing circuitry (Alvarez-Buylla and Lim, 2004; Belluzzi et al., 2003; Carleton et al., 2003; Lledo et al., 2006).

In hippocampal neurogenesis, radial glial cells in the SGZ first differentiate into intermediate progenitors and then neuroblasts. Immature neurons migrate to the dentate granule cell layer, from which they send axons to CA3 of the hippocampus and dendrites to the molecular layer (Toda et al., 2018).

The olfactory system is the only sensory system to display ongoing neurogenesis. This unique property allows the animal to respond to injury and insult of the olfactory organs with robust regeneration and repair. In the below sections, I describe in further detail adult neurogenesis in the olfactory system.

1.3.1 Adult neurogenesis in the olfactory epithelium

In the healthy OE, globose basal cells act as progenitors to OSNs and undergo continuous mitotic division to generate transitional nascent OSNs. Following injury, horizontal basal cells are activated instead to repopulate the OE (Caggiano et al., 1994; Graziadei and Graziadei, 1979; Iwai et al., 2008). The intermediate cells generated from globose or horizontal basal cells migrate apically and transiently express Achaete-scute homolog 1 (Ascl1) before differentiating into immature OSNs, which express growth-associated protein 43 (GAP43) and G-protein ɣ-subunit (Gγ8) but do not exhibit extended cilia (McIntyre et al., 2010; Murdoch and Roskams, 2007; Ryba and Tirindelli, 1995; Verhaagen et al., 1989).

Onset of OSN maturity is defined by expression of the olfactory marker protein (OMP) and concomitant downregulation of the expression of GAP43 and Gγ8 (Miragall and Graziadei, 1982; Schwob, 2002). OSNs expressing the same ORs extend their axons through the basal surface of the OE to converge onto the same glomerulus in the olfactory bulb (OB), where they provide odor input to OB neurons. The entire maturation process of an OSN is completed within 7-8 days after cell division (Liberia et al., 2019; Savya et al., 2019). The turnover time for OSNs averages one month, but another study has also found a half-life of one month (Graziadei and Graziadei, 1979; Holl, 2018).

Survival of newly generated OSNs is activity-dependent: activation extends OSNs' lifespan, and odorant stimuli enhance survival (Santoro and Dulac, 2012; Watt et al., 2004). Conversely, the number of OSNs decreases following naris occlusion (Cavallin et al., 2010). Some studies have also found that the rate of neurogenesis decreases with age, leading to a reduced overall turnover rate in aged animals (Kondo et al., 2010; Loo et al., 1996).

1.3.2 Adult neurogenesis in the olfactory bulb

The rodent OB receives a steady stream of newly generated neurons throughout the animal's life, supplied by neuroblasts originating in the SVZ. Adult neurogenesis in the OB begins with astrocytes residing in the SVZ, which lines the anterior wall of the lateral ventricle. These astrocytes act as neural stem cells that then give rise to transient amplifying cells, which differentiate into neuroblasts (Lledo et al., 2006; Ming and Song, 2011). The neuroblasts form a chain and migrate via the rostral migratory stream (RMS) to the OB. Anywhere from 30,000 to 80,000 SVZ-derived neuroblasts arrive in the OB daily (Alvarez-Buylla et al., 2001). Upon reaching the core of the GCL, they migrate radially toward the GL. The vast majority of the neuroblasts differentiate into GABAergic interneurons, with about 95% becoming GCs and the rest becoming PGCs (Lledo and Saghatelyan, 2005).

Newborn GCs exhibit dendritic spines as early as 14 days after birth, and by 30 days, all newly generated GCs show mature morphology such as elaborate dendritic arbors (Petreanu and Alvarez-Buylla, 2002). Functional maturity accompanies morphological maturity: synapses on the dendritic spines are functional by four weeks after birth. GCs generated via adult neurogenesis express $GABA_A$ and AMPA receptors while still migrating in the RMS, and NMDA receptor expression begins upon arrival in the GCL. These GCs are non-spiking for most of the maturation process, and inhibitory and excitatory synaptic events are detected before voltage-dependent Na^+ currents. This developmental pattern is the inverse of that observed in prenatally-generated GCs, in which AP generation precedes synaptic activity (Carleton et al., 2003).

Half of all postnatal-born neurons are eliminated between 15-45 days after birth (Lin et al., 2010; Petreanu and Alvarez-Buylla, 2002; Winner et al., 2002); without odor input between 14-20 days after birth, more postnatally-generated GCs die during this critical window (Yamaguchi and

Mori, 2005). Other studies have also shown that enriched olfactory experience increases postnatal neurogenesis, as do olfactory discrimination tasks (Alonso et al., 2006; Kamimura et al., 2022; Lemasson et al., 2005). Sensory deprivation via nostril occlusion, in contrast, decreases the number of postnatal-born GCs in the OB and the complexity and numbers of their dendritic spines (Saghatelyan et al., 2005). Additionally, as is the case with OSNs, GC neurogenesis decreases with age, especially during the first two months of the animal's life (Daynac et al., 2016; Enwere et al., 2004; Magavi et al., 2005).

A unique feature of postnatal neurogenesis in the OB is that postnatal-born GCs exhibit a laminar distinction in their somata location depending on birth date. GCs generated prenatally and between P3-7 occupy the superficial GCL, whereas those generated at P14 and onwards occupy the deeper regions of the GCL (Lemasson et al., 2005). The turnover rate of GCs is also much higher in GCs generated in the early postnatal period compared to those generated in the later postnatal period: by two months after terminal cell division, half of the GCs generated at P60 are eliminated, whereas virtually no GCs generated between P3-P7 are lost (Imayoshi et al., 2008). It is important to note, however, that a recent study suggested that the elimination of later postnatal-born GCs should be attributed to BrdU toxicity and that GC neurogenesis is an additive phenomenon (Platel et al., 2019).

1.3.3 Adult neurogenesis and olfactory processing

Ongoing neurogenesis in the olfactory system provides a substrate for neuronal plasticity to interact with sensory experience. On a short time scale, sensory adaptation allows neurons to modulate their stimulus-evoked responses when exposed to prolonged stimulation, restricting sensory information to only the most relevant (Benda, 2021; Martelli and Storace, 2021). On a

longer time scale, as an animal moves through different environments and encounters diverse sensory stimuli over the course of its life, its collective sensory experiences also alter the sensory system circuitry to shape the neural representations of the external world.

It has been hypothesized that the repertoire of ORs expressed in an animal's nose could be altered to reflect the animal's odor environment and to extract the maximum amount of olfactory information from its surroundings (Tesileanu et al., 2019). In support of this hypothesis, postnatal odorant exposure alters the molecular and cellular structures of OSNs (Cadiou et al., 2014), and expression of ORs and OSN subtype diversity can be altered by genetic and environmental factors (Ibarra-Soria et al., 2017). A recent study by Datta and colleagues compared OSN gene expression in mice housed in either regular home cages or in two different odor-enriched environments (Tsukahara et al., 2021). The OSNs of mice housed in each odor environment showed OR-dependent differential expression of over 70 genes related to OSN function. The particular expression profile of these genes in each OSN was also correlated with the odor response properties of the given OSN. Thus, neural representations of olfactory experiences can be altered at the level of peripheral OSNs to better inform behavioral responses to future olfactory experiences.

Postnatal-born GCs are also critical in olfactory processing, though their exact contribution has been difficult to disentangle due to variations in experimental design. When performing an odor-reward task, adult-born GCs were differentially activated compared to neonatal-born GCs, and activation of adult-born GCs via optogenetics enhanced olfactory learning (Alonso et al., 2012; Grelat et al., 2018). Ablation of adult-born GCs resulted in impaired short-term olfactory memory, but interestingly, performance in long-term olfactory memory tasks was not impaired (Breton-Provencher et al., 2009). Another study by Mandairon and colleagues showed that adult-born GCs

are necessary for olfactory perceptual learning, and their survival is modulated by olfactory experience (Moreno et al., 2009). Adult-born GCs have also been implicated in mediating responses to aversive odors, odor discrimination, and pattern separation (Enwere et al., 2004; Hardy et al., 2018; Li et al., 2018; Muthusamy et al., 2017).

1.4 Goals of the dissertation

Given that both the OE and OB are supplied with a continuous source of newly generated neurons, the mouse olfactory system is able to adapt neural representations of odor information to the environment and show robust recovery following injury and insult. Broadly, my goal in this dissertation is to study the role that postnatal neurogenesis plays in olfactory circuitry.

1.4.1 Chapter 2 overview

Due to the constant turnover of OSNs in the mammalian OE, both mature and immature OSNs coexist in a heterogeneous population (McIntyre et al., 2010). Immature OSNs express ORs as early as 4 days after basal cell division and before the onset of mature markers (Rodriguez-Gil et al., 2015). Previous studies, including work from our lab, have also shown that immature OSNs express the proteins necessary for transmitting odor stimuli to the OB and that immature OSN axons form synapses in the OB (Cheetham et al., 2016; Hanchate et al., 2015; Nickell et al., 2012). No study to date, however, has specifically studied whether these immature OSNs are capable of making monosynaptic connections with OB neurons.

In Chapter 2, I investigated whether immature OSNs make functional connections with the OB and whether these connections differ from those formed by their mature counterparts. Using optogenetics, I selectively activated either mature or immature OSN axons in OB slices and performed whole-cell patch clamp recordings of STCs in the OB. I successfully recorded monosynaptic, light-evoked excitatory currents in STCs following activation of immature OSN axons, and the kinetic properties of the light-evoked currents were similar to those of currents evoked by activation of mature OSN axons. Additionally, I showed that these connections were formed by immature OSN axons as early as five days after terminal cell division. These results collectively demonstrate that immature OSNs may play a previously unappreciated role in olfactory processing alongside mature OSNs.

1.4.2 Chapter 3 overview

The laminar organization of OB neurons has been well-described over the past few decades: morphological studies by several classic papers show that the lateral dendrites of TCs are found in the superficial EPL, whereas those of MCs are found in the deep EPL (Mori et al., 1983; Orona et al., 1984). GCs with somata in the deeper regions of the GCL have dendrites in the deep EPL, whereas GCs with somata in the superficial GCL have dendrites in the superficial EPL (Mori et al., 1983; Orona et al., 1983). Interestingly, postnatal-born GCs also show a distinct spatial segregation depending on their birth date, with GCs born in the early postnatal period occupying the superficial GCL, and GCs born in the later postnatal period occupying the deeper GCL (Lemasson et al., 2005).

The proximity of TC dendrites and superficial/early postnatal-born GC dendrites in the superficial EPL, along with the proximity of MC dendrites and deep/late postnatal-born GC

dendrites in the deep EPL, provides an intriguing possibility of differential connections between MCs and TCs and subpopulations of postnatal-born GCs. In Chapter 3, I tested whether the anatomical segregation observed led to differences in functional connectivity. I selectively activated either early postnatal-born or late postnatal-born GCs using optogenetics and recorded inhibitory currents in MCs and TCs. My results showed subtle differences in both the probability for early and late postnatal-born GCs to be connected with MCs vs. TCs and the strength of the connection when present. These data suggest that anatomical differences do indeed lead to functional differences in connectivity.

Our lab has previously demonstrated greater recruitment of superficial GCs vs. deep GCs following glomerular activation, and that MCs and TCs are subject to lateral inhibition at different firing rates—likely due to preferential recruitment of superficial vs. deep GCs by TCs and MCs (Geramita et al., 2016). Differential connectivity with subpopulations of GCs could underlie many of the differences between MCs and TCs, such as excitability, strength of OSN input, and latency of odor-evoked responses (Fukunaga et al., 2012; Gire et al., 2012; Igarashi et al., 2012). The findings described in Chapter 3 provide additional evidence that the parallel processing streams formed by MC and TC output may be mediated by subpopulations of postnatal-born GCs.

Collectively, the experiments described in this dissertation highlight a unique role for adult neurogenesis in both transducing odor signals to the OB and modulating the neural representation of odor information.

2.0 Chapter 2: Immature Olfactory Sensory Neurons Make Functional Monosynaptic Connections with Olfactory Bulb Neurons

2.1 Introduction

Olfactory sensory neurons (OSNs) in the olfactory epithelium (OE) are continuously replaced throughout an animal's life, endowing the olfactory system with significant plasticity and remarkable resilience against environmental insults and trauma (Graziadei et al., 1978; Schwob, 2002). Continuous mitotic division of globose basal cells in the OE generates transitional nascent OSNs, which express GAP43 and Gγ8, markers for immaturity; the transitional nascent OSNs migrate apically to the surface of the OE but do not yet extend cilia (McIntyre et al., 2010; Murdoch and Roskams, 2007; Ryba and Tirindelli, 1995; Verhaagen et al., 1989). OSN maturity is typically defined by the expression of OMP and decreased expression of GAP43 and Gγ8 (Miragall and Graziadei, 1982; Schwob, 2002). Mature OSNs send their axons through the basal surface of the OE and the cribriform plate to the olfactory bulb (OB), where the axons form spherical regions of neuropil called glomeruli. OSN axons expressing the same odorant receptors converge onto the same glomerulus; each glomerulus is innervated by the apical dendrites of mitral cells and tufted cells, the primary output neurons of the OB (Ressler et al., 1994; Serizawa et al., 2000).

The maturation process from terminal cell division to expression onset of the maturation marker OMP takes about 7-8 days (Liberia et al., 2019; Savya et al., 2019). Under normal conditions, the average turnover time for OSNs is one month, although one study has also suggested a mean half-life of one month for the OSN population (Graziadei and Graziadei, 1979; Holl, 2018). The continuous turnover of OSNs means that at any given time, there is a mixed

population of mature and immature OSNs of different ages (McIntyre et al., 2010). Immature OSNs thus face the challenge of integrating successfully into pre-existing circuitry without disrupting the olfactory information flow established by mature OSNs. Additionally, whether immature OSNs play any meaningful roles in odor signal transduction alongside mature OSNs is unknown.

Studies show that immature OSNs express olfactory receptors (ORs) four days after basal cell division, before onset of OMP expression, and their axons reach the OB 3-4 days after terminal cell division (Rodriguez-Gil et al., 2015). Immature OSNs also express proteins involved in the signal transduction of odor molecules (Hanchate et al., 2015; Nickell et al., 2012). Given that OSNs possess the molecular machinery required for signal transduction even in their immature state, it is possible that immature OSNs can both bind odor molecules and transduce the information to the OB. Our lab has shown using *in vivo* 2-photon imaging that immature OSN axons in many glomeruli in the OB respond to odor stimulation (Huang et al., 2021) (*under review*). Additionally, immature Gγ8-expressing OSN axons contain boutons with presynaptic vesicles apposed to the postsynaptic densities of OB neurons, suggesting that they form functional synapses with OB neurons. Optogenetic activation of Gγ8-expressing OSN axons elicited robust firing in the glomerular, external plexiform, and mitral cell layers, though the *in vivo* electrophysiology technique used precluded accurate determination of monosynaptic connectivity or the specific cell types that received input from Gγ8-expressing OSN axons (Cheetham et al., 2016).

Here, I use optogenetics to demonstrate that immature OSNs make monosynaptic connections with superficial tufted cells (STCs) in the OB, and that the excitatory inputs from immature OSNs are similar to that from their mature counterparts. I also show that immature OSNs

form these connections within five days after terminal cell division, thus providing evidence that immature OSNs may play a part in odor processing before reaching full maturity.

2.2 Results

2.2.1 Immature OSN axons can be selectively activated using an optogenetic approach.

To address the question of whether immature olfactory sensory neuron (OSN) axons provide monosynaptic input to olfactory bulb (OB) neurons, I used P18-25 Gγ8-tTA$^{+/-}$;tetO-ChIEF-Citrine$^{+/-}$ (referred to as Gγ8-ChIEF-Citrine) mice and OMP-tTA$^{+/-}$;tetO-ChIEF-Citrine$^{+/-}$ (referred to as OMP-ChIEF-Citrine) mice. In these animals, tetracycline transactivator (tTA) expression is driven by Gγ8 or OMP promoters in immature or mature OSNs, respectively (Tirindelli and Ryba, 1996). The tTA system allows for tight control of expression that can be restricted to a developmental window. Expression of the blue-light activated cation channel ChIEF fused to the yellow fluorescent protein Citrine is driven by the tetracycline-responsive promoter. For this first set of experiments, mice were raised on normal diet in the absence of doxycycline, allowing active expression of ChIEF-Citrine in OSN axons. Immature or mature OSN axons can then be selectively activated using optogenetic stimulation (Cheetham et al., 2016) (Figure 2).

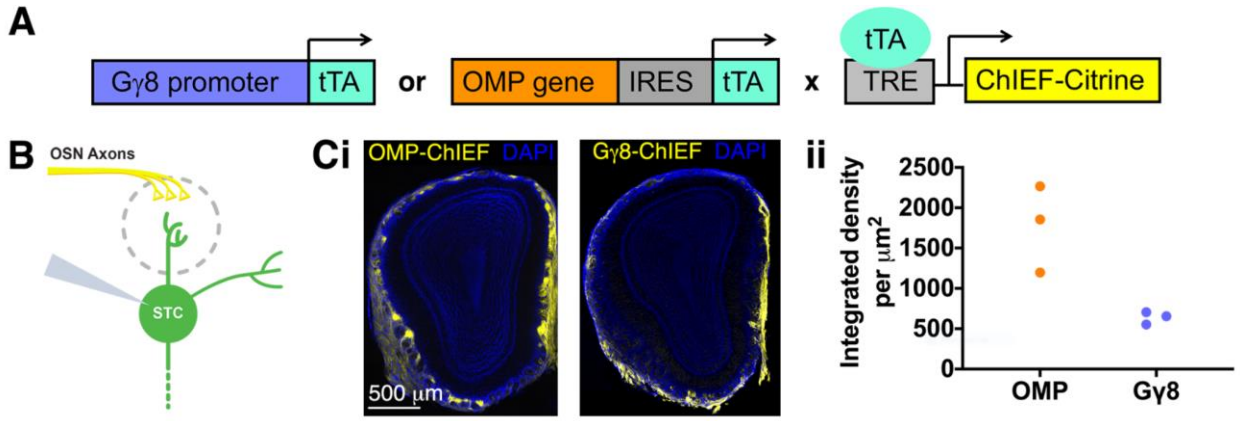

Figure 2. Expression of ChIEF-Citrine in immature (Gγ8$^+$) and mature (OMP$^+$) OSN axons.

A. Schematic of breeding strategy to generate mice expressing CHIEF-Citrine in either immature or mature OSNs under control of the Gγ8 or OMP promote, respectively. **B.** Schematic of relevant OB glomerular circuitry. Whole-cell voltage clamp recordings were made from STCs in either Gγ8-ChIEF-Citrine or OMP-ChIEF-Citrine mice. **C.** Quantification of the density of ChIEF-Citrine-expressing axons in OMP-ChIEF-Citrine and Gγ8-ChIEF-Citrine mice. **i.** Widefield fluorescence images showing ChIEF-Citrine-expressing axons in OMP-ChIEF-Citrine and Gγ8-ChIEF-Citrine mice. **ii.** Integrated density of Citrine fluorescence per μm^2 of the glomerular layer in OMP-ChIEF-Citrine and Gγ8-ChIEF-Citrine mice (n = 3 per group). Symbols: values for individual mice. The data in Figure 1C were collected by Alyssa Lauer and Alex Rangel.

I then made whole-cell recordings of superficial tufted cells (STCs), which are known to receive direct monosynaptic input from mature OSNs (Sun et al., 2020). These recordings were made in slices of olfactory bulbs. STCs were identified using morphological and physiological criteria: they reside at the border between the glomerular layer (GL) and external plexiform layer (EPL), possess a lateral dendrite in the EPL in addition to a primary apical dendrite, and exhibit regular or irregular non-bursting spiking patterns without the depolarizing envelope characteristic of external tufted cells (ETCs) (Antal et al., 2006; De Saint Jan et al., 2009; Hayar et al., 2004b; Jones et al., 2020; Liu et al., 2012; Liu and Shipley, 2008; Sun et al., 2020) (Figure 3A, B). I targeted STCs located close to the glomeruli innervated by ChIEF-expressing axons, voltage

clamped them at -70 mV, and recorded their excitatory responses to multiglomerular optogenetic stimulation (Figure 3C, D). Responses were made with APV (20 μM) in the bath to isolate fast AMPA-mediated currents; light-evoked responses were observed following optogenetic stimulation of both immature and mature ChIEF-Citrine-expressing axons.

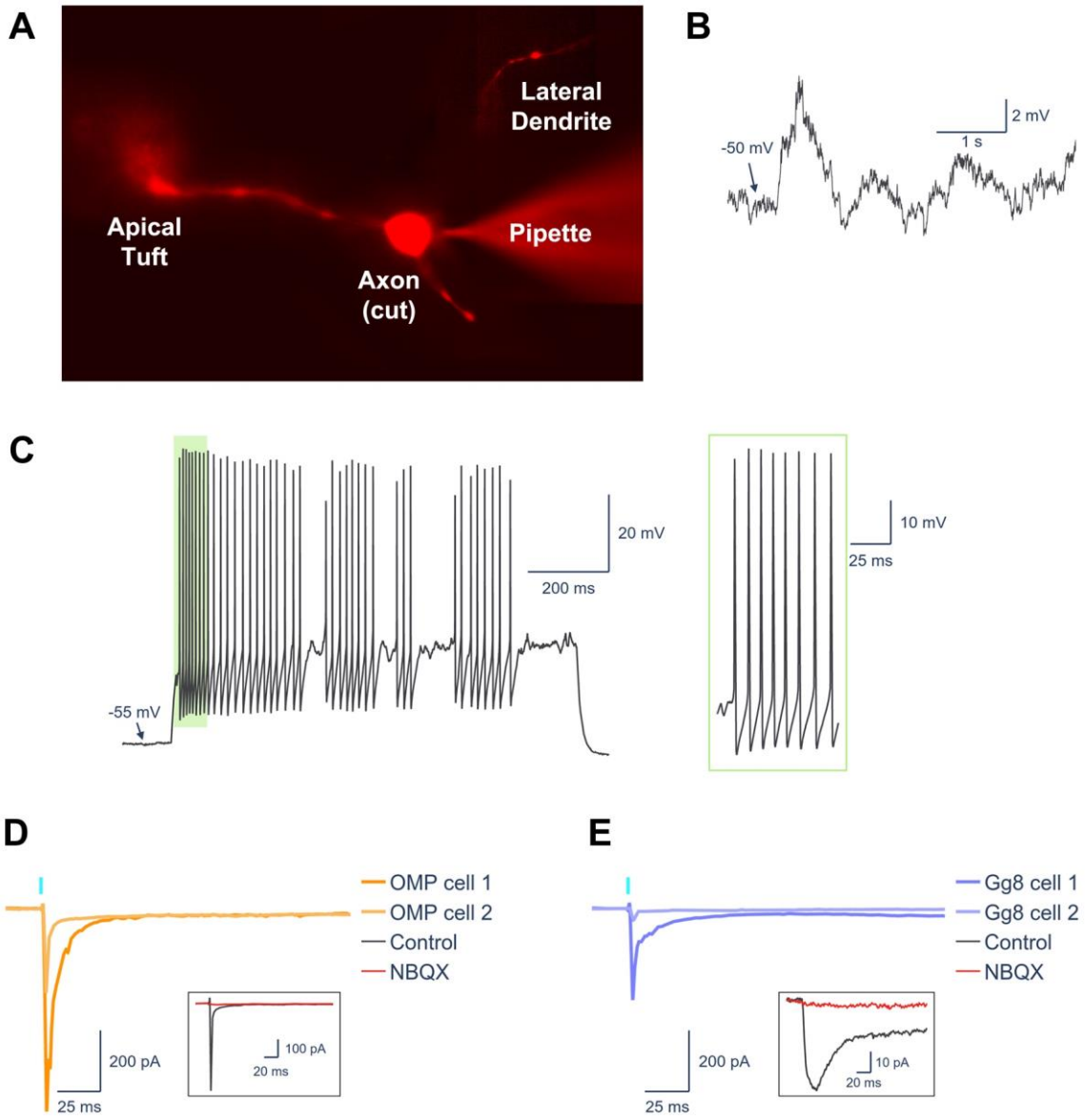

Figure 3. Identification and whole-cell patch-clamp recordings of superficial tufted cells (STCs).

A. Visualization of a STC filled with AF594, showing an apical dendrite, a lateral dendrite, and a cut axon. **B.** Example trace of membrane oscillations in a STC, indicative of an intact apical dendrite. **C.** Example of a STC spike train evoked by step current injection, showing an irregular spiking pattern without a depolarizing envelope or rhythmic bursting. **D-E:** Recordings from STCs made in normal ACSF containing 20 µM APV (control) and in ACSF containing 10 µM NBQX in addition to APV, demonstrating the presence of monosynaptic input from OSN axons. **D.** Example responses from two STCs elicited by 1 ms, 100% intensity light pulse photoactivation of immature Gγ8-

ChIEF-Citrine-expressing OSN axons. **E.** Example responses from two STCs elicited by 1 ms, 100% intensity light pulse photoactivation of mature OMP-ChIEF-Citrine-expressing OSN axons. All traces are averages of 10 trials. Blue line: 1 ms light pulse photostimulation.

2.2.2 A similar proportion of STCs receive monosynaptic input from mature and immature OSNs.

I generated a power curve for each STC by systematically increasing the LED intensity (from 10 to 20, 50, 80, and 100%) for each of three light stimulus durations (0.25, 1, and 2 ms) (Figure 4). The shortest stimulus condition that reliably and consistently evoked responses (1 ms at 100% light intensity) was selected and used for all subsequent analyses.

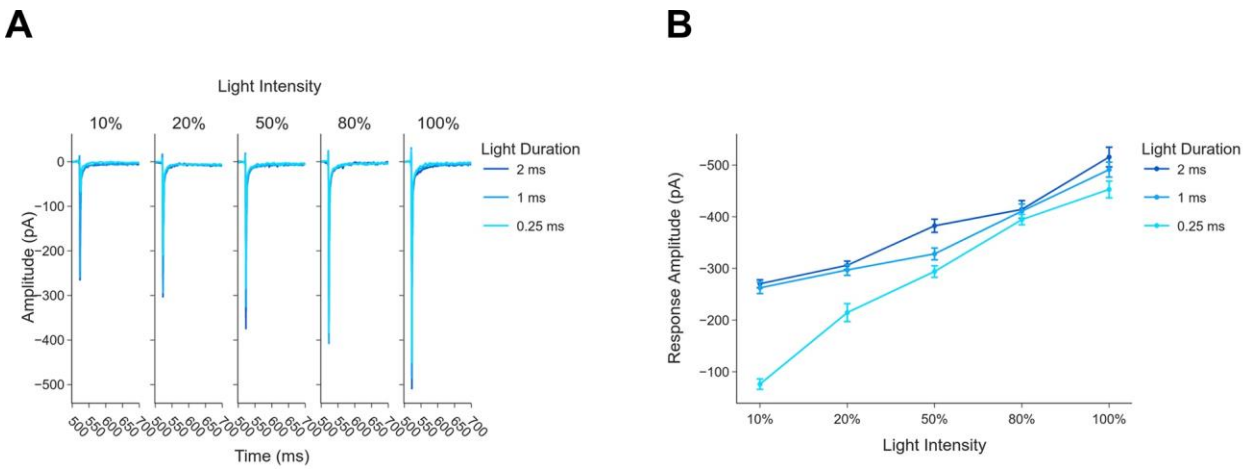

Figure 4. Power curve for a STC recorded in an OMP-ChIEF-Citrine mouse.

A. Light-evoked EPSCs recorded in response to light pulses of increasing duration and light intensity. **B.** Relationship between light pulse intensity and duration and EPSC amplitude for the same STC. All traces are averages of 10 trials per stimulus condition.

I compared responses evoked by photoactivation of mature vs. immature OSN axons and considered a cell as receiving monosynaptic input from OSNs if the onset latency of its photoactivated response was shorter than 2 ms (Sun et al., 2020). A similar proportion of STCs from OMP-ChIEF-Citrine and Gγ8-ChIEF-Citrine mice showed inward currents in response to optogenetic stimulation (OMP-ChIEF-Citrine responsive cells: 7/19; Gγ8-ChIEF-Citrine responsive cells: 4/11; Fisher's exact test, $p > 0.99$) (Figure 5A). For a subset of recorded neurons, I confirmed that the responses were AMPA-mediated as they were completely abolished by bath application of NBQX (10 μM) (Figure 3C, D).

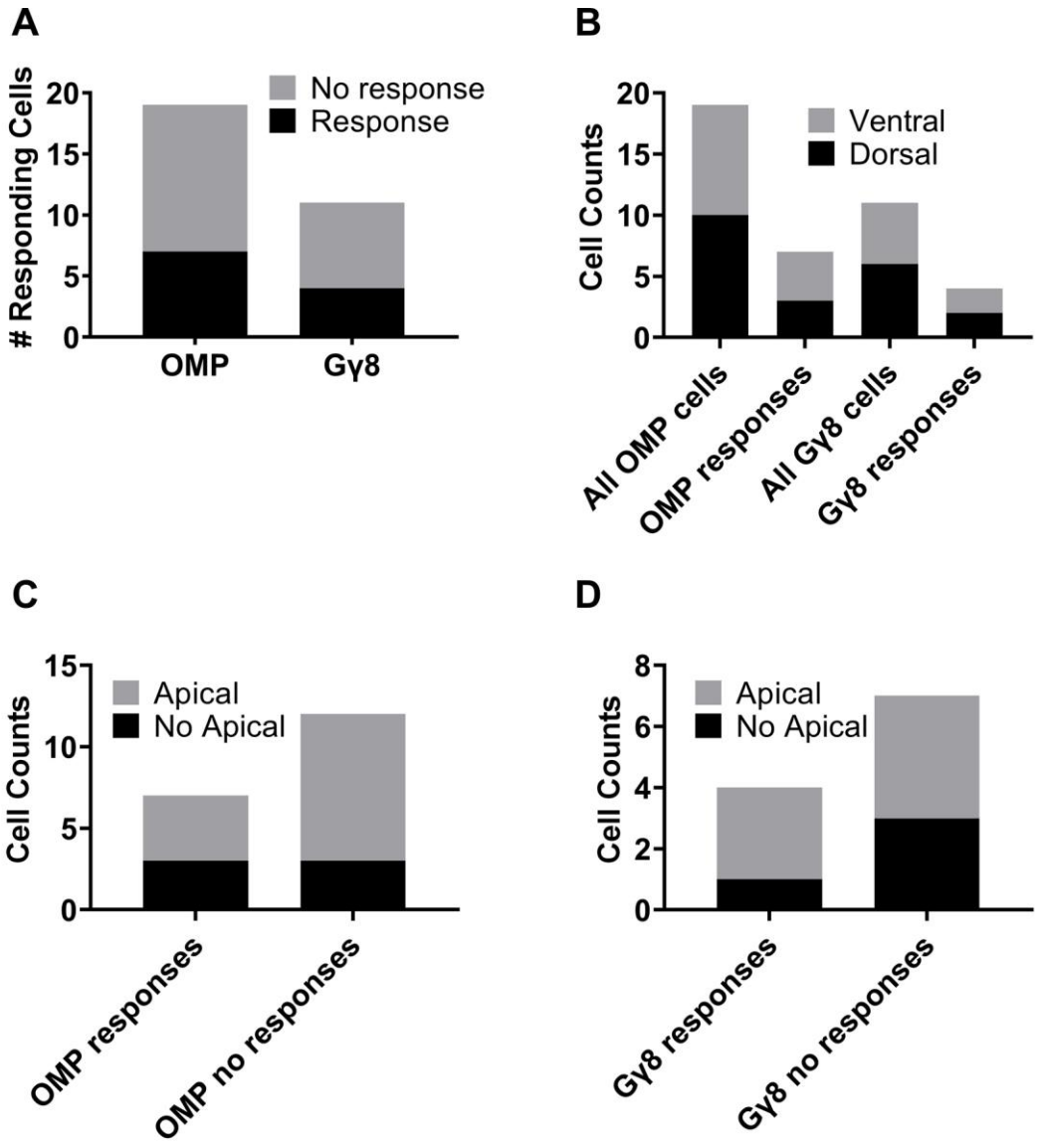

Figure 5. A similar proportion of STCs from both OMP-ChIEF-Citrine and Gγ8-ChIEF-Citrine mice show light-evoked responses.

A. A similar proportion of recorded STCs from both OMP-ChIEF-Citrine and Gγ8-ChIEF-Citrine mice responded monosynaptically to photoactivation (Fisher's exact test, $p > 0.99$, n = 19 cells from 10 OMP-ChIEF-Citrine mice and n = 11 cells from 5 Gγ8-ChIEF-Citrine mice). One STC from the Gγ8-ChIEF-Citrine group showed a monosynaptic response to optogenetic stimulation with a 1 ms, 50% intensity light pulse, but its dataset was incomplete and lacked sweeps for the 1 ms, 100% intensity light stimulation, so it was not included for further analysis (see Methods). **B.** I recorded roughly numbers of dorsal and ventral STCs, and the proportion of responsive STCs that were dorsal or ventral did not differ between the two genotypes (OMP responses vs. Gγ8 responses: Fisher's exact test, $p > 0.99$, n

= 7 cells from 5 OMP-ChIEF-Citrine mice and n = 4 responsive cells from 3 Gγ8-ChIEF-Citrine mice). **C.** The visualization of an apical dendrite or tuft did not guarantee the presence of a light-evoked monosynaptic response in recorded STCs from OMP-ChIEF-Citrine mice. A similar proportion of responsive cells and cells without light-evoked responses showed the presence of an apical dendrite or tuft (Fisher's exact test, $p = 0.62$, n = 19 cells from 10 OMP-ChIEF-Citrine mice). **D.** The visualization of an apical dendrite or tuft did not guarantee the presence of a light-evoked monosynaptic response in recorded STCs from Gγ8-ChIEF-Citrine. A similar proportion of responsive cells and cells without light-evoked responses showed the presence of an apical dendrite or tuft (Fisher's exact test, $p > 0.99$, n = 11 cells from 5 OMP-ChIEF-Citrine mice).

Approximately equal numbers of STCs from the dorsal and the ventral surfaces of the OB for both genotypes were recorded (OMP-ChIEF-Citrine: 10 dorsal, 9 ventral; Gγ8-ChIEF-Citrine: 6 dorsal, 5 ventral). This enabled me to corroborate our *in vivo* calcium imaging data demonstrating odor-evoked responses in immature OSN axons (Huang et al., 2021) (*under review*), which were obtained from the dorsal OB. I also obtained recordings from the ventral OB, which receives robust innervation by immature OSN axons at this age (Cheetham et al., 2016; Eerdunfu et al., 2017). The proportion of responsive cells that were dorsal or ventral was not significantly different between OMP-ChIEF-Citrine and Gγ8-ChIEF-Citrine mice, suggesting that there was no difference in whether dorsal vs. ventral STCs were more likely to receive input from either mature or immature OSN axons (OMP-ChIEF-Citrine responsive cells: 3/7 dorsal, 4/7 ventral; Gγ8-ChIEF-Citrine responsive cells: 2/4 dorsal, 2/4 ventral; Fisher's exact test, $p > 0.99$) (Figure 5B).

The presence of an intact apical dendrite may be correlated with the responsiveness of an STC. To account for this factor, I filled every recorded cell with AF594 to visualize cell morphology on the rig microscope and noted whether I was able to see an apical tuft or intact apical dendrite (Figure 3A). I also observed oscillatory membrane potentials in some cells, which is indicative of an intact apical dendrite (Figure 3B) (Carlson et al., 2000; Hayar et al., 2005;

Schoppa and Westbrook, 2001). There were responsive cells in which I could not visualize an apical dendrite, and there were also cells that displayed apical dendrites but no responses (Figure 5C, D). In both OMP-ChIEF-Citrine and Gγ8-ChIEF-Citrine mice, a similar proportion of responsive cells and non-responsive cells showed the presence of an apical dendrite or tuft (OMP-ChIEF-Citrine cells with apical dendrite/tuft: 4/7 responsive cells, 9/12 non-responsive cells, Fisher's exact test, p = 0.62; Gγ8-ChIEF-Citrine cells with apical dendrite/tuft: 3/4 responsive cells, 4/7 non-responsive cells, Fisher's exact test, $p > 0.99$). The inability to visualize apical dendrites in some responsive cells may be explained by their apical dendrites running deep within the slice.

2.2.3 The excitatory input from immature OSNs does not differ from input from mature OSNs.

Next, I compared the properties of the excitatory inputs received by STCs from OMP-ChIEF-Citrine axons vs. Gγ8-ChIEF-Citrine axons (n = 7 cells from 5 OMP-ChIEF-Citrine mice; n = 3 cells from 2 Gγ8-ChIEF-Citrine mice) (Figure 6A). There was no significant difference in the peak amplitude of EPSCs evoked by optogenetic stimulation of mature vs. immature OSN axons (OMP-ChIEF-Citrine: -667.8 (565.4) pA, Gγ8-ChIEF-Citrine: -74.6 (1050) pA, Mann-Whitney test, p = 0.517; data are reported as median (IQR)) (Figure 6B). Light-evoked EPSCs recorded in STCs from both genotypes displayed short onset latencies (OMP-ChIEF-Citrine: 1.4 (0.6) ms, Gγ8-ChIEF-Citrine: 1.4 (0.8) ms, Mann-Whitney test, p = 0.667) and had low trial-to-trial jitter (OMP-ChIEF-Citrine: 0.07 (0.2), Gγ8-ChIEF-Citrine: 0.9 (0.8), Mann-Whitney test, p = 0.067) (Figure 6C, D), consistent with previously reported kinetics of monosynaptic transmission from OSNs to STCs (Sun et al., 2020; Vaaga and Westbrook, 2016). EPSC time to

peak was also similar between the two genotypes (OMP-ChIEF-Citrine: 1.4 (0.7) ms, Gγ8-ChIEF-Citrine: 2.3 (1.0) ms, Mann-Whitney test, $p = 0.667$) (Figure 6E). Overall, the responses evoked by stimulation of Gγ8-ChIEF-Citrine axons were kinetically similar to responses evoked by stimulation of OMP-ChIEF-Citrine axons, providing clear evidence that immature OSNs form monosynaptic glutamatergic connections with STCs. Due to the difficulty and low probability of recording monosynaptic responses in STCs following photoactivation of Gγ8-ChIEF-Citrine-expressing OSN axons, the sample size of STCs from Gγ8-ChIEF-Citrine mice is quite small. Future experiments with a larger and sufficiently powered sample size could unveil robust differences in the kinetic properties of inputs from mature vs. immature OSN axons.

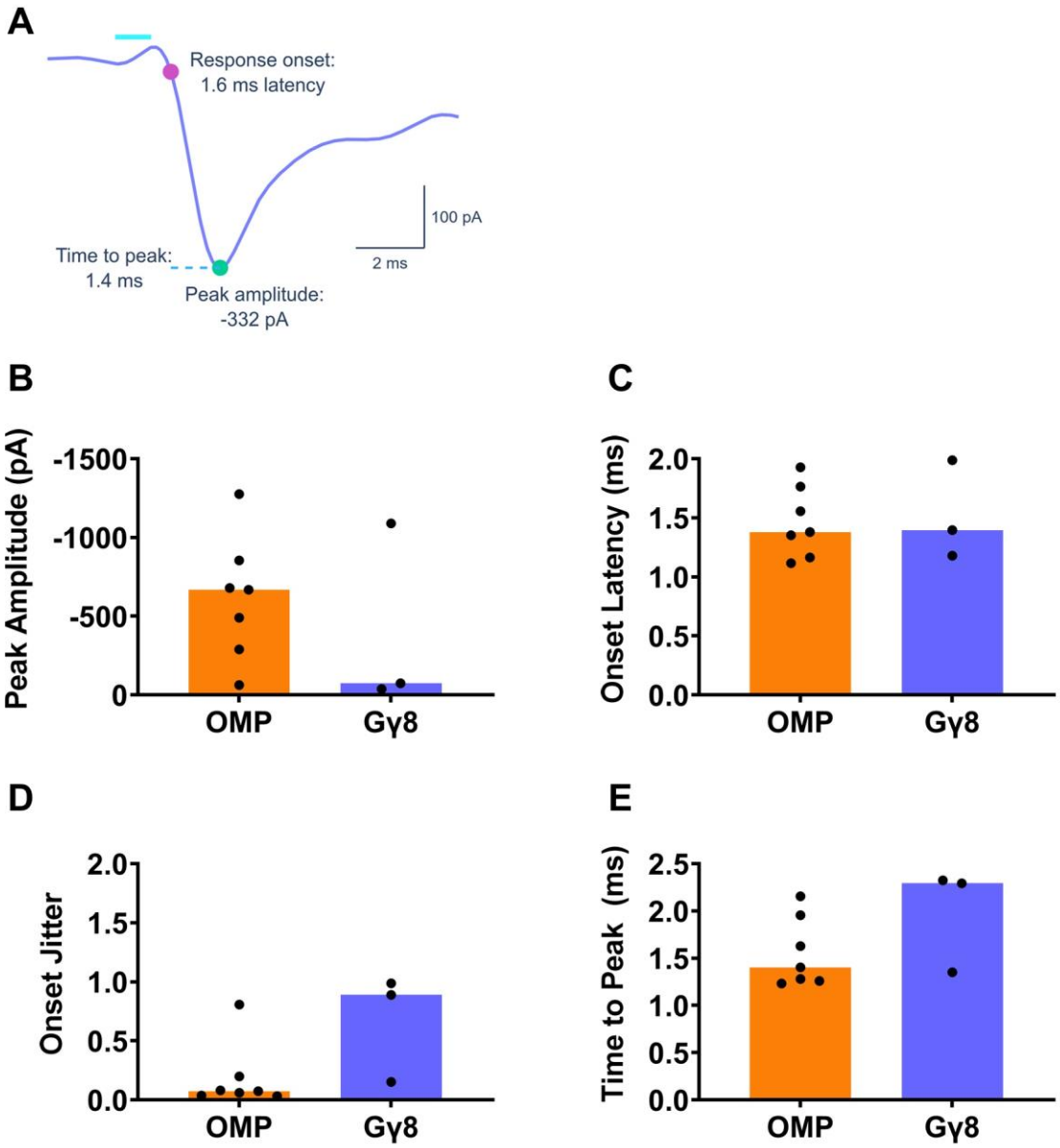

Figure 6. The kinetic properties of excitatory inputs from mature vs. immature OSN axons are similar.

A. Properties of each light-evoked response analyzed: time to peak, response onset, and peak amplitude. **B.** Median peak amplitude was not significantly different between OMP-ChIEF-Citrine and Gγ8-ChIEF-Citrine mice (Mann-Whitney test, $p = 0.517$). **C.** Median onset latency was not significantly different between OMP-ChIEF-Citrine and Gγ8-ChIEF-Citrine mice (Mann-Whitney test, $p = 0.667$). **D.** Median onset jitter was not significantly different between OMP-ChIEF-Citrine and Gγ8-ChIEF-Citrine mice (Mann-Whitney test, $p = 0.067$). **E.** Median time to peak was not significantly different between OMP-ChIEF-Citrine and Gγ8-ChIEF-Citrine mice (Mann-Whitney test, $p =$

0.183). n = 7 cells from 5 OMP-ChIEF-Citrine mice, and n = 3 cells from 2 Gγ8-ChIEF-Citrine mice. Bars: median, symbols: values for individual neurons.

2.2.4 Photoactivation of OSN axons 3-5 days after methimazole treatment elicits light-evoked responses in STCs.

My data thus far demonstrate that immature Gγ8-ChIEF-Citrine axons can be photoactivated and provide monosynaptic glutamatergic input onto STCs, but the exact birth date of these axons is unknown. In order to investigate whether newly generated Gγ8-expressing OSNs can synapse with OB neurons, I generated a mouse model with its mature OSNs ablated. Methimazole (MMZ) is an antithyroid drug that selectively induces cell death in OSNs when injected intraperitoneally in rodents (Bergstr¨om et al., 2003; Kikuta et al., 2015; Sakamoto et al., 2007). The progenitor basal cells in the olfactory epithelium (OE) are spared and generate new OSNs over the next month (Bergman et al., 2002). At early time points after MMZ injection, the OE should contain only immature but not mature OSNs.

Histological analysis of mice injected with MMZ validated this assumption (Figure 7), showing that OE width and the number of immature $GAP43^+$ OSNs increased in number from 3-7 dpi MMZ (Figure 7B-E), whereas mature OMP^+ OSNs were absent until 7 dpi (Figure 7Fi). Even at 7 dpi, OMP-expressing OSNs were only present in very small numbers (0.48% of the saline-injected control mice, vs. Gγ8-expressing axons, which recovered to 55.9% of control levels) (Figure 7Fii).

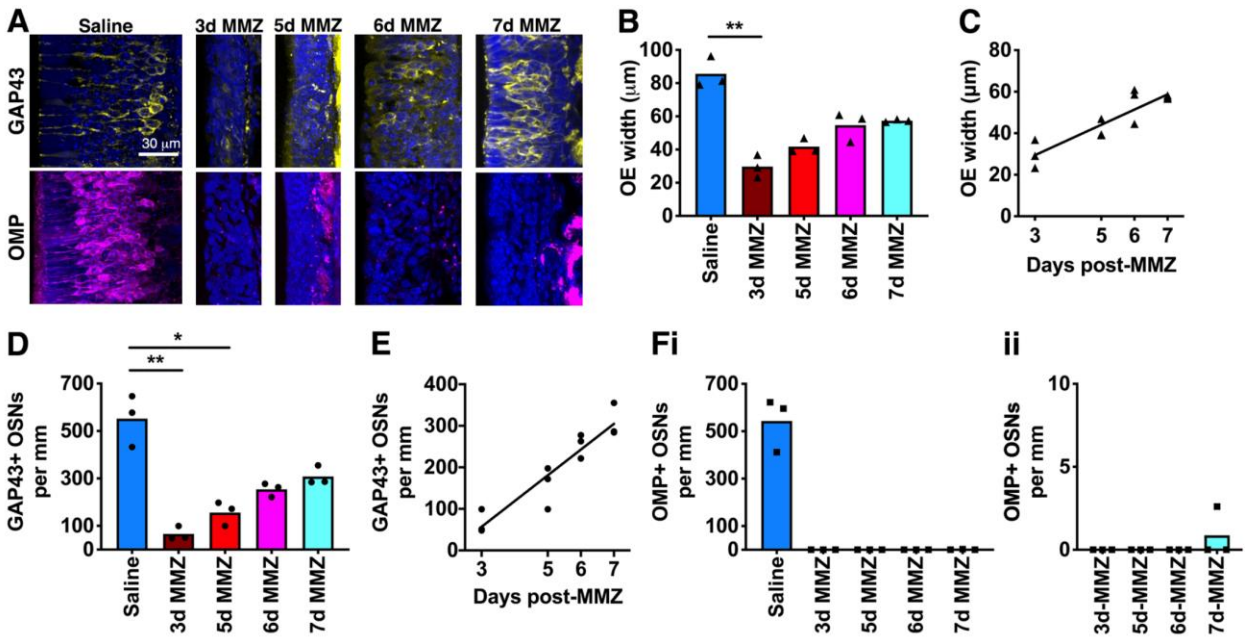

Figure 7. The olfactory epithelium contains immature but not mature OSNs at early time points after methimazole administration.

A. Maximum intensity projections of 2-photon z-stacks of coronal OE sections stained for GAP43 or OMP from mice that had received either MMZ 3 – 7 d previously or saline. **B.** OE width is significantly reduced 3 days post-MMZ compared to saline-injected mice (One-way ANOVA on Ranks, $p < 0.001$, Kruskal-Wallis statistic = 12.4. Dunn's multiple comparisons tests, 3-day, $p = 0.004$, Z = 3.29; 5d, $p = 0.071$, Z = 2.37; 6d, $p = 0.94$, Z = 1.19; 7d, $p = 0.68$, Z = 1.37; vs. saline. n = 3 mice per group). **C.** OE width increases linearly between 3 and 7 days post-MMZ (Linear regression, $R^2 = 0.80$, $p < 0.001$, n = 3 mice per group). **D.** Linear density of $GAP43^+$ OSNs is significantly reduced at 3 and 5 days post-MMZ compared to saline-injected mice (One-way ANOVA on Ranks: $p < 0.001$, Kruskal-Wallis statistic = 13.4. Dunn's multiple comparisons tests. 3d MMZ, $p = 0.005$, Z = 3.24; 5d MMZ, $p = 0.048$, Z = 2.51; 6d MMZ, $p = 0.40$, Z = 1.65; 7d MMZ, $p = 1.00$, Z = 0.82; vs. saline-injected mice. n = 3 mice per group). **E.** Linear density of $GAP43^+$ OSNs increases linearly between 3 and 7 days post-MMZ (Linear regression. $R^2 = 0.88$, $p < 0.001$, n = 3 mice per group). **F.** OMP^+ OSNs are absent from the septal OE at 3-6 days post-MMZ and very sparse at 7 days post-MMZ. Note different y-axis scales in **i** and **ii**. **B-F.** Bars: mean values per group, symbols: values for individual mice. The data in this figure were collected and analyzed by Claire Cheetham.

With this validation that MMZ administration results in only the presence of immature OSNs at early time points post injection, three separate cohorts of mice were injected for slice electrophysiology experiments at different time points (Figure 8A): Gγ8-ChIEF-Citrine mice sacrificed for slice experiments at 3 dpi (n = 3 mice), when I expect no newly generated immature OSN axons in the OB, OMP-ChIEF-Citrine mice sacrificed at 5 dpi (n = 3 mice), when there should be no mature OSN axons present, and Gγ8-ChIEF-Citrine mice sacrificed at 5 dpi (n = 3 mice), when newly generated immature OSN axons have begun to recover in meaningful numbers in the OB (Figure 7D). Light-evoked responses in recorded STCs following photoactivation of OSN axons in these mice would suggest that newly generated OSNs do make monosynaptic connections with OB neurons.

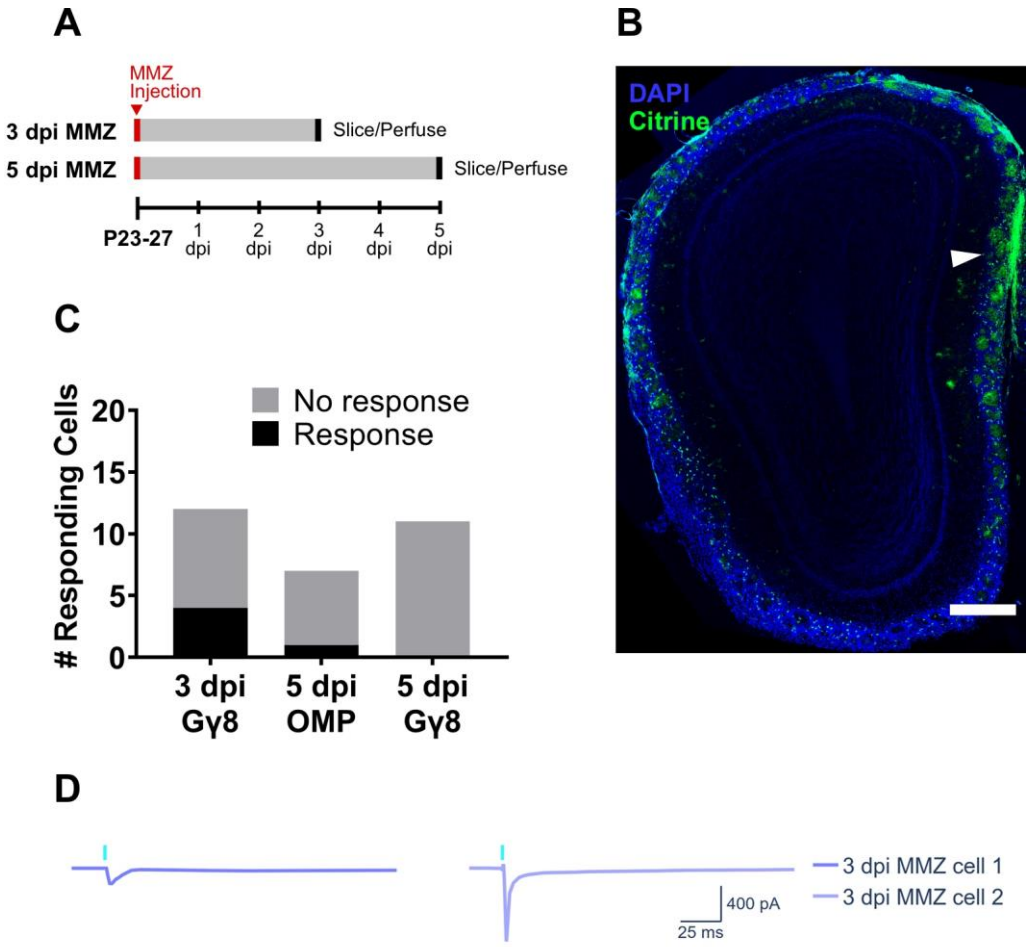

Figure 8. Photoactivation of methimazole-treated OSN axons elicits light-evoked responses in STCs.

A. Schematic of the methimazole (MMZ) injection timeline for OMP-ChIEF-Citrine and Gγ8-ChIEF-Citrine mice. **B.** Widefield fluorescence images showing ChIEF-expressing axons in an Gγ8-ChIEF-Citrine mouse 3 days after MMZ injection (3 dpi). Note that lipofuscin, which is commonly observed in MMZ-injected animals due to debris clearance, is visible as autofluorescent puncta. Scale bars: 150 μm. **C.** STCs from both Gγ8-ChIEF-Citrine mice sacrificed at 3 dpi and OMP-ChIEF-Citrine mice sacrificed at 5 dpi responded monosynaptically to photoactivation (n = 12 cells from 3 Gγ8-ChIEF-Citrine mice at 3 dpi, n = 7 cells from 3 OMP-ChIEF-Citrine mice at 5 dpi, and n = 11 cells from 3 Gγ8-ChIEF-Citrine mice at 5 dpi). **D.** Example responses from two STCs elicited by 1 ms 100% intensity light pulse photoactivation of Gγ8-ChIEF-Citrine-expressing OSN axons at 3 dpi MMZ. Blue line: 1 ms light pulse photostimulation. The data in Figure 8B were collected by Taryn Brechbill, Alex Rangel, and Claire Cheetham. MMZ injections were performed by Taryn Brechbill, Alex Rangel, and Tenzin Kunkhyen.

To my surprise, I was able to identify ChIEF-expressing axons in the OB of an Gγ8-ChIEF-Citrine mouse three days after MMZ injection. (Figure 8B). Equally surprisingly, I also recorded monosynaptic responses in STCs after photoactivation of axons in 3 dpi Gγ8-ChIEF-Citrine mice, in which there should be no newly generated Gγ8-ChIEF-Citrine-expressing axons present in the OB (n = 4/12 responsive cells), and in 5 dpi OMP-ChIEF-Citrine mice, in which there should be no newly generated OMP-ChIEF-Citrine-expressing axons present in the OB (n = 1/7 responsive cells). Photoactivation of Gγ8-ChIEF-Citrine-expressing axons five days after MMZ injection did not elicit any monosynaptic responses (n = 0/11 responsive cells) (Figure 8C).

Light-evoked responses in 3 dpi Gγ8-ChIEF-Citrine mice resembled those recorded in untreated Gγ8-ChIEF-Citrine mice (Figure 8D). Comparison of the kinetic properties of light-evoked responses in 3 dpi Gγ8-ChIEF-Citrine mice vs. untreated Gγ8-ChIEF-Citrine mice also revealed no significant differences, with the peak amplitude (3 dpi: -95.7 (675.4) pA, untreated: -74.6 (1050) pA, Mann-Whitney test, $p = 0.629$), onset latency (3 dpi: 1.5 (0.6) ms, untreated: 1.4 (0.8) ms, Mann-Whitney test, $p > 0.99$), trial-to-trial jitter (3 dpi: 0.7 (1.8), untreated: 9 (0.8), Mann-Whitney test, $p > 0.99$), and time to peak (3 dpi: 20.1 (37.4) ms, untreated: 2.3 (1.0) ms, Mann-Whitney test, $p = 0.257$) all being similar between STCs recorded in the two groups (Figure 9).

No newly generated mature or immature OSNs should be present in the OB at the time of slice recordings in these animals; photostimulation in these OB slices should not evoke neurotransmitter release in the absence of ChIEF-Citrine-expressing OSN axons. Therefore, I hypothesized that the light-evoked responses I observed were mediated by release from the axons of degenerating ChIEF-Citrine-expressing OSNs. Previous studies have reported the persistence of high numbers of degenerating immature OSN axons at 5-6 dpi MMZ (Blanco-Hernández et al.,

2012; Kikuta et al., 2015; Tsai and Barnea, 2014). Here, I was unable to differentiate between the two possible sources of light-evoked input onto STCs: 1) the degenerating axons of pre-existing ChIEF-Citrine-expressing OSNs, whose somata in the OE were ablated by MMZ administration, and 2) newly generated OSNs, which emerged after MMZ administration.

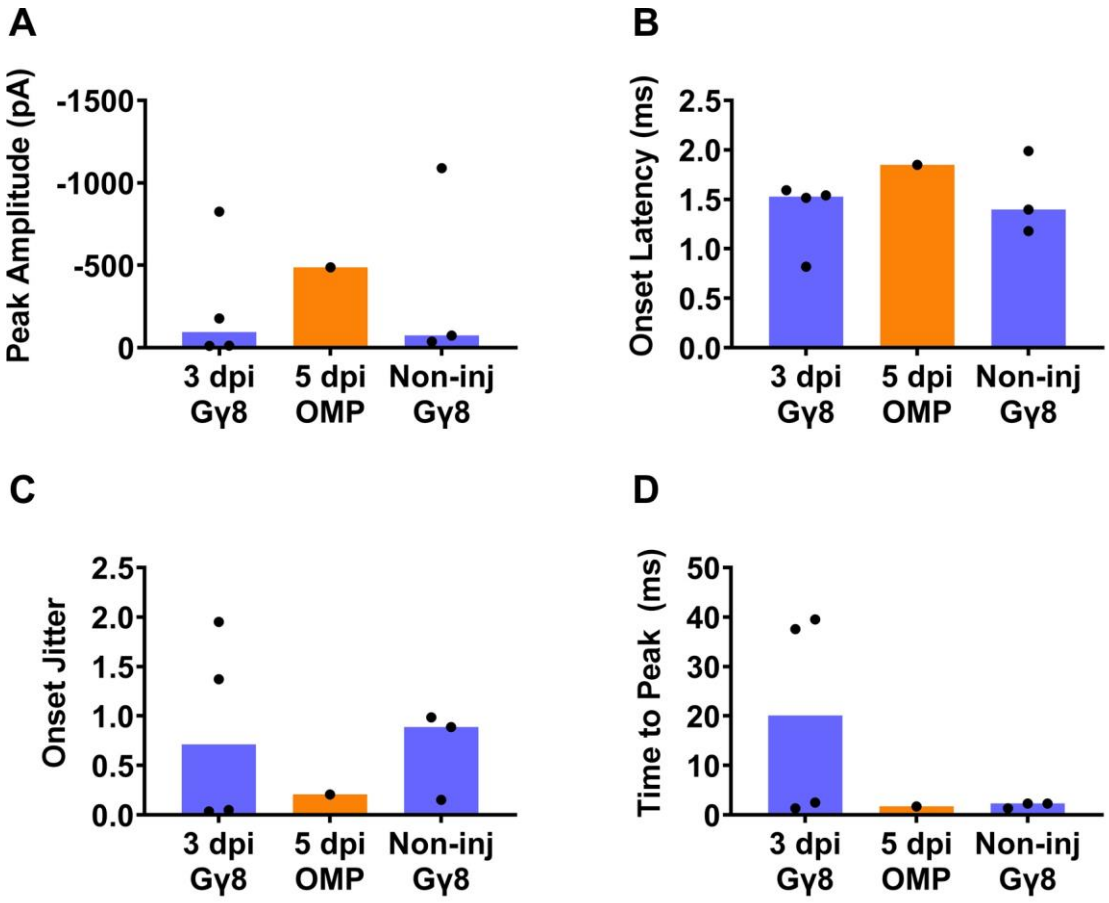

Figure 9. The kinetic properties of excitatory inputs from immature OSNs at 3 dpi MMZ are similar to those from untreated immature OSNs.

A. Median peak amplitude was not significantly different between Gγ8-ChIEF-Citrine mice at 3 dpi MMZ and untreated Gγ8-ChIEF-Citrine mice (Mann-Whitney test, $p = 0.629$). **B.** Median onset latency was not significantly different between Gγ8-ChIEF-Citrine mice at 3 dpi MMZ and untreated Gγ8-ChIEF-Citrine mice (Mann-Whitney test, $p > 0.99$). **C.** Median onset jitter was not significantly different between Gγ8-ChIEF-Citrine mice at 3 dpi MMZ and untreated Gγ8-ChIEF-Citrine mice (Mann-Whitney test, $p > 0.99$). **D.** Median time to peak was not significantly different between Gγ8-ChIEF-Citrine mice at 3 dpi MMZ and untreated Gγ8-ChIEF-Citrine mice (Mann-Whitney test, $p = 0.257$). n = 4 cells from 2 Gγ8-ChIEF-Citrine mice at 3 dpi MMZ, and n = 3 cells from 2 untreated Gγ8-ChIEF-Citrine mice. Bars: median, symbols: values for individual neurons.

2.2.5 Restricting ChIEF-Citrine expression to newly generated OSNs reveals that newly generated immature OSNs provide monosynaptic input to STCs.

In order to disentangle photoactivated release mediated by degenerating Gγ8-ChIEF-Citrine-expressing axons from that mediated by newly generated Gγ8-ChIEF-Citrine-expressing axons, I leveraged theTet-Off expression system to suppress ChIEF-Citrine expression in OSNs prior to MMZ ablation. Four cohorts of Gγ8-ChIEF-Citrine mice were given doxycycline-fortified chow (Dox food) starting at P7 and injected with MMZ. Six hours after MMZ injection, the mice were taken off Dox food and given normal chow until they were sacrificed for slice electrophysiology experiments (Figure 10A). This strategy ensured that any OSNs that pre-existed before MMZ ablation did not express ChIEF-Citrine, since expression was suppressed by doxycycline. Removal of Dox food after MMZ injection allowed newly generating OSN axons to express ChIEF, enabling the selective activation of newly generated OSN axons without activating degenerating axons.

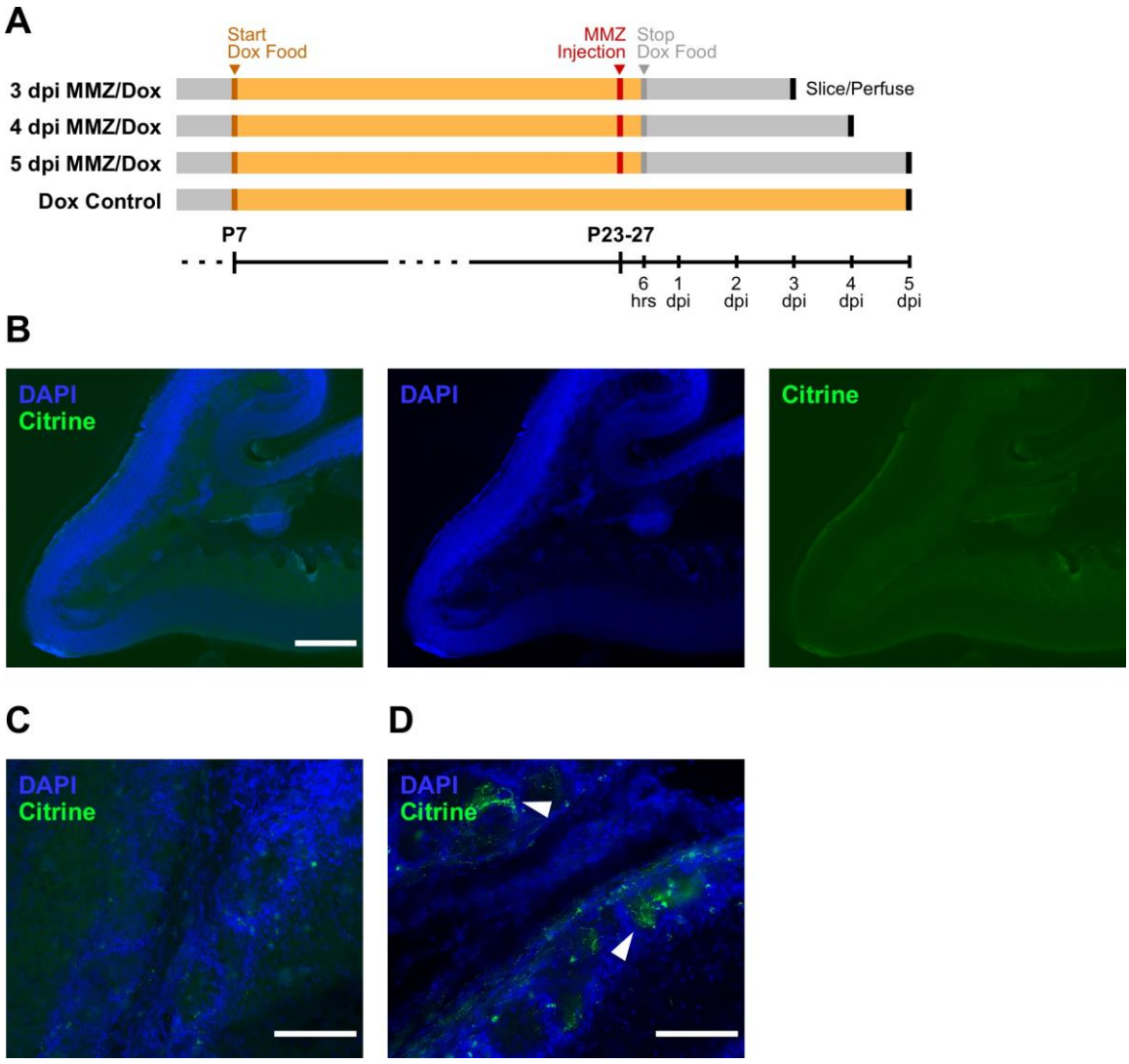

Figure 10. Doxycycline restricts expression of ChIEF-Citrine expression to newly generated OSN axons.

A. Schematic of the methimazole (MMZ) injection and Dox food administration timeline for Gγ8-ChIEF-Citrine mice. **B.** Widefield fluorescence images showing no ChIEF-Citrine fluorescence in the OE of a Gγ8-ChIEF-Citrine mouse that was kept on Dox food until time of sacrifice (Dox Control). Scale bars: 150 µm. **C.** Widefield fluorescence images showing no ChIEF-Citrine fluorescence in the OB of a Gγ8-ChIEF-Citrine mouse at 3 dpi MMZ/Dox. Note that lipofuscin, which is commonly observed in MMZ-injected animals due to debris clearance, is visible as autofluorescent puncta. Scale bars: 100 µm. **D.** Widefield fluorescence images showing the presence of ChIEF-Citrine fluorescence OSN axons in the OB of a Gγ8-ChIEF-Citrine mouse at 5 dpi MMZ/Dox. Scale bars: 100 µm. The data in this figure were collected by Taryn Brechbill, Jordan Gregory, Alex Rangel, and Claire Cheetham.

Unless otherwise specified, the following experiments used mice that were given Dox food from P7 until six hours after MMZ injection; “dpi MMZ/Dox" refers to days post MMZ injection and removal of Dox food. In these mice, ChIEF-Citrine expression should be absent in degenerating axons. The absence of ChIEF-Citrine fluorescence in the OE of a non-injected control animal that was given Dox food until time of sacrifice confirmed that ChIEF-Citrine expression was suppressed by Dox food (Figure 10B). There was also no ChIEF-Citrine fluorescence in a Gγ8-ChIEF-Citrine mouse at 3 dpi MMZ/Dox (Figure 10C). By 5 dpi MMZ/Dox, I was able to observe some ChIEF-Citrine-expressing OSN axons in the OB, suggesting that newly generated immature OSN axons do arrive into the bulb five days after terminal cell division (Figure 10D).

In a control mouse that was given Dox food until being sacrificed for slice recording at 3 dpi MMZ, I did not observe any light-evoked responses in STCs following photostimulation as expected (n = 0/6 responsive cells). Similarly, I did not observe light-evoked responses in STCs from animals sacrificed at 3 and 4 dpi MMZ/Dox (n = 0/3 and 0/10 responsive cells, respectively). By 5 dpi MMZ/dox, however, I observed evidence for monosynaptic input onto one STC (n = 1/13 responsive cells) following photoactivation of Gγ8-ChIEF-Citrine-expressing axons (Figure 11A). Gγ8-ChIEF-Citrine-expressing axons were also visible in a fixed electrophysiology OB slice from a Gγ8-ChIEF-Citrine mouse at 5 dpi MMZ/Dox (Figure 11B). The light-evoked response in the STC resembled those recorded in untreated Gγ8-ChIEF-Citrine mice, albeit with a larger onset jitter and longer time to peak (peak amplitude: -24.5 pA; onset latency: 1.7 ms; onset jitter: 2.7; time to peak: 17.0 ms; Figure 11C).

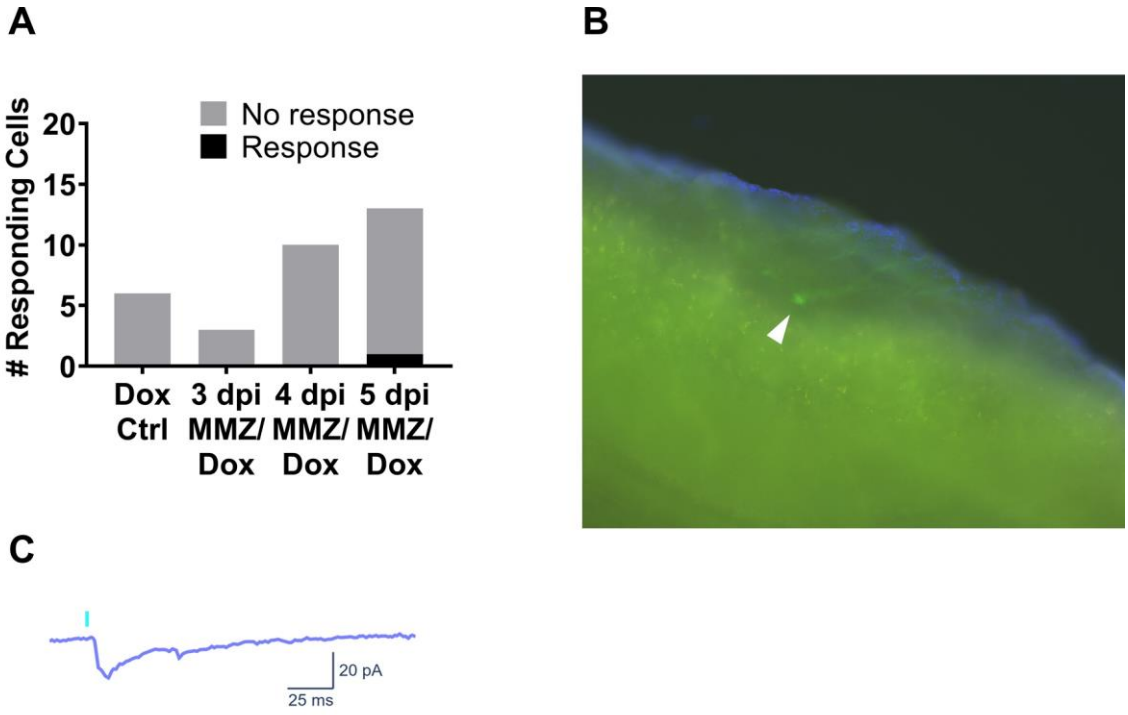

Figure 11. Newly regenerated immature OSN axons provide monosynaptic input to STCs.

A. Immature OSNs treated with MMZ and Dox food do not provide monosynaptic input onto recorded STCs until 5 dpi MMZ/Dox food (n = 6 cells from 1 Gγ8-ChIEF-Citrine mouse at 3 dpi MMZ and stayed on Dox food (Dox Ctrl), n = 3 cells from 1 Gγ8-ChIEF-Citrine mouse at 3 dpi MMZ/Dox, n = 10 cells from 2 Gγ8-ChIEF-Citrine mice at 4 dpi MMZ/Dox, and n = 13 cells from 3 Gγ8-ChIEF-Citrine mice at 5 dpi MMZ/Dox). **B.** Example of a Gγ8-ChIEF-Citrine-expressing axon in an OB slice from a Gγ8-ChIEF-Citrine mouse at 5 dpi MMZ/Dox, fixed after slice recording. Note that the axon is well within the glomerular layer. **C.** Example response from an STC elicited by 1 ms 100% intensity light pulse photoactivation of Gγ8-ChIEF-Citrine-expressing OSN axons at 5 dpi MMZ/Dox. Blue line: 1 ms light pulse photostimulation.

The low probability of recording from an STC with a light-evoked response in an animal sacrificed at 5 dpi MMZ/Dox was likely due to the sparsity of newly generated Gγ8-ChIEF-Citrine-expressing axons in the OB at that time point. Despite this sparsity, the possibility that the light-evoked response I observed was mediated by monosynaptic input onto STCs is supported by

previous behavioral work in our lab. At 3 dpi MMZ, all mice were unable to perform odor detection when assessed by the buried food task but showed recovery in odor detection ability by 5 dpi MMZ (Figure 12A-C). A two-choice odor detection assay also showed that mice failed to detect the food odorant at 3 dpi MMZ, but, as in the buried food assay, showed recovery of food detection by 5 dpi MMZ (Figure 12D, E). In both these tasks, mice showed improvement in olfactory detection from 5-7 dpi MMZ, suggesting that the mice were able to detect odors using only immature OSNs.

The ability for some mice to successfully perform odor detection at just 5 dpi MMZ necessitates that newly generated immature OSNs extend their axons into the OB and make monosynaptic connections with OB neurons. Thus, these data collectively demonstrate that newly generated immature OSNs are capable of forming functional synapses with STCs in the OB just five days after terminal cell division.

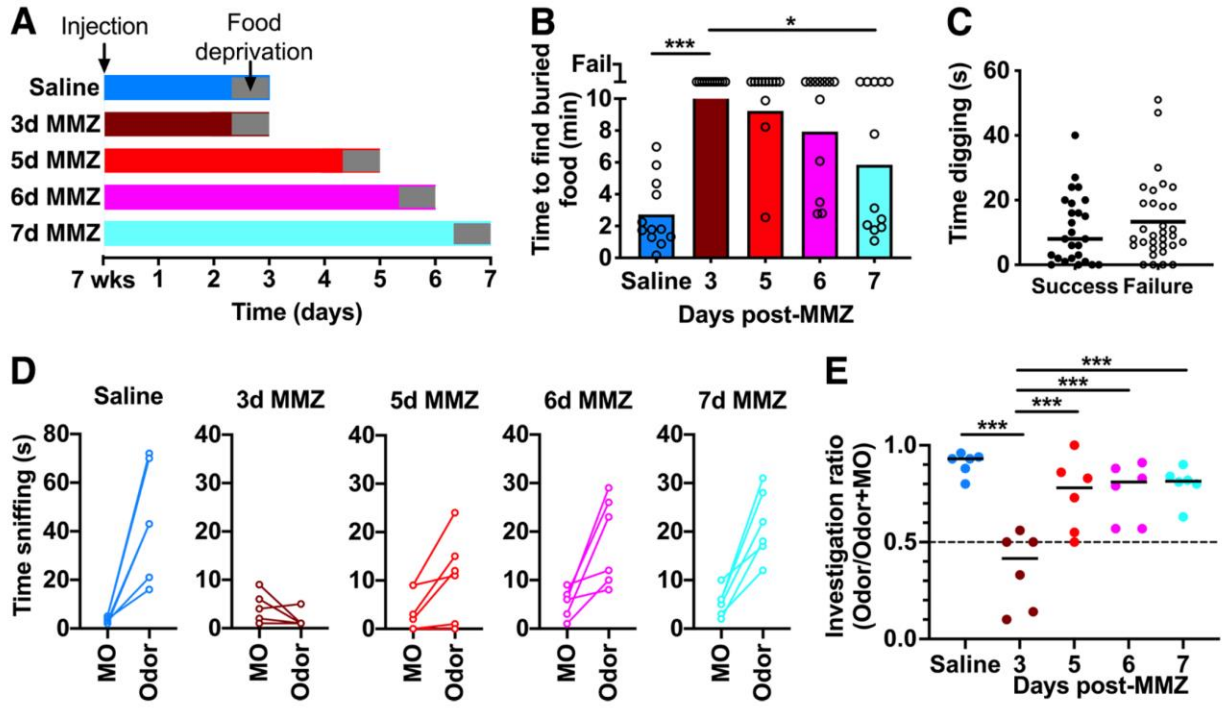

Figure 12. Mice show recovery of olfactory deficits starting at 5 dpi MMZ.

A. Experimental design for behavior assays. Mice received an i.p. injection of MMZ or saline and were food deprived for 16 h prior to beginning the behavior assays. **B.** All mice failed to detect the buried food at 3 days post-MMZ; food detection behavior then gradually improved with increasing time post-MMZ (One-way ANOVA on Ranks, $p < 0.001$, Kruskal-Wallis statistic = 31.6. Dunn's multiple comparisons tests, Saline, $p < 0.001$, Z = 5.10; 5d MMZ, $p > 0.99$, Z = 0.86; 6d MMZ, $p = 0.47$, Z = 1.56; 7d MMZ, $p = 0.017$, Z = 2.86; all vs. 3d MMZ, n = 12 per group). Bars: mean per group. Filled circles: values for individual mice. **C.** No difference between time spent digging during the 5 min acclimation period for mice that found the buried food (success) or failed to find the buried food (Mann-Whitney test, $p = 0.44$, U = 367, n = 58 mice). Lines: median. Circles: values for individual mice. **D.** Time spent sniffing mineral oil (MO) vs. Nutter Butter (Odor) for mice injected with saline or MMZ. MO and Odor values for individual mice are linked by solid lines. **E.** Investigation ratio is significantly higher in saline, 5d MMZ, 6d MMZ and 7d MMZ mice than in 3d MMZ mice (One-way ANOVA, $p < 0.001$, $F_{4,26} = 11.96$. Sidak's multiple comparisons test, Vs. saline: 3d MMZ, $p < 0.001$, t = 6.43; 5d MMZ, $p = 0.20$, t = 1.88; 6d MMZ, $p = 0.20$, t = 1.73; 7d MMZ, $p = 0.23$, t = 1.24. Vs. 3d MMZ: 5d MMZ, $p < 0.001$, t = 4.54; 6d MMZ, $p < 0.001$, t = 4.70; 7d MMZ, $p < 0.001$, t = 5.18). The data presented in this figure were collected and analyzed by Tenzin Kunkhyen, Alex Rangel, and Claire Cheetham.

2.3 Discussion

Here, I have shown that immature OSNs provide monosynaptic input onto OB neurons. By activating immature Gγ8-ChIEF-Citrine-expressing OSN axons and recording light-evoked EPSCs in STCs, I demonstrate that the input received by STCs from immature OSNs is similar to that from mature OSNs. I also restricted ChIEF-Citrine expression to only newly generated Gγ8 axons and show that these monosynaptic connections are formed within 5 days of the OSN's birth date. Together, these findings corroborate data from our previous *in vivo* study showing that photoactivation of immature OSNs elicits firing of neurons in multiple OB layers (Cheetham et al., 2016).

2.3.1 Immature OSNs provide direct monosynaptic input to STCs.

My goal in this study was to determine whether immature OSNs provide monosynaptic input to OB neurons. In order to address this question, I chose to record from STCs (Figure 3), which reside at the border between the glomerular layer (GL) and the external plexiform layer (EPL), and are known to receive monosynaptic input from mature OSNs (Sun et al., 2020). STCs are less specialized than ETCs and more closely resemble the classic category of middle TCs (mTCs) that function as OB output neurons (De Saint Jan et al., 2009; Griff et al., 2008; Hayar et al., 2004a; Hayar et al., 2004b; Jones et al., 2020). Compared to mTCS, however, STCs are easier to identify and more homogeneous as a population than mTCs, whose cell bodies are scattered sparsely throughout the EPL (Nagayama et al., 2014; Shepherd, 2004b). As a practical consideration, the apical dendrites of STCs are also more likely to be intact following slicing than those of deeper TCs.

The light-evoked responses I observed in STCs following photoactivation of Gγ8-ChIEF-Citrine-expressing OSN axons are characteristic of monosynaptic responses (Figure 6). Light-evoked EPSCs showed onset latencies of less than 2 ms with low trial-to-trial jitter, which is consistent with previously reported monosynaptic mature OSN input to STCs (Sun et al., 2020).

I also observed that the presence of a visualized apical dendrite did not guarantee monosynaptic input from photoactivated mature or immature OSNs (Figure 5C). Aside from the obvious explanation that perhaps the recorded STC was not connected to a ChIEF-Citrine-expressing OSN, the lack of a light-evoked response could also be explained by the subtypes of STCs I recorded from. For example, vasopressin-expressing STCs do not show excitatory input following electrical olfactory nerve stimulation (Lukas et al., 2019). Although I did not distinguish between the possible subtypes of STCs included in my dataset, it is plausible that some non-responsive cells belonged to a physiologically distinct group from the responsive cells. The inability to visualize apical dendrites/tufts in some responsive cells may be explained by their apical dendrites running deep within the slice. Indeed, I observed oscillatory resting membrane potentials in many of the cells, which is correlated with intact apical dendrites (Figure 3B) (Carlson et al., 2000; Hayar et al., 2005; Schoppa and Westbrook, 2001).

2.3.2 Degenerating OSN axons are capable of neurotransmitter release.

After demonstrating that immature OSNs form monosynaptic connections with STCs, I wanted to investigate whether these connections were formed within a certain time window after terminal cell division. My initial strategy consisted of first ablating all OSNs in the OE using MMZ, then performing slice recording experiments at various time points after MMZ injection. Intraperitoneal injection of MMZ results in almost total loss of all OSNs in the OE, with less than

0.2% of OSNs remaining (Figure 8A) (Blanco-Hernández et al., 2012; Kikuta et al., 2015; Tsai and Barnea, 2014). Given our previous histological analysis of animals injected with MMZ (Figure 7), I was surprised to observe light-evoked responses at time points at which there should be no newly generated ChIEF-Citrine-expressing axons present in the OB (Figure 8).

The most logical explanation for the light-evoked responses that I observed in these animals is that the degenerating axons of MMZ-ablated ChIEF-Citrine-expressing OSNs are still capable of neurotransmitter release. OSN axons are slow to degenerate following MMZ treatment; a high density of degenerating immature OSN axons remain in the OB up to 5-7 days post-MMZ (Blanco-Hernández et al., 2012; Kikuta et al., 2015; Tsai and Barnea, 2014). Beyond noting the presence of degenerating axons, however, previous studies using MMZ do not characterize or identify release from degenerating axons. The response kinetics evoked by activating these putative degenerating Gγ8-ChIEF-Citrine-expressing axons were similar to those evoked by activating healthy Gγ8-ChIEF-Citrine-expressing axons from untreated mice (Figure 9). To my knowledge, there are few or no physiological studies characterizing neurotransmitter release from degenerating synapses or axons; most studies are found within the field of neurodegeneration or spinal injury and describe the cellular and anatomical changes occurring in synaptic degeneration (Gillingwater and Ribchester, 2001; Neukomm and Freeman, 2014; Pemberton et al., 2020).

Beyond the immediate relevance to my study, neurotransmitter release mediated by degenerating axons also bears significant consequences. Optogenetic stimulation of acutely severed axons in slices is widely used to look at long-distance inputs to neurons (Boyd et al., 2012; Markopoulos et al., 2012), and it is assumed that acutely severed axons are sufficiently similar to intact axons such that release from severed axons can provide insight into release from intact axons under physiological conditions. This assumption is difficult to test due to the nature of slice

electrophysiology experiments. In the OB slice electrophysiology experiments described in this chapter, the degenerating axons mediating release have already lost their somata several days ago due to MMZ treatment and are thus already severed, in a sense, prior to being cut during tissue slicing for slice electrophysiology. Release from degenerating axons in an OB slice could be affected by both the initial loss of these axons' somata and by the subsequent severance during tissue slicing.

Physiological characterization of degenerating axons would also be complicated by the fact that most studies of synaptic transmission involve presynaptic manipulations and postsynaptic response measurements, and there are likely limitations to how degenerating axons can be manipulated. It would be interesting in the context of this study to characterize the time course of axonal release mediated by degenerating axons. To do this, I could administer Dox food to an OMP-ChIEF-Citrine mouse starting at P7 and inject the mouse with MMZ to ablate OSN somata in the OE. The mouse would be maintained on Dox food until time of sacrifice to suppress ChIEF-Citrine expression in newly generated OSN axons; only OSNs axons that were generated before P7 and whose somata were ablated with MMZ treatment would express ChIEF-Citrine. I could then record light-evoked responses in these OMP-ChIEF-Citrine mice and see when the responses begin to disappear over time.

2.3.3 Newly generated immature OSNs form monosynaptic connections with STCs.

In order to restrict ChIEF-Citrine expression to only newly generated Gγ8-ChIEF-Citrine OSN axons, I revised my experimental design to incorporate the use of Dox food. Administration of Dox food prior to MMZ injection ensured that ChIEF-Citrine expression was suppressed in OSNs existing prior to MMZ ablation, and replacement of Dox food with normal chow after MMZ

injection allowed ChIEF-Citrine to be expressed in only newly generated immature OSNs (Figure 10A). This enabled me to selectively activate only newly generated Gγ8-ChIEF-Citrine OSN axons without the confounding contribution of ChIEF-Citrine expression in degenerating Gγ8-ChIEF-Citrine axons. I observed a light-evoked response in one STC at 5 dpi MMZ/Dox (Figure 11), suggesting that immature OSNs are capable of providing monosynaptic input onto STCs just 5 days after terminal cell division. This finding is corroborated by previous behavioral data from our lab showing partial recovery of odor detection behavior by 5 dpi MMZ (Figure 12).

Ample evidence exists for immature OSNs to be functional. Both $GAP43^{+}$ and $G\gamma8^{+}$ OSNs express ORs before reaching maturity. The P2 OR is expressed well before the downregulation of GAP43 (Iwema and Schwob, 2003), and mRNA transcripts for multiple ORs are expressed in immature OSNs (Hanchate et al., 2015; Tan et al., 2015). Additionally, immature OSNs also express some proteins involved in the signal transduction of odor molecules (Hanchate et al., 2015; Nickell et al., 2012). Transmission electron microscopy also shows that Gγ8-expressing axons have boutons that contain presynaptic vesicles and are structurally similar to those found on OMP-expressing axons, and synaptophysin is present in immature OSNs at five days after terminal cell division, suggesting that immature OSN axons can form axodendritic synapses with OB neurons (Cheetham et al., 2016; Marcucci et al., 2011).

Together, my data provide evidence that immature OSNs form functional monosynaptic connections with STCs in the OB, and that these connections are formed as early as five days after an OSN's terminal cell division. Although beyond the scope of this study, it would be interesting to catalog the different types of OB cell types that receive monosynaptic inputs from immature OSNs and whether those types differ from cell types that receive input from mature OSNs. Future directions could also include more extensive characterization of the properties of immature OSNs,

such as release probability (Murphy et al., 2004) and the presynaptic inhibition received from periglomerular cells or short axon cells (Kiyokage et al., 2010; McGann, 2013; Shao et al., 2009), and how these properties could vary with OSN developmental timeline. Increased understanding of immature OSNs would provide valuable insights into the role they play in regeneration as well as olfactory processing alongside their mature counterparts.

2.4 Materials and Methods

2.4.1 Experimental design and animals

All animal procedures were in compliance with guidelines established by the Institutional Animal Care and Use Committee at the University of Pittsburgh. Genotypes of mice used were Gγ8-ChIEF-Citrine [Gγ8-tTA$^{+/-}$;tetO-ChIEF-Citrine$^{+/-}$] or OMP-ChIEF-Citrine [OMP-tTA$^{+/-}$;tetO-ChIEF-Citrine$^{+/-}$]. Generation of the Gγ8-tTA (Nguyen et al., 2007), OMP-IRES-tTA (Yu et al., 2004), and tetO-ChIEF-Citrine (Cheetham et al., 2016) mice have been described previously.

2.4.2 Slice electrophysiology

For non-MMZ-treated data sets (Figures 2-6), P18-25 Gγ8-ChIEF-Citrine (n = 5) and OMP-ChIEF-Citrine (n = 10) mice were deeply anesthetized with isoflurane and decapitated into ice-cold oxygenated artificial cerebrospinal fluid (ACSF). The olfactory bulbs (OB) were dissected, and horizontal slices (310 μm thick) were prepared using a vibratome (Ci 5000 mz2; Campden Instruments). Slices recovered in ACSF at 35°C for 20 min. ACSF contained (in mM):

125 NaCl, 25 glucose, 2.5 KCl, 25 $NaHCO_3$, 1.25 NaH_2PO_4, 1 $MgCl_2$, and 2.5 $CaCl_2$, pH 7.4. Slices were then incubated in ACSF at room temperature until recording. Slices were continuously superfused in ACSF at 35°C while recording. Current clamp and voltage clamp recordings were made using electrodes filled with (in mM): 120 K-gluconate, 2 KCl, 10 HEPES, 10 Na-phosphocreatine, 4 Mg-ATP, 0.3 Na_3GTP, 0.2 EGTA and 0.025 Alexa Fluor 594.

Whole-cell patch-clamp recordings were made using a Multiclamp 700A amplifier (Molecular Devices) and an ITC-18 acquisition board (Instrutech) controlled by Igor Pro (WaveMetrics). STCs were identified under an upright microscope (SliceScope, Scientifica) with IR-DIC by their shape and location in OB laminae. Their identity was confirmed by visualization of AF594-filled lateral dendrites and/or spike patterns characteristic of STCs (Figure 3A, C) (Antal et al., 2006; Sun et al., 2020). STCs close to glomeruli innervated by ChIEF-Citrine-expressing OSN axons were selected for recording. Pharmacological agents used were the NMDA receptor antagonist DL-2-amino-5-phosphonovaleric acid (APV, 20 mM), and the AMPA receptor antagonist 2,3-dihydroxy-6-nitro-7-sulfamoyl-benzo(F)quinoxaline (NBQX, 10 mM). Cells were excluded from analysis if their resting membrane potential was depolarized above -45 mV.

2.4.3 Optogenetic stimulation

At least 10 minutes elapsed between cell selection and the start of photoactivation experiments. For photoactivation of immature or mature OSN axons, slices were illuminated using a 490 nm CoolLED (pe-100; CoolLED Ltd) passed through a 40x/0.8NA water-immersion objective (Olympus) centered on the GL. An open field stop was used to enable multiglomerular activation. Light evoked EPSCs were isolated in the presence of APV. I generated a power curve for each STC by systematically increasing the LED intensity (from 10 to 20, 50, 80 and 100 %)

for each of three light stimulus durations (0.25, 1 and 2 ms) (Figure 4).10 trials per stimulus condition were recorded for each cell. NBQX was applied at the end of a subset of recordings to confirm that the recorded responses were AMPA-mediated.

2.4.4 Electrophysiology data analysis

For analysis of my recordings, I selected the shortest stimulus (1 ms at 100 % intensity) that reliably and consistently evoked responses and used data from these trials for all subsequent analysis. For each recording, the mean baseline over a 350 ms window before stimulus onset was subtracted from the recorded current trace. EPSC peak amplitude was defined as the most negative value of the baseline-subtracted current trace in a 250 ms window after stimulus onset for each trial. The response onset latency was defined as the time interval from optogenetic stimulus onset to the time at which the current trace reaches 5% of its peak value. Jitter was calculated by taking the standard deviation of the onset latencies of all trials collected using the same stimulus parameters (Diez et al., 2019). The time to peak was defined as the interval of time from response onset to the time of the EPSC peak.

A cell was classified as having a response if the EPSC peak amplitude exceeded three standard deviations of the pre-stimulus baseline current. Only STCs showing responses with an onset latency shorter than 2 ms were defined as receiving monosynaptic input from OSN axons (Sun et al., 2020; Vaaga and Westbrook, 2016). In the dataset from Gγ8-ChIEF-Citrine mice, one STC showed consistent light-evoked monosynaptic responses, but its power curve was incomplete and lacked response sweeps for the 100% intensity and 1 ms duration stimulus parameter. Therefore, I included this cell in the response counts but not in the amplitude and kinetic analysis due to stimulus parameter mismatch.

2.4.5 Methimazole ablation of olfactory sensory neurons for electrophysiology experiments

P23-27 Gγ8-ChIEF-Citrine (n = 13) and OMP-ChIEF-Citrine (n = 3) mice received a single intraperitoneal injection of methimazole (MMZ; 75 mg/kg in sterile saline). Animals were weighed each day after injection to ensure normal growth and health. At 3-5 dpi, mice were deeply anesthetized with isoflurane and transcardial perfusion was performed with ice-cold oxygenated Ringer solution containing the following (in mM): 125 NaCl, 25 glucose, 2.5 KCl, 25 $NaHCO_3$, 1.25 NaH_2PO_4, 3 $MgCl_2$, and 1 $CaCl_2$, pH 7.4. Slices were then transferred to ACSF at 35°C for 20 min. The Ringer solution used for recovery and recording was identical to that used for perfusion and slicing except with lower $MgCl_2$, (1 mM) and higher $CaCl_2$ (2.5 mM) concentrations. Whole-cell patch-clamp recording and optogenetic stimulation were performed as described previously.

2.4.6 Dox food administration

The normal diet of Gγ8-ChIEF-Citrine mice was replaced with mouse chow formulated with 200 mg/kg doxycycline (Dox food) (Bio-Serv) once the pups reached the age of P7. Upon weaning, mice were still given the doxycycline-supplemented diet until receiving MMZ injections. With the exception of control mice that remained on Dox food until time of sacrifice, six hours after each mouse received the MMZ injection, Dox food was replaced with normal diet until time of sacrifice.

2.4.7 Perfusion, immunohistochemistry, and image analysis

Mice were anesthetized with either 200 mg/kg ketamine and 20 mg/kg xylazine or 5 % isoflurane in 1 l/min O_2. Transcardial perfusion, preparation and immunohistochemical staining of OB and OE sections were performed as described previously (Cheetham et al., 2016). All sections were mounted with Vectashield containing DAPI (Vector Labs).

Citrine fluorescence was quantified for 3 OB sections per mouse (left and right OBs at 25%, 50% and 75% along the anterior-posterior axis) for Gγ8-ChIEF-Citrine and OMP-ChIEF-Citrine mice (n = 3 per group). Images (pixel size 0.64 mm) of entire sections were collected using an Eclipse 90i large area-scanning widefield microscope equipped with a Plan-Apo 10x/ 0.45NA air objective and Elements software (Nikon). Camera settings were the same for all images. Total integrated fluorescence intensity in the Citrine channel was normalized to the area of the GL for each section using Fiji.

For histological analysis in MMZ- and saline-injected mice, OE sections (3 per antibody per mouse at 25%, 50% and 75% along the anterior-posterior axis) were stained for GAP43 as a marker of immature OSNs (anti-GAP43 primary antibody, 1:1000 for 48 h at 4 °C, NB300-143, Novus Biologicals; donkey anti-rabbit-Alexa Fluor 546 secondary antibody, 1:500 for 1 h at room temperature), or OMP (anti-OMP primary antibody, 1:5000, 96 h at 4 °C, catalog #544-10001, Wako Chemicals; donkey anti-goat-Alexa Fluor 546 secondary antibody, 1:500, 1 h at room temperature) as a marker of mature OSNs. 2-photon z-stacks of ~1 mm of the dorsal septal OE were collected using the Bergamo system with 2-photon excitation at 800 nm. Image analysis was performed in Fiji. OE width (from the basal lamina to the apical surface) was measured at 3 different locations each on the left and right sides of the OE and averaged for each section. The grand mean width for the three sections per mouse was then calculated. $GAP43^+$ and OMP^+ OSNs

were counted in each image, and the mean value expressed as linear density (cells per mm) was calculated for each mouse. Widefield fluorescence images of turbinates were collected using a Revolve widefield microscope equipped with an Olympus Plan-Apo 20x/ 0.80NA air objective and Echo software (Echo).

2.4.8 Odor detection and discrimination assays

A buried food assay (Yang and Crawley, 2009) and two-choice odor detection assay (Pankevich et al., 2004) were used to test odor detection. Mice were transported to the behavioral testing room at least 30 min prior to commencing the assay(s). All trials were videoed.

8-week-old C57BL/6J mice performed the buried food assay (12 mice per group, injected with MMZ or saline 3 – 7 d prior to testing). Protocols were based on a previously published method (Yang and Crawley, 2009), with some refinements. Mice were food deprived for 16 h prior to the assays. Videos were collected from two angles for analysis. Each mouse that performed the buried food assay received a single Froot Loop (Kellogg's) for odorant familiarization at the start of food deprivation. All mice consumed this Froot Loop. For the buried food assay each mouse had 5 min to acclimate to the test cage, which contained a 1.5 cm depth of Sani-Chips bedding (P.J. Murphy). Time digging during this 5 min session was quantified from videos. The mouse was then briefly removed, a Froot Loop was buried near the center of the cage, and the mouse was returned to the test cage. The time to locate the buried Froot Loop was then measured; mice failed the task if they had not located the buried food within 10 min.

A separate group of 8-week-old C57BL/6J mice performed the two-choice odor detection assay (6 mice per group). Male and female mice were housed in groups of three. For two consecutive days, each mouse was transferred to a clean cage and given 1.5 g Nutter Butter cookie

(Nabisco). Mice were returned to their home cage once they had eaten the cookie. The next day, mice received a saline or MMZ injection. Mice were food deprived for 16 hours prior to testing, which occurred 3 – 7 d after saline or MMZ injection. Each mouse was transferred to a test cage and given 10 min to acclimate. Mice then had 10 minutes to investigate filter paper squares odorized with mineral oil (MO) or Nutter Butter cookie suspended in mineral oil (Odor). Mice could not make direct contact with the filter paper squares. The total time spent sniffing each filter paper square was scored manually from videos. Investigation ratio was calculated as the time spent sniffing Odor divided by the total time spent sniffing Odor plus MO, i.e., a value of 0.5 indicates no odor detection. An investigation ratio of 0.75 (i.e., duration sniffing Odor was three times that of sniffing MO) was defined as indicating significant odor detection.

2.4.9 Statistical analyses

Electrophysiological recordings were analyzed using custom scripts written in Python. All statistical analyses were performed using Prism 9 (GraphPad). Fisher's exact test was used to compare proportions of responding neurons. Mann-Whitney rank sum tests were used to compare two groups, whereas one-way ANOVA on Ranks with Dunn's multiple comparisons were used to compare multiple groups. Data are reported as median (IQR) in the text.

Table 1 Key Resources

Reagent or Resource	Source	Identifier
Goat polyclonal anti-olfactory marker protein	Wako Chemicals	#544-10001 RRID:AB_664696
Rabbit polyclonal anti-GAP43	Novus Biologicals	NB300-143 RRID:AB_10001196
Donkey anti-goat IgG (H+L) Alexa Fluor 546 conjugated	Thermo Fisher Scientific	A11056 RRID:AB_142628
Donkey anti-rabbit IgG (H+L) Alexa Fluor 546 conjugated	Thermo Fisher Scientific	A10040 RRID:AB_2534016
Donkey anti-rabbit IgG (H+L) Alexa Fluor 647 conjugated	Thermo Fisher Scientific	A31573 RRID:AB_2536183
GFP-Booster-Atto-488	Chromotek	gba-488-100 RRID:AB_2631386
VECTASHIELD Antifade Mounting Medium with DAPI	Vector Labs	H-1200
Methimazole	Millipore Sigma	M8506-25G CAS: 60-56-0
Mouse: OMP-IRES-tTA B6;129-Omptm1(tTA)Gogo/J	The Jackson Laboratory	JAX:017754, RRID:IMSR_JAX:017754
Mouse: tetO-ChIEF-Citrine	(Cheetham et al., 2016)	N/A
Mouse: Gg8-tTA	(Nguyen et al., 2007)	N/A
Primers for Gg8-tTA, OMP-IRES-tTA, tetO-ChIEF-Citrine	(Cheetham et al., 2016)	N/A
Fiji	(Schindelin et al., 2012)	https://imagej.net/Fiji
Python	Python 3.8 Pyzo	https://python.org https://pyzo.org
Prism	GraphPad	
Nikon Elements	Nikon	
ThorImage	ThorLabs	
Igor Pro	Wavemetrics	
Echo	Echo	

3.0 Chapter 3: Early and Late Postnatal-Born Granule Cells Show Differential Functional Connectivity with Mitral and Tufted Cells

3.1 Introduction

In rodents, about 30,000 to 80,000 subventricular zone (SVZ)-derived neuroblasts arrive in the olfactory bulb (OB) daily; 95% percent of these neuroblasts differentiate into olfactory granule cells (GCs), and the remaining differentiate into periglomerular cells (PGCs) and other cell juxtaglomerular cell types (Alvarez-Buylla et al., 2001; Belluzzi et al., 2003; Kaplan et al., 1985; Lledo and Saghatelyan, 2005). About 50% of postnatal-born GCs are lost within four weeks; the surviving GCs mature and integrate into the preexisting circuitry (Mouret et al., 2009; Petreanu and Alvarez-Buylla, 2002; Yamaguchi and Mori, 2005). The cell bodies of GCs born in the prenatal and early postnatal periods (P3-7) occupy more superficial regions of the granule cell layer (GCL) and those born in the later postnatal period (P14-60) occupy the deeper regions (Lemasson et al., 2005). The morphological differences of GCs based on which GCL regions they occupy are well-established: the dendrites of deeper GCs are found in the deeper regions of the external plexiform layer (EPL), and those of superficial GCs are found in more superficial regions of the EPL (Mori et al., 1983; Orona et al., 1983). Therefore, the dendrites of GCs born early in life will tend to be found in the more superficial regions of the EPL, whereas those of GCs born later will predominantly be found in the deeper portions of the EPL.

Olfactory GCs form dendrodendritic synapses with mitral cells (MCs) and tufted cells (TCs), whose secondary dendrites travel in the EPL (Isaacson and Strowbridge, 1998; Mori et al., 1983). At these synapses, GCs are excited via glutamatergic input from MCs and TCs and in return

provide GABAergic inhibition back onto the principal neurons (Pressler and Strowbridge, 2020; Schoppa et al., 1998). Early anatomical work indicates that TC cell bodies can be found throughout the EPL, with their secondary dendrites occupying the middle and superficial regions of the EPL. In contrast, MC cell bodies are only found in the mitral cell layer (MCL), and the majority of their dendrites are found in the deeper EPL (Orona et al., 1984).

Differential connectivity with GC subpopulations may explain the differences in how MCs and TCs encode odor information (Ezeh et al., 1993; Griff et al., 2008). Compared to MCs, TCs receive stronger monosynaptic excitatory input from OSNs (Burton and Urban, 2014; Gire et al., 2012; Kikuta et al., 2013). In response to odor presentation and OSN stimulation, TCs display higher firing rates than MCs (Nagayama et al., 2014). Our lab has demonstrated that the much higher intrinsic excitability of TCs is a strong predictor of their higher OSN-evoked firing rates (Burton and Urban, 2014). Additionally, odor-evoked activity of TCs and not MCs is correlated with that of OSN inputs, suggesting that odor response maps are transformed differently by the two cell types (Adam et al., 2014).

In response to odor presentation, TCs respond with a shorter latency and lower concentration threshold compared to MCs (Igarashi et al., 2012; Kikuta et al., 2013). Interestingly, odor-evoked responses in MCs were subject to lateral inhibition when the odorant was mixed with another odorant that activated a nearby glomeruli. Lateral inhibition was not observed in the odor responses of TCs, however (Nagayama et al., 2014). This observation is supported by work from our lab showing that MCs receive stronger lateral inhibition than TCs (Geramita et al., 2016). Both MCs and TCs exhibit subthreshold membrane oscillations that are coupled with the animal's sniff cycles, but they are locked to different phases: TCs are locked to the exhalation phase, whereas MCs are locked, with a delay, to the inhalation phase. Increasing the odor concentration causes

TCs to increase their odor-evoked firing rates, whereas MCs show phase advancement. Inhibition onto MCs is responsible for the delay in their phase lock (Fukunaga et al., 2012). As a population, TCs show greater subthreshold resonance, which results in strong synchrony among TCs in both the fast and slow gamma frequencies; MC synchrony, however, is weak and restricted to the slow gamma frequencies (Burton and Urban, 2021).

If different subtypes of GCs mediate inhibition at different depths of a single glomerular microcircuit, then the representation of the odor signal could be different at each layer depending on connectivity with MCs or TCs. Different components of the odor signal would be processed and sent to different cortical areas for further processing (Fukunaga et al., 2012; Kikuta et al., 2013; Nagayama et al., 2010; Nagayama et al., 2004). This possibility is supported by the fact that the projection targets of MCs and TCs are also spatially segregated, with TC axons projecting to the anterior olfactory nucleus (AON) and the anterior piriform cortex (PCx), and MC axons projecting to all areas of the olfactory cortex (Igarashi et al., 2012; Nagayama et al., 2014). The two segregated projection pathways from MCs and TCs could represent parallel processing streams that provide different components of the odor signal to higher cortical areas. Given the differences in odor-evoked responses between the two cell types, TCs may be primarily used in coarse olfactory behaviors requiring speed and fast reaction times, whereas MCs could be recruited later for more difficult olfactory discrimination or decision tasks (Nagayama et al., 2014).

This anatomical segregation of MC and TC dendrites and of deep vs. superficial GCs in the EPL suggests that different populations of GCs may form different preferential contacts with either MC or TC dendrites. It is thus plausible that early postnatal-born GCs preferentially form synapses with TCs, whereas later postnatal-born GCs preferentially form synapses with MCs. A direct link between subpopulations of postnatal-born GCs and their differential connectivity with

MCs and TCs has yet to be established. Here, I selectively label and activate an early postnatal-born (P2) subpopulation of GCs and a late postnatal-born (P14) subpopulation of GCs and assess the strength of their inhibition onto MCs and TCs. I find subtle differences in the strength of the inhibition from early and late postnatal-born GCs onto MCs and TCs.

3.2 Results

3.2.1 Timed viral injections label postnatal-born GC subpopulations with different birth dates

To label two subpopulations of postnatal-born GCs, one in the early postnatal period and one in the later postnatal period, I performed virus injections in two cohorts of mice at P2 and P14, respectively (Figure 13A, right). The adeno-associated virus AAV2-hSyn-hChR2(H134R)-EYFP was targeted into the rostral migratory stream (RMS) to transduce migrating neuroblasts (Figure 13A, left). Slice electrophysiology experiments were performed at four weeks post injection in both cohorts to allow neuroblasts to develop into mature GCs (Carleton et al., 2003; Petreanu and Alvarez-Buylla, 2002). This timeline ensured that the GCs activated by photostimulation in both P2- and P14-injected cohorts were of similar developmental age, despite differences in the animals' ages. Both P2 and P14 injections resulted in reliable expression of ChR2-EYFP in postnatal-born GCs in the olfactory bulb (OB) (Figure 13B). Transduced GCs displayed spiny branched dendrites that extended to the glomerular layer (GL). Consistent with previous work (Lemasson et al., 2005), I observed that the somata of $EYFP^+$ GCs tended to occupy more

superficial regions of the GCL in P2-injected animals, whereas they occupied deeper regions of the GCL in P14-injected animals (Figure 13C).

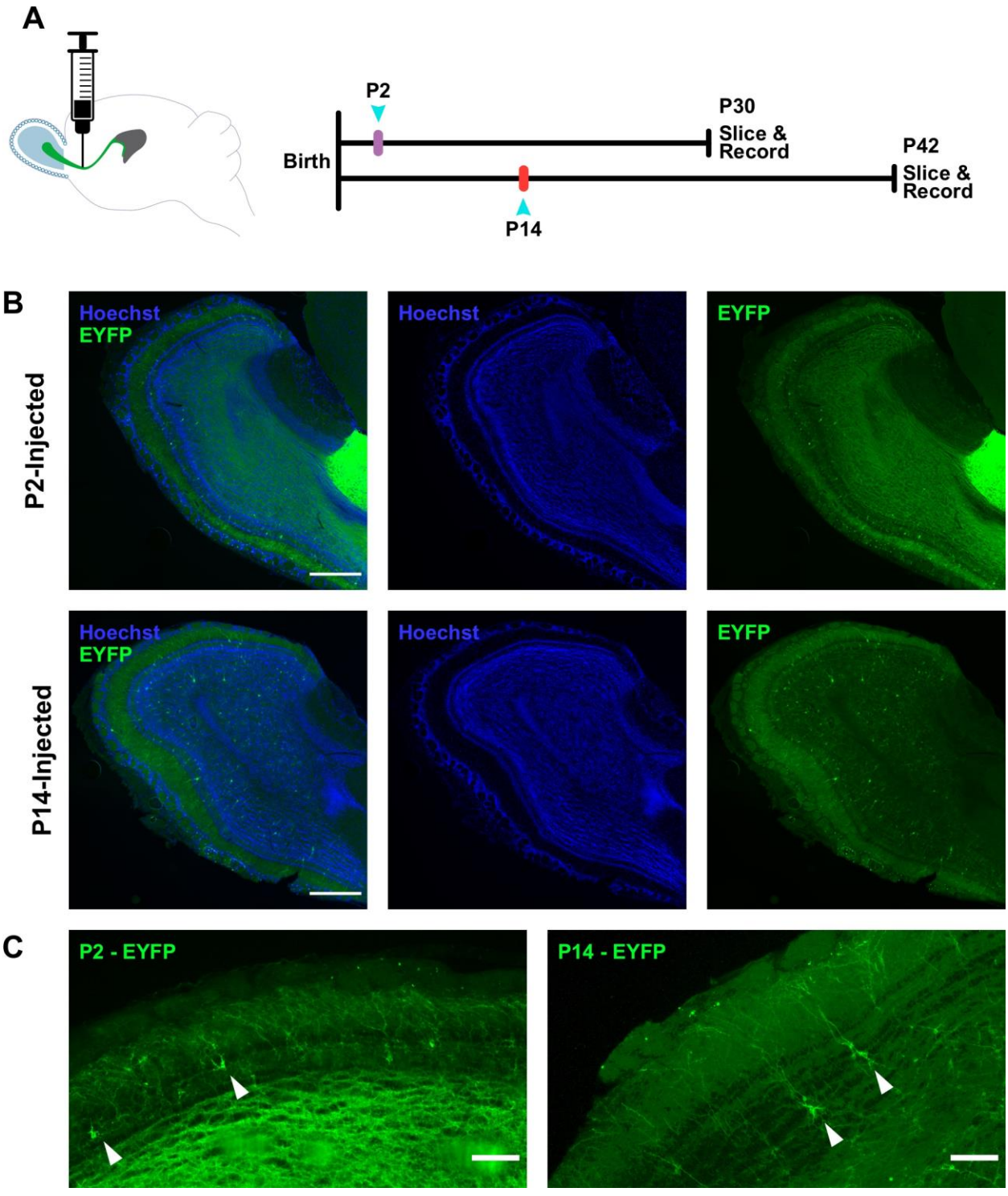

Figure 13. Timed virus injections label postnatal-born GC subpopulations with different birth dates.

A. Schematic of virus injection strategy (left) and timeline of virus injection and slice experiments for P2- and P14-injected cohorts. **B.** Example sagittal OB sections from a P2-injected mouse (top row) and P14-injected mouse (bottom

row). Scale bars: 500 μm. **C.** Closer view of superficial EYFP$^+$ GCs in a P2-injected mouse (left) and deeper EYFP$^+$ GCs in a P14-injected mouse (right). Scale bars: 200 μm.

3.2.2 Timed viral injections enable optogenetic activation of transduced postnatal-born GC subpopulations.

I next demonstrated that transduced postnatal-born GCs (Figure 14A) can be activated via photostimulation in slice electrophysiology. Photostimulation was performed using a 100 ms blue light pulse to mimic physiological sniff conditions (Geramita et al., 2016; Labarrera et al., 2013) while performing whole-cell voltage recordings from fluorescent GCs. Light pulses evoked spikes and photoactivated currents in EYFP$^+$ transduced GCs (P2: n = 1 cell, max firing rate = 80 Hz; P14: n = 1 cell, max firing rate = 30 Hz) (Figure 14B).

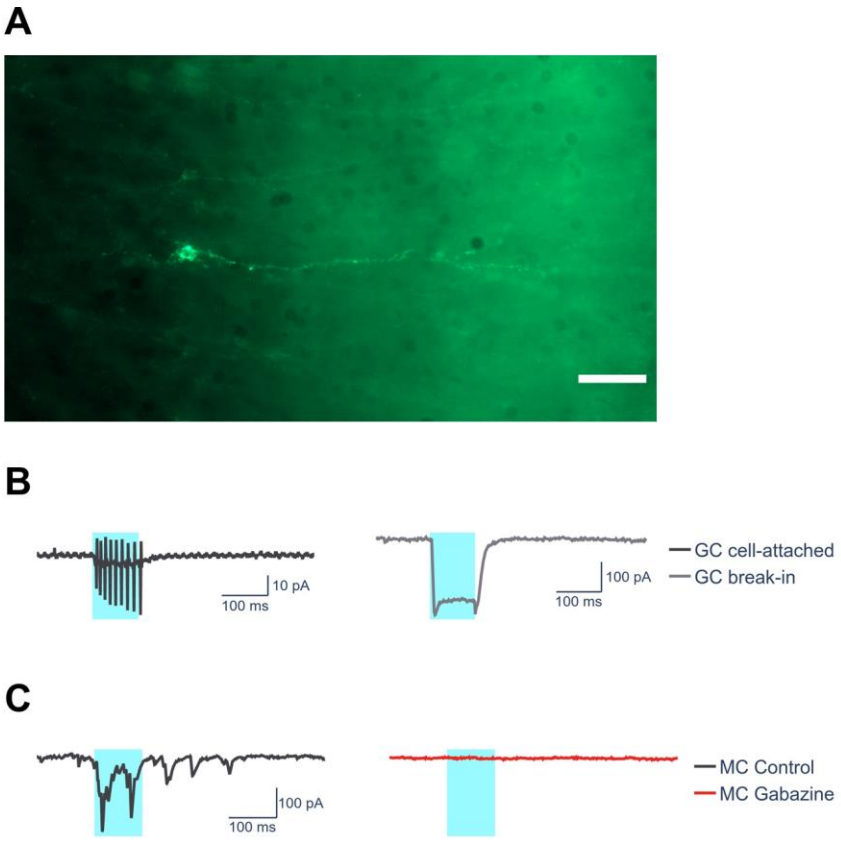

Figure 14. Virus injections enable optogenetic activation of transduced postnatal-born GCs.

A. Example of an EYFP^{+} transduced GC in a OB slice from a P14-injected animal, fixed after slice recording. Scale bar: 200 µm. **B.** Example cell-attached (left) and after break-in (right) recordings of an EYFP^{+} GC from a P2-injected animal during photostimulation. Blue rectangles: 100 ms light pulse photostimulation. **C.** Light stimulation evoked reliable IPSCs (left) in a MC from a P14-injected animal that were (right) abolished by bath application of 50 µM gabazine. Control recording solution included 20 µM APV and 10 µM NBQX.

I then tested whether I could observe GABAergic input from light-activated GCs in MCs and TCs, as has been observed previously (Bardy et al., 2010; Mandairon et al., 2018; Valley et al., 2013). I recorded MCs and TCs in P2- and P14-injected animals using a high-chloride internal. I held the cells at -70 mV while activating GCs using 100 ms light pulses and demonstrated light-evoked inward currents that were observable in the presence of APV (20 µM) and NBQX (10 µM)

but abolished by bath application of gabazine (50 μM) (Figure 14C), confirming the GABAergic nature of the light-evoked response. In both the MCs and TCs of the P2- and P14-injected cohorts, photoactivation of postnatal-born GCs resulted in IPSCs that were diverse in amplitude, frequency, and latency (Figure 15), suggestive of asynchronous release of GABA from GCs (Schoppa et al., 1998). Barrages of IPSCs, when present, also resembled IPSCs observed in MCs after glomerular stimulation, activation of lateral inhibition, or depolarizing local GC dendrites (Isaacson and Strowbridge, 1998). Together, these results showed that photostimulation of transduced postnatal-born GCs resulted in GABAergic inhibition onto MCs and TCs.

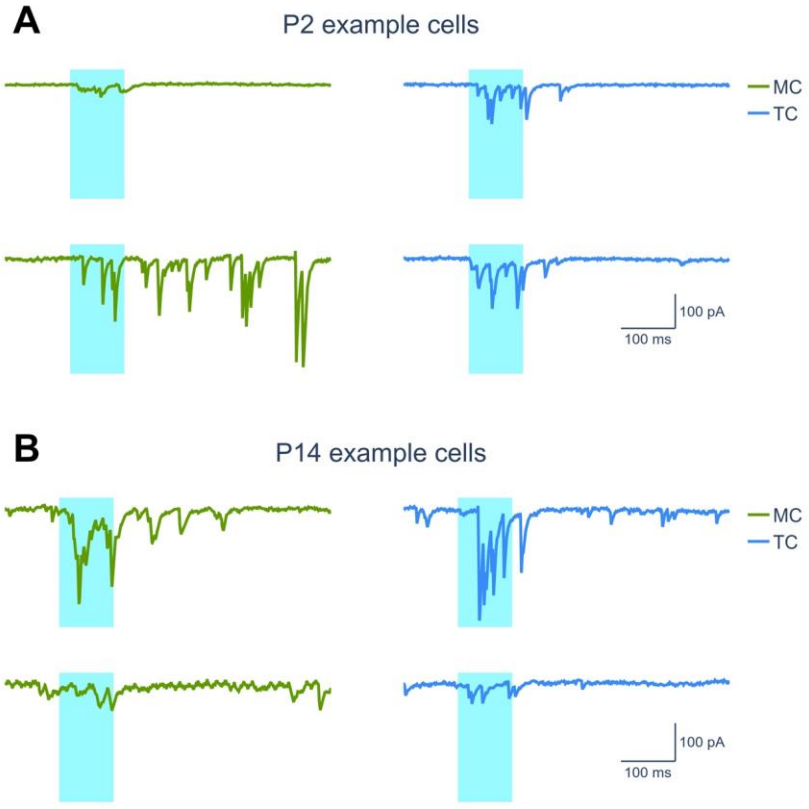

Figure 15. Examples of IPSCs evoked by optogenetic activation of postnatal-born GCs.

A. Example light-evoked IPSCs in MCs and TCs from P2-injected animals. **B.** Example light-evoked IPSCs in MCs and TCs from P14-injected animals. Blue rectangles: 100 ms light pulse photostimulation. Traces are individual trials.

3.2.3 The MC population receives greater overall inhibitory input from both P2- and P14-transduced GCs than does the TC population.

Having established that I can photoactivate GCs and that these cells then provide inhibitory input to MCs and TCs, I was interested in determining whether there were any differences in the photoactivated currents observed in MCs and TCs. I calculated the mean current traces from all the stimulation trials for each recorded cell and measured the peak amplitude of the mean current trace. The mean trace peak amplitudes of MCs and TCs recorded from the same slice did not show statistically significant correlations (Spearman rank-order test, P2: $r_s = 0.468$, $p = 0.091$; P14: $r_s = 0.468$, $p = 0.091$; Figure 16), which allowed me to pool cells from across different slices together into one dataset for each cell type per injection cohort.

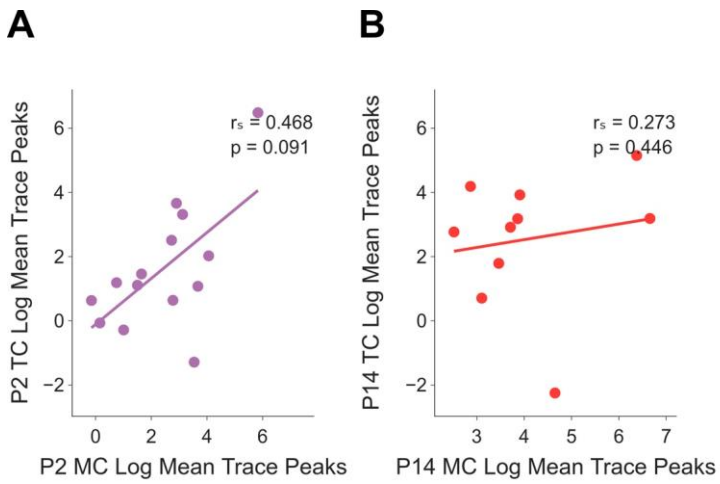

Figure 16. The mean current trace peak amplitudes of MCs and TCs recorded from the same slice are not correlated.

A. The average MC mean trace peak amplitude was not correlated with the average TC mean trace peak amplitude from the same slice in P2-injected animals (Spearman rank-order test, $r_s = 0.468$, $p = 0.091$; n = 23 MCs and 18 TCs from 16 slices and 8 animals). **B.** The average MC mean trace peak amplitude was not correlated with the average TC mean trace peak amplitude from the same slice in P14-injected animals (Spearman rank-order test, $r_s = 0.468$, $p = 0.091$; n = 21 MCs and 15 TCs from 10 slices and 7 animals).

I found that the peak amplitude of the mean traces of MCs was larger than that of TCs following activation of both P2- and P14-transduced GCs (P2: MC = -19.1 ± 5.5 pA, TC = -5.7 ± 1.3 pA, unpaired t-test, $p = 0.046$; P14: MC = -131.5 ± 47.7 pA, TC = -16.5 ± 8.8 pA; unpaired t-test, $p = 0.020$; values are reported as mean ± SEM; Figure 17). This result suggests that, on the whole, MCs receive greater inhibition from postnatal-born GCs compared to TCs.

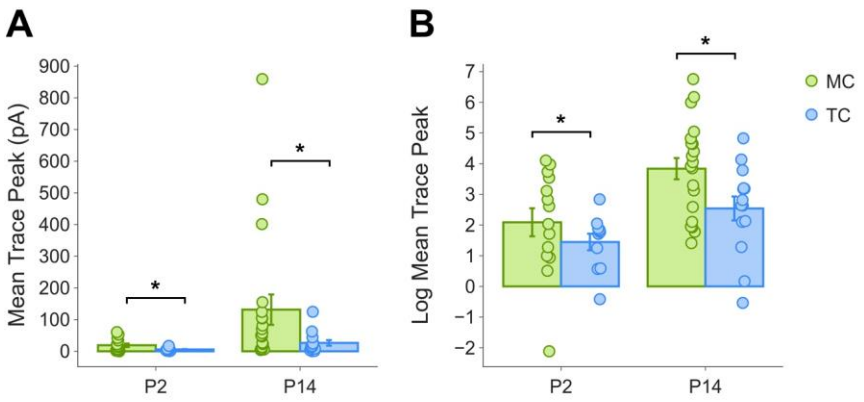

Figure 17. The mean current trace peak amplitude of MCs is higher than that of TCs.

A. The peak amplitude of mean current traces was higher in MCs than in TCs, for both P2- and P14-injected animals (P2: unpaired t-test on magnitudes, $p = 0.046$, n = 14 MCs and 11 TCs from 5 animals; P14: unpaired t-test on log-transformed magnitudes, $p = 0.020$, n = 20 MCs and 14 TCs from 7 animals). **B.** Plot of the log-transformed mean trace peak amplitudes shown in A. to display the spread of individual values. Bars: mean ± SEM, symbols: individual cells.

Next, I compared the mean current trace peak amplitudes between MCs and TCs recorded from the same slice for both cohorts (Figure 18A, B). In order to determine whether the average mean trace peak amplitude of MCs was larger than that of TCs from the same slice, I calculated the ratio of the average TC mean trace peak amplitude/the average MC mean trace peak amplitude and plotted the distribution of the ratios for both P2- and P14-injected cohorts (Figure 18C). The distribution of ratios in the P2-injected cohort showed a strong trend toward being smaller than 1, but the difference did not reach significance (P2: 0.67 (1.3); one-sample t-test on log-transformed ratios, $p = 0.060$; values are reported as median (IQR)). In P14-injected animals, however, the ratios were significantly smaller than 1 (P14: 0.32 (1.2); one-sample t-test on log-transformed ratios, $p < 0.001$; Figure 18C). I counted the number of MC-TC pairs in which the mean trace peak amplitude of the MC was larger than that of the MC and compared the proportion of those pairs

between the P2- and P14-injected cohorts. Although the proportion of MC-TC pairs with larger MC mean trace peak amplitudes was higher in the P14-injected cohort than the P2-injected cohort, the difference was not statistically significant (P2: MC > TC = 59.3%, P14: MC > TC = 70.6%, Fisher's exact test, $p = 0.422$; Figure 18D). Nevertheless, P14-transduced GCs provided stronger inhibition onto MCs than TCs as quantified by the mean trace peak amplitudes.

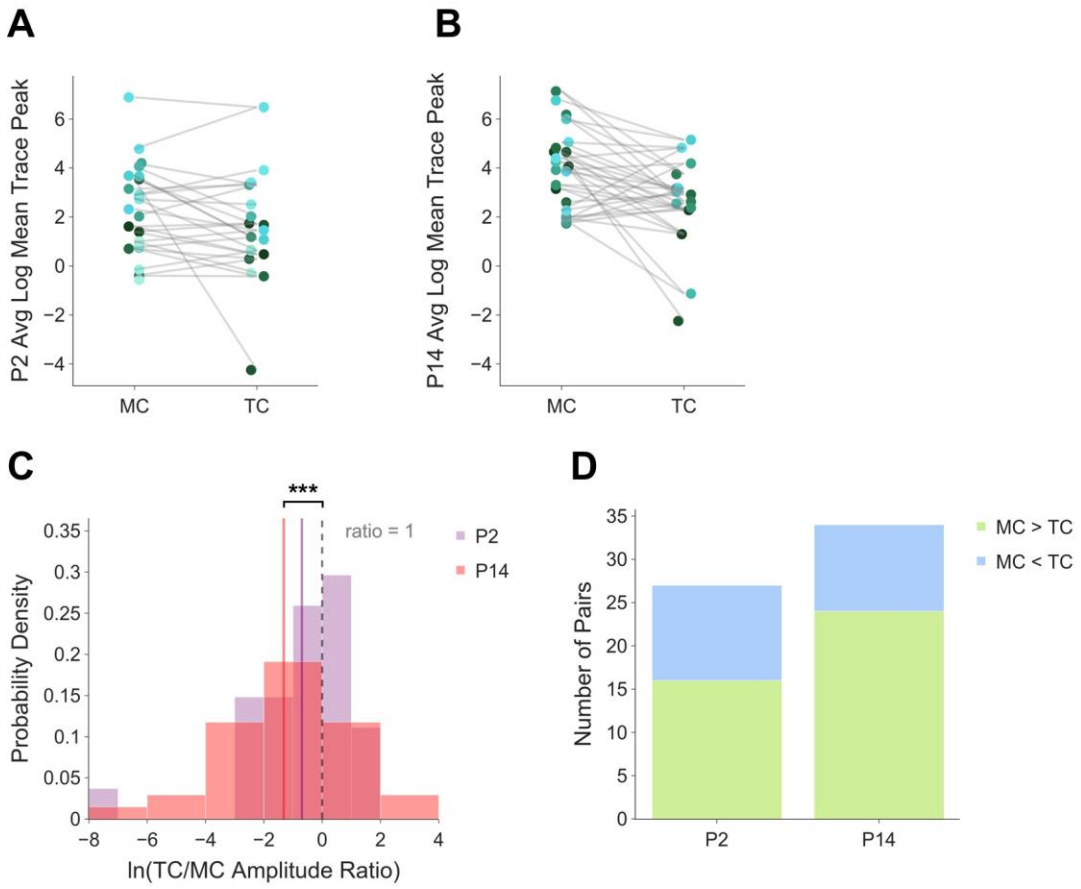

Figure 18. Within-slice comparisons for MC and TC mean current trace peak amplitude.

A. The average log-transformed peak amplitudes of mean current traces from MCs and TCs in P2-injected animals. Shades of blue represent individual slices, and lines connect MCs and TCs recorded from the same slice. **B.** The average log-transformed peak amplitudes of mean traces from MCs and TCs in P14-injected animals. **C.** The distribution of log-transformed TC/MC amplitude ratios from P2 and P14-injected animals. Dashed line represents TC/MC ratio = 1. Solid colored lines indicate mean ratios for each cohort. The ratios from P2-injected animals did not differ significantly from 1. The ratios from P14-injected animals were significantly less than 1. (One-sample t-tests on log-transformed ratios, P2: $p = 0.060$, P14: $p < 0.001$). **D.** The proportion of MC-TC pairs in which the MC mean trace peak amplitude was larger than that of the TC mean trace peak amplitude was not significantly different between the P2- and P14-injected animals (Fisher's exact test, $p = 0.422$). P2: n = 27 pairs from 14 slices and 8 animals; P14: n = 34 pairs from 10 slices and 7 animals.

3.2.4 The probability of a connection with P2- and P14-transduced GCs is not significantly different between MCs vs. TCs.

For subsequent analyses, I performed comparisons between cell types within the same injection cohort. Comparisons were not made between injection cohorts due to differences in P2 vs. P14 injection techniques, which may lead to differences in expression levels and introduce confounding variables in these comparisons (see Section 3.3.1). Moreover, the most direct method to address whether postnatal-born GCs born at a particular age make preferential connections with MCs or TCs is to compare inhibition in MCs vs. TCs following activation of postnatal-born GCs with the same birth date.

Following the initial analysis comparing the mean traces of all recorded cells in both P2- and P14-injected cohorts, I next compared only the inhibition received by MCs and TCs connected to either P2- or P14-transduced GCs. For each recorded cell, in addition to calculating the peak amplitude of the mean current trace (Figure 17, Figure 19A bottom), I calculated the frequency of light-evoked IPSCs over a 1500 ms response window following stimulus onset (Figure 19A top, middle). The frequency of IPSCs was first used to determine the connectivity of the recorded cell; subsequent analysis of IPSC frequency will be discussed in Results section 3.2.6. A cell was considered to have a light-evoked response and be connected to the transduced GCs if 1) the average frequency of IPSCs within the stimulus window was statistically higher than the frequency of IPSCs in the baseline window preceding stimulus onset (as evaluated by paired t-tests, Figure 19B), and 2) the peak amplitude of its mean current trace exceeded 4 standard deviations of the baseline current.

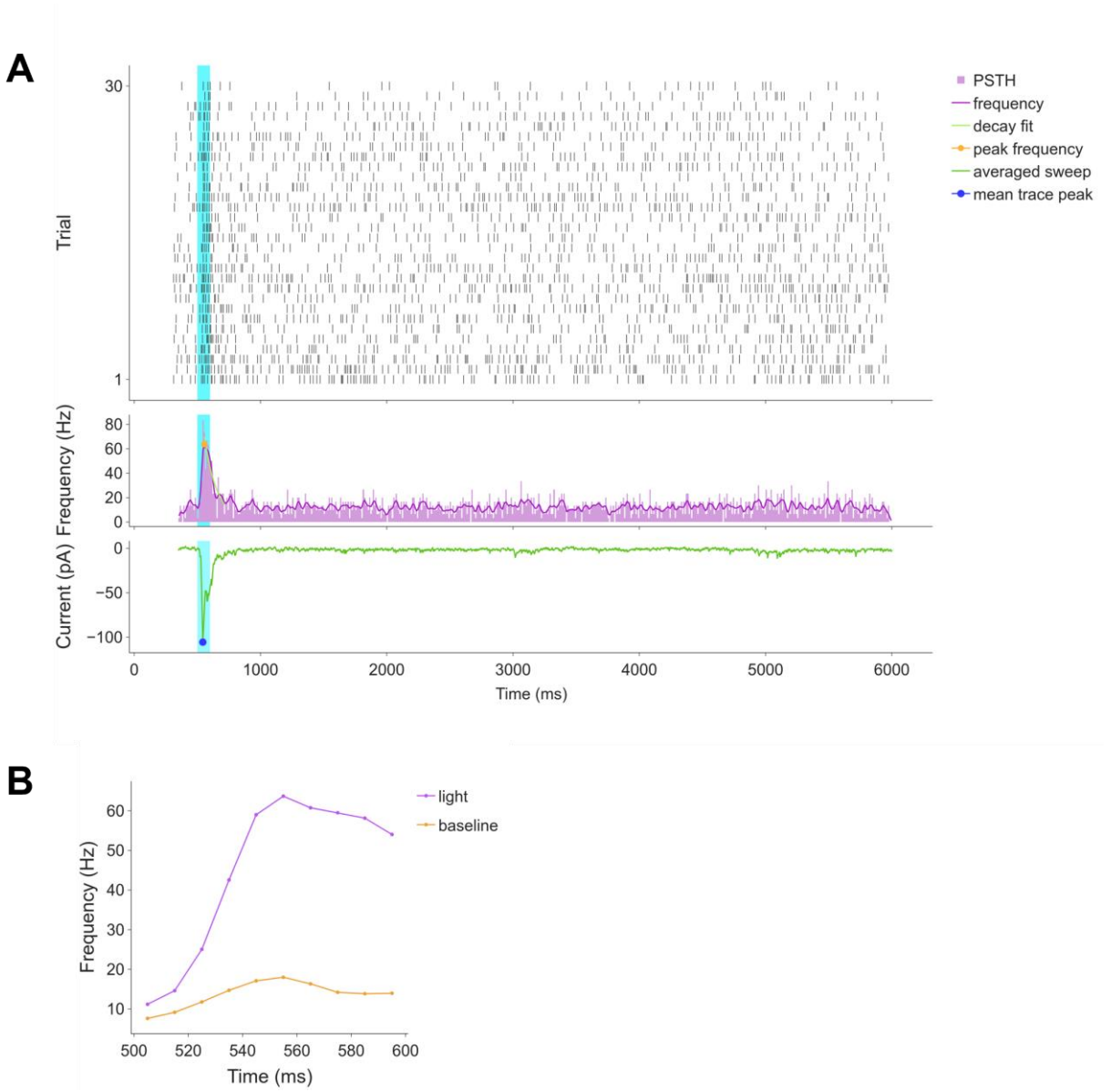

Figure 19. Example analysis for one cell.

A. Raster plot of IPSC times across multiple trials (top), the PSTH of IPSC times with frequency shown in the purple line (middle), and the mean current trace of all 30 trials (bottom). Blue rectangles: 100 ms light pulse photostimulation. **B.** Comparison of IPSC frequency between light-evoked vs. baseline conditions from the same cell shown in **A** (Paired t-test, $p = 0.003$).

In the P2-injected cohort, about half of both MCs and TCs showed light-evoked IPSCs, suggesting similar connectivity in both cell types with P2-transduced GCs (P2: MC responses =

52.2%, n = 12/23 cells; TC responses = 50.0%, n = 9/18 cells; Fisher's exact t test, $p > 0.999$; Figure 20A). In the P14-injected cohort, a higher proportion of MCs showed light-evoked IPSCs than TCs, but the difference did not reach statistical significance (P14: MC responses = 81.0%, n = 17/21 cells; TC responses = 46.7%, n = 7/15 cells; Fisher's exact t test, $p = 0.071$; Figure 20B).

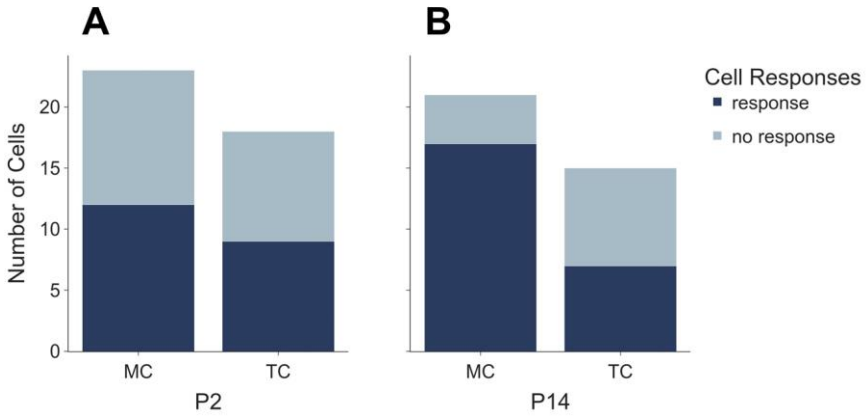

Figure 20. Late postnatal-born GCs show a trend of being preferentially connected to MCs

A. A similar proportion of MCs and TCs showed light-evoked IPSCs in response to photoactivation of P2-transduced GCs (Fisher's exact test, $p > 0.999$, n = 23 MCs and 18 TCs from 8 animals). **B.** A higher proportion of MCs responded to photoactivation of P14-transduced GCs than TCs, but the difference in proportions between the cell types was not statistically significant (Fisher's exact test, $p = 0.071$, n = 21 MCs and 15 TCs from 7 animals).

To test whether the variations I observed (in both the proportion of cells with light-evoked responses and the IPSC frequency in those cells) were due to differences in the number of transduced GCs in each recorded slice, I fixed a subset of OB slices after recordings were concluded and quantified the $EYFP^+$ fluorescence of the GCL in each slice. The fluorescence intensity was normalized to the area of the GCL to obtain the integrated intensity density. The integrated intensity density for each slice was then plotted against 1) the proportions of cells with a response from that slice (Spearman rank-order test, $r_s = -0.292$, $p = 0.272$; Figure 21A) and 2)

the mean peak frequency of IPSCs observed in the cells from that slice (Spearman rank-order test, r_s = -0.077, p = 0.803; Figure 21B). I did not observe any correlations in either comparison, suggesting that differences in the probability of a cell showing a light-evoked response and in the frequency of light-evoked IPSCs were independent of slice-to-slice variations in slicing or animal-to-animal differences in virus infection rate. A potential caveat to this analysis is that the fixed slices could be subject to bleaching following ChR2 photoactivation. More robust methods to control for variations in GC transduction will be described in the Discussion section 3.3.1.

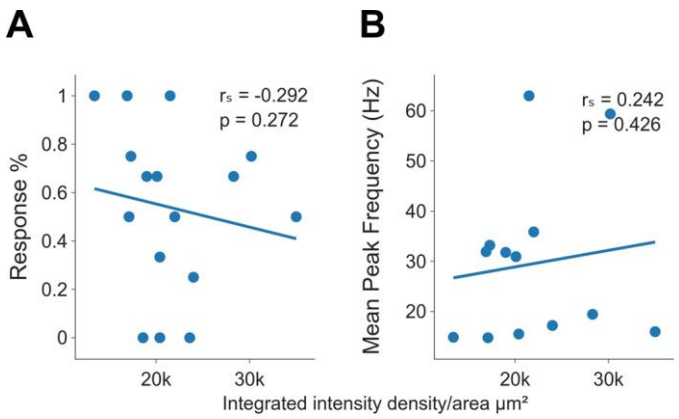

Figure 21. Fluorescence intensity in electrophysiology slices does not correlate with the probability or frequency of light-evoked IPSCs.

A. The proportion of cells that showed light-evoked IPSCs was not correlated with the EYFP fluorescence intensity in that slice (Spearman rank-order test, r_s = -0.292, p = 0.272). **B.** The peak frequency of light-evoked IPSC events in recorded cells was not correlated with the EYFP fluorescence intensity of the slice recorded (Spearman rank-order test, r_s = -0.077, p = 0.803). n = 52 cells from 16 slices and 10 animals. Symbols: averaged value from all the cells within a given slice (at least 2 cells per slice).

3.2.5 Connected MCs and TCs show no difference in the strength of inhibitory input from P2- and P14-transduced GCs

Previously, I showed that, for all recorded cells, the peak amplitude of the mean current traces of MCs was larger than that of TCs in both P2- and P14-injected cohorts (Figure 17). I repeated this analysis but only included the peak amplitudes of cells showing light-evoked responses. In other words, I restricted my subsequent analyses to only cells with a clear connection to transduced postnatal-born GCs. The mean trace peak amplitude of light-evoked responses was similar between MCs and TCs in the P2-injected cohort (P2: MC = -117.4 ± 78.7 pA, TC = -88.5 ± 70.8 pA; Anderson-Darling test, $p = 0.103$). Although the mean trace peak amplitude was slightly larger in MCs than in TCs in the P14-injected cohort, this difference did not reach statistical significance (P14: MC = -227.5 ± 83.8 pA, TC = -65.4 ± 23.1 pA; Anderson-Darling test, $p > 0.250$; Figure 22A, B). The time to peak of the mean trace was similar between cell types in both cohorts (P2: MC = 68.5 ± 13.5 ms, TC = 50.6 ± 12.7 ms; Anderson-Darling test, $p > 0.250$; P14: MC = 26.5 ± 5.9 ms, TC = 31.0 ± 9.1 ms; $p > 0.250$; Figure 22C).

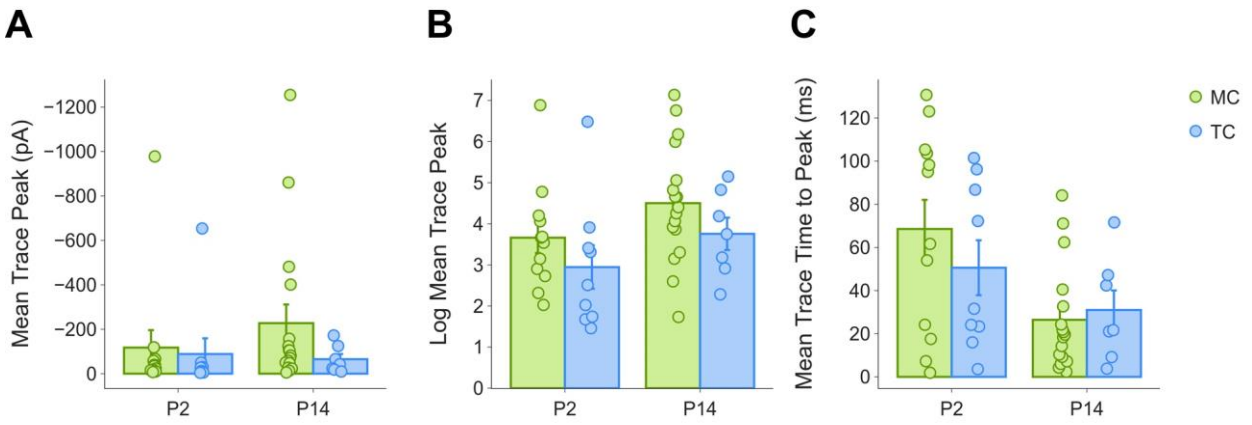

Figure 22. The mean trace peak amplitude of connected MCs trends larger than that of connected TCs.

A. The mean trace peak amplitude of light-evoked responses was similar between MCs and TCs in the P2-injected cohort but slightly larger in MCs than in TCs in the P14-injected cohort, though the difference was not statistically significant (Two-sample Anderson-Darling tests, P2: $p = 0.103$; P14: $p > 0.250$). **B.** Plot of the log-transformed mean trace peak amplitudes shown in A. to display the spread of individual values. **C.** The time to peak of the mean trace was slightly higher in MCs than in TCs in the P2-injected cohort, but the difference was not statistically significant. The time to peak was similar between MCs and TCs in the P14-injected cohort (Two-sample Anderson-Darling tests, P2: $p > 0.250$; P14: $p > 0.250$). P2: n = 12 MCs and 9 TCs from 5 animals; P14: n = 17 MCs and 7 TCs from 7 animals. Bars: mean ± SEM, symbols: individual cells.

I next compared the IPSC event frequency observed in MCs and TCs in the P2- (Figure 23) and P14-injected (Figure 24) cohorts and analyzed properties of the IPSC frequency (Figure 25A), which would provide insight into the properties of the postnatal-born GC subpopulations activated by photostimulation.

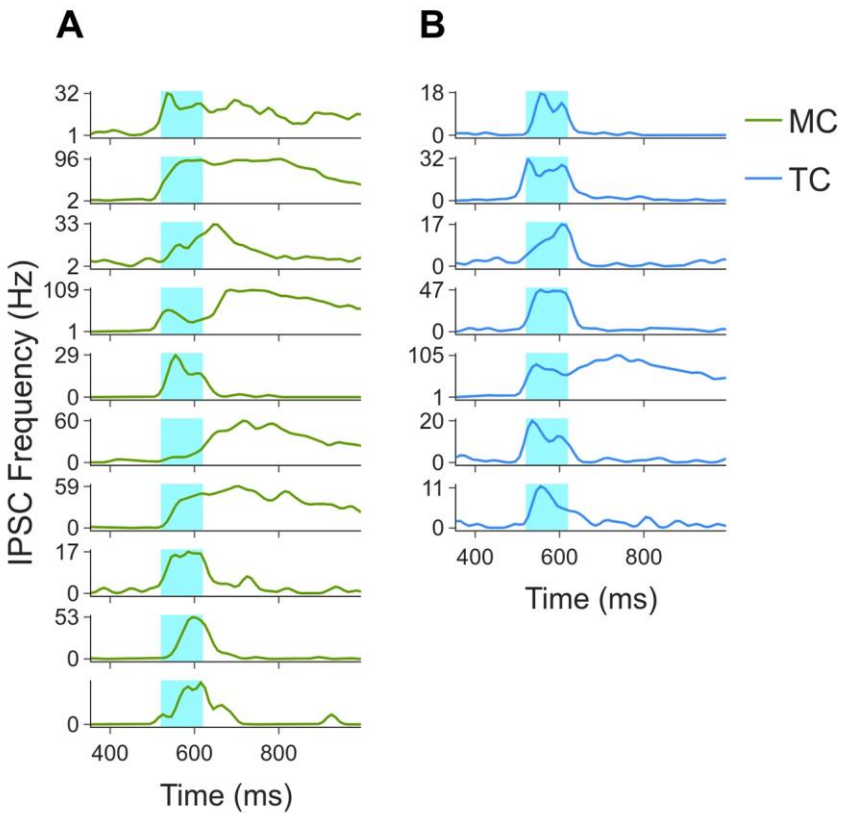

Figure 23. Example IPSC frequency of MCs and TCs in the P2-injected cohort.

The IPSC frequency of example MCs (**A**) and TCs (**B**) in the P2-injected cohort. IPSC frequency was calculated by gaussian smoothing of the PSTH. Blue rectangles: 100 ms light pulse photostimulation.

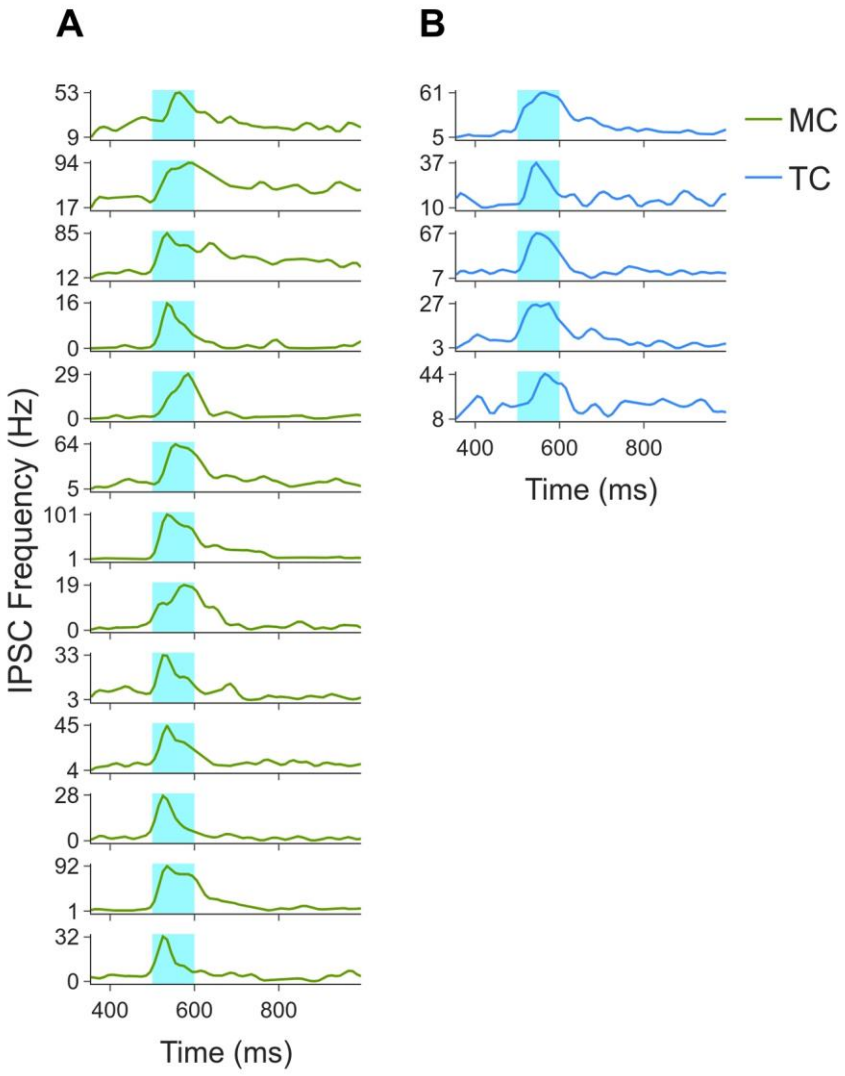

Figure 24. Example IPSC frequency of MCs and TCs in the P14-injected cohort.

The IPSC frequency of example MCs (**A**) and TCs (**B**) in the P14-injected cohort. IPSC frequency was calculated by gaussian smoothing of the PSTH. Blue rectangles: 100 ms light pulse photostimulation.

Similar to the trends observed in the mean traces, the peak IPSC frequency was higher in MCs than in TCs for both P2- and P14-injected cohorts, though the differences did not reach statistical significance (P2: MC = 38.2 ± 8.2 Hz, TC = 25.0 ± 7.8 Hz; Anderson-Darling test, $p > 0.250$; P14: MC = 37.3 ± 6.7 Hz, TC = 30.5 ± 6.1 Hz; $p > 0.250$; Figure 25B). Interestingly, both

MCs and TCs of the P14-injected cohort had a higher baseline IPSC frequency compared to the P2-injected cohort, but because the baseline frequency was not different between cell types in either cohort, the higher baseline frequency at P14 was likely due to age-related differences in the overall OB circuitry (P2: MC = 1.8 ± 0.5 Hz, TC = 1.6 ± 0.5 Hz; Anderson-Darling test, $p > 0.250$; P14: MC = 8.1 ± 2.1 Hz, TC = 10.8 ± 1.9 Hz; $p > 0.250$; Figure 25C). The rise time was similar between MCs and TCs in both cohorts (P2: MC = 45.8 ± 11.2 ms, TC = 33.3 ± 9.9 ms; Anderson-Darling test, $p = 0.077$; P14: MC = 32.4 ± 4.4 ms, TC = 37.1 ± 4.7 ms; $p = 0.224$; Figure 25D).

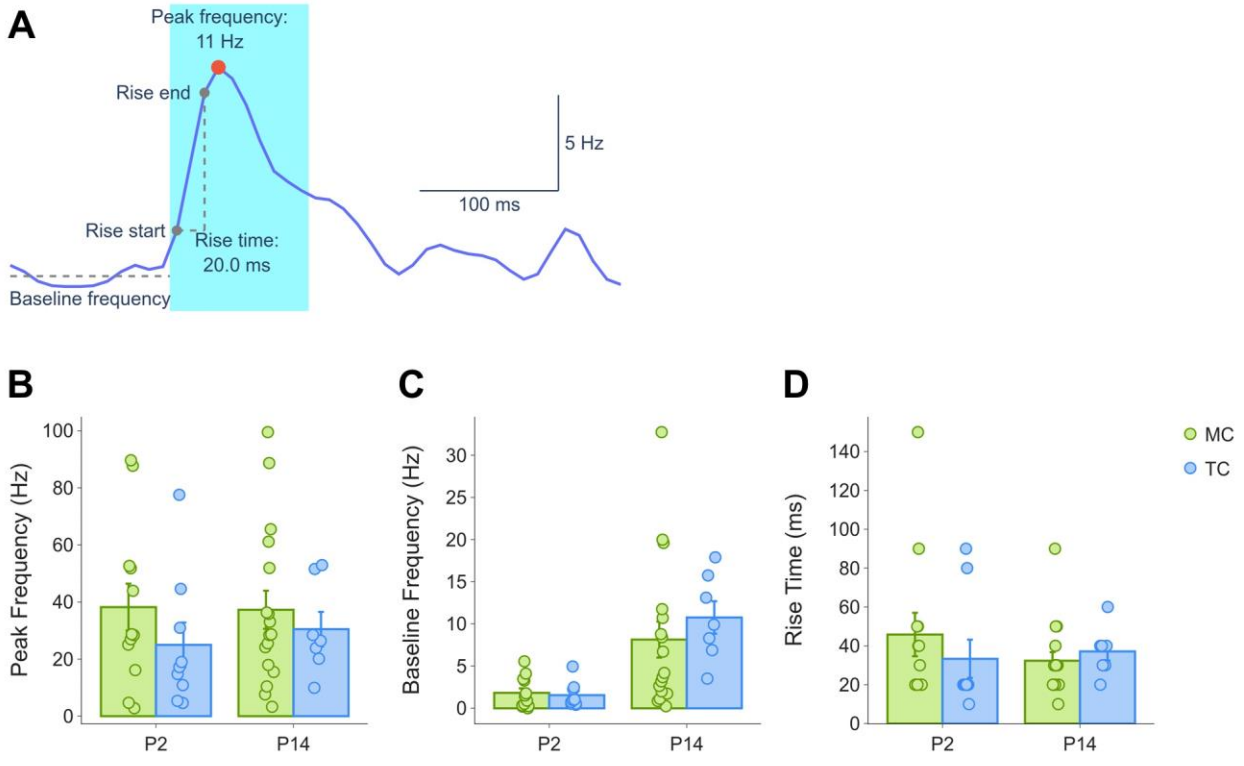

Figure 25. The kinetics of the population IPSC frequency are similar between MCs and TCs.

A. Schematic of the IPSC frequency properties quantified for each cell. **B.** The peak frequency of light-evoked IPSCs were higher in MCs than in TCs in both P2- and P14-injected cohorts, but the difference was not statistically significant (Two-sample Anderson-Darling tests, P2: $p > 0.250$; P14: $p > 0.250$). **C.** The baseline frequency of IPSCs outside the photostimulation window was similar between MCs and TCs in both P2- and P14-injected cohorts. Note the higher baseline frequency displayed by both MCs and TCs in the P14-injected cohort compared to cells in the P2-injected cohort, likely due to age-related differences (Two-sample Anderson-Darling tests, P2: $p > 0.250$; P14: $p > 0.250$). **D.** The rise time of peak IPSC frequency was higher in MCs than in TCs in both P2- and P14-injected cohorts, but the difference was not statistically significant (Two-sample Anderson-Darling tests, P2: $p = 0.077$; P14: $p = 0.224$). P2: n = 12 MCs and 9 TCs from 5 animals; P14: n = 17 MCs and 7 TCs from 7 animals. Bars: mean ± SEM, symbols: individual cells.

In some cells, light stimuli evoked barrages of IPSCs that persisted over a longer post-stimulus window (Figure 15A, bottom left) than other cells in which light-evoked IPSCs were

fewer in number and restricted to a shorter post-stimulus window (Figure 15A, top left). I wanted to see whether a correlation between the peak frequency and the rise time to peak frequency could capture some of these features. Neither the P2- nor P14-injected cohorts showed significant correlations between the peak frequency and peak frequency rise time in either MCs or TCs (P2: MC: Spearman rank-order test, $r_s = 0.404$, $p = 0.193$; TC: $r_s = -0.495$, $p = 0.175$; P14: MC: $r_s = -0.334$, $p = 0.191$, n = 17 cells; TC: $r_s = 0.318$, $p = 0.487$; Figure 26). The lack of correlation between the peak frequency and peak frequency rise time, along with similar a peak frequency rise time between MCs and TCs in both cohorts (Figure 25D), suggests that the timing of the barrages of light-evoked IPSCs was not different between cell types.

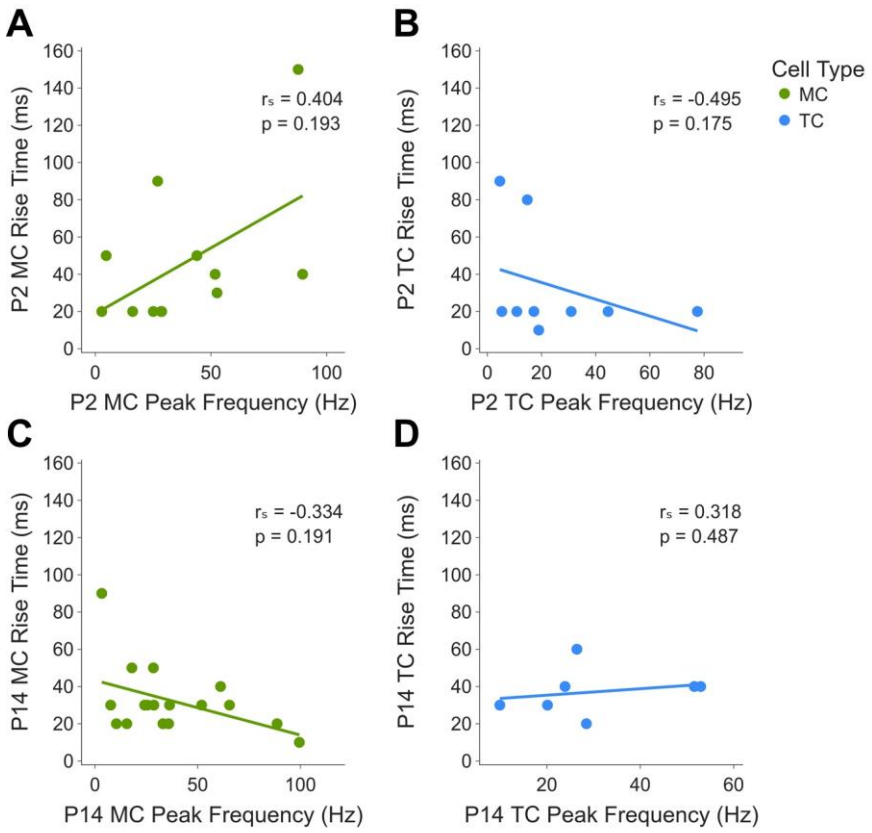

Figure 26. The peak frequency of IPSC events is not correlated with the rise time of the peak frequency in MCs and TCs from the P14 cohort.

A-B. The rise time of the peak frequency of IPSC events was not significantly correlated with the peak frequency in either MCs (**A**) or TCs (**B**) in the P2-injected cohort (Spearman rank-order tests: MCs: r_s = 0.404, p = 0.193, n = 11 cells; TC: r_s = -0.495, p = 0.175, n = 9 cells). **C-D.** The rise time of the peak frequency of IPSC events was not significantly correlated with the peak frequency in MCs (**C**) and in TCs (**D**) from the P14-injected cohort (Spearman rank-order tests: MCs: r_s = -0.334, p = 0.191, n = 17 cells; TC: r_s = 0.318, p = 0.487, n = 7 cells). Symbols: individual cells.

3.2.6 Photoactivating P2- and P14-transduced GCs results in larger IPSCs in MCs compared to trials without photostimulation.

Following the analyses of the overall population of light-evoked IPSCs, I next compared the properties of individual light-evoked IPSCs. First, for each cohort and within each cell type, I compared the kinetics of IPSCs in two stimulus conditions (Light vs. Light Off) and in two windows (Response Window (RW) and Outside Window (OW)). RW is defined as the 1500 ms following stimulus onset; OW is defined as the rest of the trial after RW; Tables 2 and 4). In the P2-injected cohort, the IPSC amplitude of MCs in the Light RW condition was significantly larger than the IPSC amplitude in both the Light Off RW and Light Off OW conditions (Figure 27A; Tables 2-4). The absence of a significant difference in IPSC amplitude between Light RW and Light OW could be due to the persistence of some light-evoked events beyond the 1500 ms window following photostimulation (Table 4). In contrast to MCs, the IPSC amplitude of TCs was similar across all conditions (Figure 27B; Tables 2, 3). The rise time and decay constant tau of MCs and TCs were also similar across all conditions in the P2-injected cohort (Figure 27C-F; Tables 2, 3).

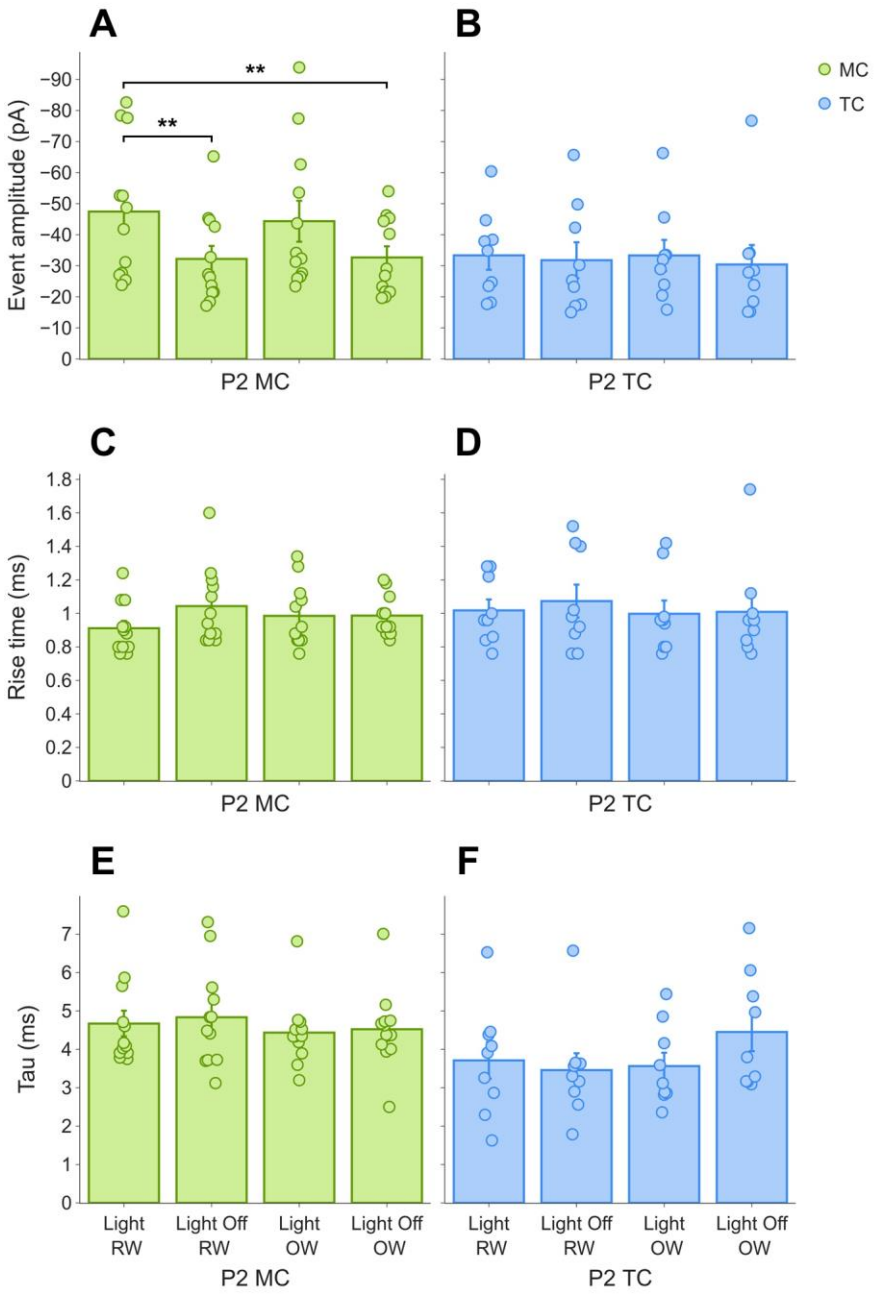

Figure 27. The IPSC amplitude is larger in MCs following activation of P2-transduced GCs.

A. The IPSC amplitude of MCs within the response window during Light condition (Light RW) was larger than the amplitude both within the response window but without Light (Light Off RW) and outside the response window and without light (Light Off OW) (Two-way repeated measures ANOVA, effect of light: $p = 0.046$, $F_{1, 11} = 5.055$; effect of response window: $p = 0.603$, $F_{1, 11} = 0.286$; interaction: $p = 0.505$, $F_{1, 11} = 0.476$. Dunnett's multiple comparisons: Light RW vs. Light Off RW: $p = 0.004$; Light RW vs. Light OW: $p = 0.741$; Light RW vs. Light Off OW: $p = 0.005$).

B. IPSC amplitude was similar in TCs across all Light and window conditions. (Two-way repeated measures ANOVA, effect of light: $p = 0.503$, $F_{1, 8} = 0.492$; effect of response window: $p = 0.675$, $F_{1, 8} = 0.190$; interaction: $p = 0.758$, $F_{1, 8} = 0.101$). **C-D.** The rise time of IPSCs within and outside the response window, in both Light and Light Off trials, was similar in MCs (**C**) and TCs (**D**) (Two-way repeated measures ANOVAs, MC: effect of light: $p = 0.243$, $F_{1, 11} = 1.524$; effect of response window: $p = 0.800$, $F_{1, 11} = 0.067$; interaction: $p = 0.073$, $F_{1, 11} = 3.919$; TC: effect of light: $p = 0.685$, $F_{1, 8} = 0.177$; effect of response window: $p = 0.430$, $F_{1, 8} = 0.693$; interaction: $p = 0.321$, $F_{1, 8} = 1.120$). **E-F.** The decay constant of IPSCs within and outside the response window, in both Light and Light Off trials, was similar in MCs (**E**) and TCs (**F**) (Two-way repeated measures ANOVAs, MC: effect of light: $p = 0.466$, $F_{1, 11} = 0.570$; effect of response window: $p = 0.513$, $F_{1, 11} = 0.457$; interaction: $p = 0.786$, $F_{1, 11} = 0.077$; TC: effect of light: $p = 0.464$, $F_{1, 8} = 0.592$; effect of response window: $p = 0.304$, $F_{1, 8} = 1.209$; interaction: $p = 0.070$, $F_{1, 8} = 4.364$). n = 12 MCs and 9 TCs from 5 animals. Bars: mean ± SEM, symbols: individual cells.

Table 2. IPSC kinetic properties of MCs and TCs in the P2-injected cohort

Injection Cohort	Cell Type	Window	IPSC Amplitude (pA)	Rise time (ms)	Tau (ms)
P2	MC	Light RW	-47.4 ± 6.3	0.91 ± 0.04	4.7 ± 0.3
P2	TC	Light RW	-33.4 ± 4.6	1.02 ± 0.07	3.7 ± 0.5
P2	MC	Light Off RW	-32.2 ± 4.2	1.04 ± 0.07	4.8 ± 0.4
P2	TC	Light Off RW	-31.8 ± 5.8	1.07 ± 0.10	3.5 ± 0.4
P2	MC	Light OW	-44.4 ± 6.6	0.99 ± 0.05	4.4 ± 0.3
P2	TC	Light OW	-33.3 ± 5.0	1.00 ± 0.08	3.6 ± 0.3
P2	MC	Light Off OW	-32.7 ± 3.6	0.99 ± 0.03	4.5 ± 0.3
P2	TC	Light Off OW	-30.4 ± 6.3	1.01 ± 0.10	4.5 ± 0.50

Table 3. Results of two-way repeated measures ANOVA on IPSC kinetic properties in the P2-injected cohort

Cohort	Cell Type	Measure	Light effect	Window effect	Interaction
P2	**MC**	**Amplitude**	***p* = 0.046** **$F_{1, 11} = 5.055$**	*p* = 0.603 $F_{1, 11} = 0.286$	*p* = 0.505 $F_{1, 11} = 0.476$
P2	TC	Amplitude	*p* = 0.503 $F_{1, 8} = 0.492$	*p* = 0.675 $F_{1, 8} = 0.190$	*p* = 0.758 $F_{1, 8} = 0.101$
P2	MC	Rise time	*p* = 0.243 $F_{1, 11} = 1.524$	*p* = 0.800 $F_{1, 11} = 0.067$	*p* = 0.073 $F_{1, 11} = 3.919$
P2	TC	Rise time	*p* = 0.685 $F_{1, 8} = 0.177$	*p* = 0.430 $F_{1, 8} = 0.693$	*p* = 0.321 $F_{1, 8} = 1.120$
P2	MC	Tau	*p* = 0.466 $F_{1, 11} = 0.570$	*p* = 0.513 $F_{1, 11} = 0.457$	*p* = 0.786 $F_{1, 11} = 0.077$
P2	TC	Tau	*p* = 0.464 $F_{1, 8} = 0.592$	*p* = 0.304 $F_{1, 8} = 1.209$	*p* = 0.070 $F_{1, 8} = 4.364$

Table 4. Dunnett's multiple comparisons IPSC kinetic properties with significant Light effect in the P2-injected cohort

Cohort	Cell Type	Measure	Comparison	*p* value
P2	**MC**	**Amplitude**	**Light RW vs. Light Off RW**	**0.004**
P2	MC	Amplitude	Light RW vs. Light OW	0.741
P2	**MC**	**Amplitude**	**Light RW vs. Light Off OW**	**0.005**

In the P14-injected cohort, the amplitude of light-evoked IPSCs in MCs was significantly higher in Light RW than in Light Off RW, Light OW, and Light Off OW, suggesting that photostimulation elicits IPSCs with larger amplitudes than when no stimulus is present (Figure 28A; Tables 5-7). In contrast, the IPSC amplitude of P14 TCs was similar across all conditions (Figure 28B; Tables 5, 6). The rise time and decay constant of both cell types were also similar across all conditions, similar to the P2-injected cohort (Figure 28C-F; Tables 5, 6). There was a significant Window effect (i.e. RW vs. OW) on the decay constant of MCs in the P14 cohort, but given that there was not a significant Light effect, the difference observed was likely not directly related to the activation of transduced GCs (Table 6).

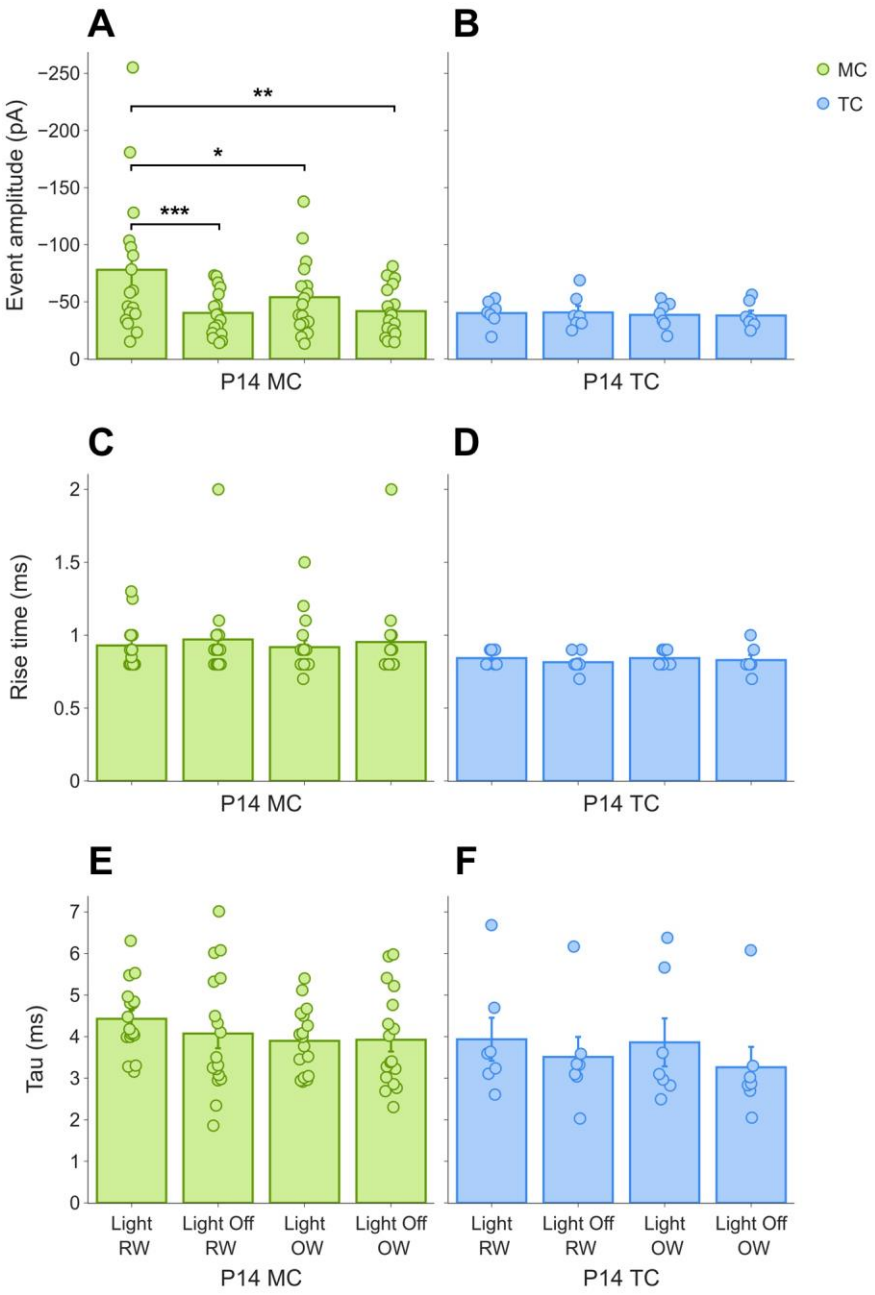

Figure 28. The IPSC amplitude is larger in MCs following activation of P14-transduced GCs.

A. The IPSC amplitude of MCs within the response window during Light condition (Light RW) was larger than the amplitude within the response window but without Light (Light Off RW), outside of the response window but with light (Light OW), and outside the response window and without light (Light Off OW) (Two-way repeated measures ANOVA, effect of light: $p = 0.015$, $F_{1, 16} = 7.467$; effect of response window: $p = 0.073$, $F_{1, 16} = 3.674$; interaction: $p = 0.045$, $F_{1, 16} = 4.716$. Dunnett's multiple comparisons: Light RW vs. Light Off RW: $p = 0.001$; Light RW vs. Light

OW: $p = 0.028$; Light RW vs. Light Off OW: $p = 0.001$). **B.** IPSC amplitude was similar in TCs across all Light and window conditions. (Two-way repeated measures ANOVA, effect of light: $p = 0.996$, $F_{1, 6} = 2.611e\text{-}005$; effect of response window: $p = 0.292$, $F_{1, 6} = 1.337$; interaction: $p = 0.697$, $F_{1, 6} = 0.167$). **C-D.** The rise time of IPSCs within and outside the response window, in both Light and Light Off trials, was similar in MCs (**C**) and TCs (**D**) (Two-way repeated measures ANOVAs, MC: effect of light: $p = 0.385$, $F_{1, 16} = 0.797$; effect of response window: $p = 0.418$, $F_{1, 16} = 0.691$; interaction: $p = 0.795$, $F_{1, 16} = 0.070$; TC: effect of light: $p = 0.356$, $F_{1, 6} = 1.000$; effect of response window: $p = 0.356$, $F_{1, 6} = 1.000$; interaction: $p = 0.356$, $F_{1, 6} = 1.000$). **E-F.** The decay constant of IPSCs within and outside the response window, in both Light and Light Off trials, was similar in MCs (**E**) and TCs (**F**) (Two-way repeated measures ANOVAs, MC: effect of light: $p = 0.431$, $F_{1, 16} = 0.654$; effect of response window: $p = 0.006$, $F_{1, 16} = 10.24$; interaction: $p = 0.008$, $F_{1, 16} = 9.016$; TC: effect of light: $p = 0.121$, $F_{1, 6} = 3.265$; effect of response window: $p = 0.146$, $F_{1, 6} = 2.784$; interaction: $p = 0.512$, $F_{1, 6} = 0.485$). n = 17 MCs and 7 TCs from 7 animals. Bars: mean ± SEM, symbols: individual cells.

Table 5. IPSC kinetic properties of MCs and TCs from the P14-injected cohort

Injection Cohort	Cell Type	Window	IPSC Amplitude (pA)	Rise time (ms)	Tau (ms)
P14	MC	Light RW	-78.1 ± 15.2	0.93 ± 0.04	4.4 ± 0.2
P14	TC	Light RW	-40.2 ± 4.2	0.84 ± 0.02	3.9 ± 0.5
P14	MC	Light Off RW	-40.3 ± 4.9	0.97 ± 0.07	4.1 ± 0.4
P14	TC	Light Off RW	-40.6 ± 5.7	0.81 ± 0.03	3.5 ± 0.5
P14	MC	Light OW	-54.0 ± 8.0	0.92 ± 0.05	3.9 ± 0.2
P14	TC	Light OW	-38.6 ± 4.3	0.84 ± 0.02	3.9 ± 0.6
P14	MC	Light Off OW	-41.8 ± 5.2	0.95 ± 0.07	3.9 ± 0.3
P14	TC	Light Off OW	-38.1 ± 4.3	0.83 ± 0.04	3.3 ± 0.5

Table 6. Results of two-way repeated measures ANOVA on IPSC kinetic properties in the P14-injected cohort

Cohort	Cell Type	Measure	Light effect	Window effect	Interaction
P14	**MC**	**Amplitude**	***p* = 0.015** **$F_{1, 16}$ = 7.467**	*p* = 0.073 $F_{1, 16}$ = 3.674	***p* = 0.045** **$F_{1, 16}$ = 4.716**
P14	TC	Amplitude	*p* = 0.996 $F_{1, 6}$ = 2.611e-005	*p* = 0.292 $F_{1, 6}$ = 1.337	*p* = 0.697 $F_{1, 6}$ = 0.167
P14	MC	Rise time	*p* = 0.385 $F_{1, 16}$ = 0.797	*p* = 0.418 $F_{1, 16}$ = 0.691	*p* = 0.795 $F_{1, 16}$ = 0.070
P14	TC	Rise time	*p* = 0.356 $F_{1, 6}$ = 1.000	*p* = 0.356 $F_{1, 6}$ = 1.000	*p* = 0.356 $F_{1, 6}$ = 1.000
P14	MC	Tau	*p* = 0.431 $F_{1, 16}$ = 0.654	*p* = 0.006 $F_{1, 16}$ = 10.24	*p* = 0.008 $F_{1, 16}$ = 9.016
P14	TC	Tau	*p* = 0.121 $F_{1, 6}$ = 3.265	*p* = 0.146 $F_{1, 6}$ = 2.784	*p* = 0.512 $F_{1, 6}$ = 0.485

Table 7. Dunnett's multiple comparisons IPSC kinetic properties with significant Light effect in the P14-injected cohort

Cohort	Cell Type	Measure	Comparison	*p* value
P14	**MC**	**Amplitude**	**Light RW vs. Light Off RW**	**0.001**
P14	**MC**	**Amplitude**	**Light RW vs. Light OW**	**0.028**
P14	**MC**	**Amplitude**	**Light RW vs. Light Off OW**	**0.001**

I next restricted my analyses to only IPSCs recorded in Light trials during the Response Window (Light RW) and compared the kinetic properties between cell types in each cohort. The amplitude of light-evoked IPSCs in MCs was slightly higher than that in TCs, but the difference was not statistically significant (P2: MC = -47.4 ± 6.3 pA, TC = -33.4 ± 4.6 pA; Anderson-Darling test, $p = 0.108$; P14: MC = -78.1 ± 15.2 pA, TC = -40.2 ± 4.2 pA; $p = 0.156$; Figure 29A). The rise time was comparable between the cell types in both cohorts (P2: MC = 0.91 ± 0.04 ms, TC = 1.02 ± 0.07 ms; Anderson-Darling test, $p = 0.222$; P14: MC = 0.93 ± 0.04 ms, TC = 0.84 ± 0.02 ms; $p = 0.176$; Figure 29B). In both P2- and P14-injected cohorts, the decay constant tau showed a non-significant trend of being larger in MCs than in TCs (P2: MC = 4.7 ± 0.3 ms, TC = 3.7 ± 0.5 ms; Anderson-Darling test, $p = 0.136$; P14: MC = 4.4 ± 0.2 ms, TC = 3.9 ± 0.5 ms; $p = 0.062$; Figure 29C).

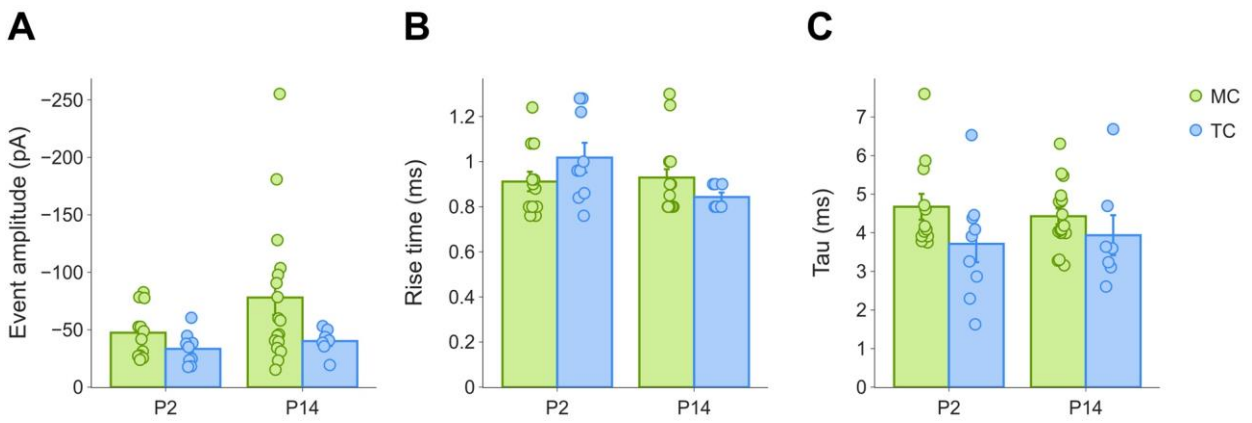

Figure 29. The amplitude of individual IPSCs in connected MCs trends larger than that of connected TCs.

A. The amplitude of light-evoked IPSCs was slightly higher in MCs than in TCs for both P2- and P14-injected cohorts, but the difference was not statistically significant (Two-sample Anderson-Darling tests, P2: $p = 0.108$; P14: $p = 0.156$). **B.** The rise time of light-evoked IPSCs was similar between MCs and TCs for both P2- and P14-injected cohorts (Two-sample Anderson-Darling tests, P2: $p = 0.222$; P14: $p = 0.176$). **C.** The decay constant of light-evoked IPSCs was slightly larger in MCs than in TCs for both P2- and P14-injected cohorts, but the difference was not statistically significant (Two-sample Anderson-Darling tests, P2: $p = 0.136$; P14: $p = 0.062$). P2: n = 12 MCs and 9 TCs from 5 animals; P14: n = 17 MCs and 7 TCs from 7 animals. Bars: mean ± SEM, symbols: individual cells.

Next, I tested for correlations between kinetic properties of the events. First, I plotted the peak amplitude of light-evoked IPSCs against the rise time and observed significant negative correlations between the two measurements in the MCs of both P2- and P14-injected cohorts (P2 MC: Spearman rank-order test, $r_s = -0.878$, $p < 0.001$; P14 MC: $r_s = -0.548$, $p = 0.023$; Figure 30A, C). In contrast, there was no significant correlation in the TCs of either cohort (P2 TC: Spearman rank-order test, $r_s = -0.395$, $p = 0.293$; P14 TC: $r_s = 0.577$, $p = 0.175$; Figure 30B, D).

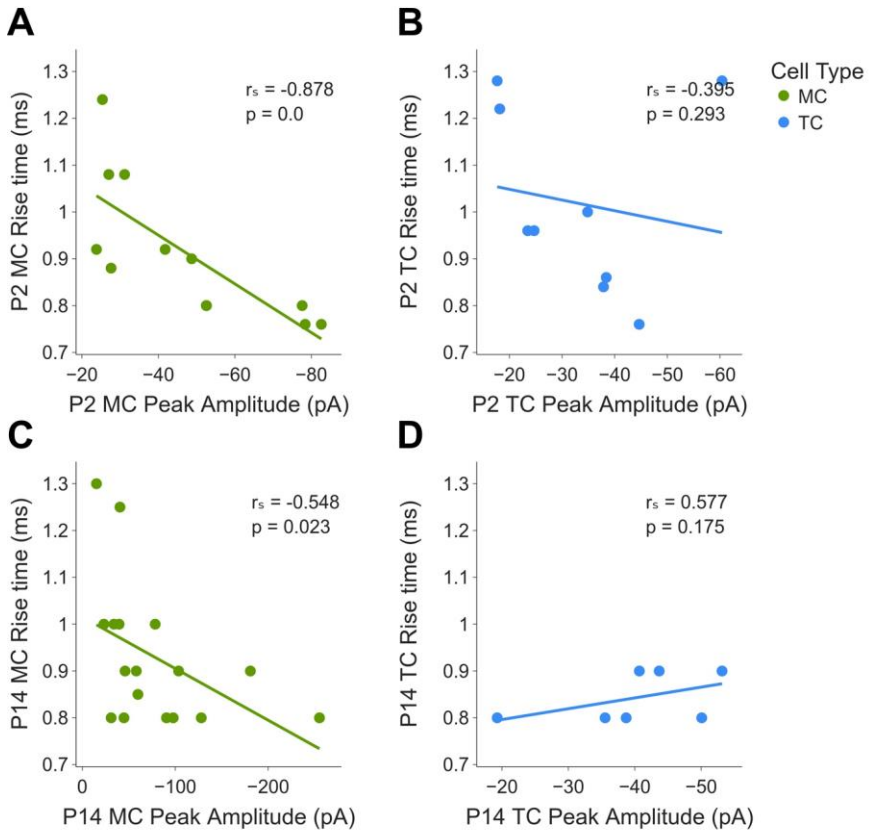

Figure 30. The peak amplitude of IPSCs in MCs is negatively correlated with the rise time.

A-B. The peak amplitude of light-evoked IPSCs was negatively correlated with the rise time in MCs (**A**) but not in TCs (**B**) in the P2-injected cohort (Spearman rank-order tests, MC: $r_s = -0.878$, $p < 0.001$, n = 11 cells; TC: $r_s = -0.395$, $p = 0.293$, n = 9 cells). **C-D.** The peak amplitude of light-evoked IPSCs was negatively correlated with the rise time in MCs (**C**) but not in TCs (**D**) in the P14-injected cohort (Spearman rank-order tests, MC: $r_s = -0.548$, $p = 0.023$, n = 17 cells; TC: $r_s = 0.577$, $p = 0.175$, n = 7 cells). Symbols: individual cells.

Further analyses did not reveal strong correlations between the peak amplitude and decay constant (P2: MC: Spearman rank-order test, $r_s = 0.021$, $p = 0.948$; TC: $r_s = -0.433$, $p = 0.244$; P14: MC: $r_s = -0.252$, $p = 0.328$, n = 17 cells; TC: $r_s = 0.714$, $p = 0.071$; Figure 31) or between the rise time and decay constant (P2: MC: Spearman rank-order test, $r_s = 0.120$, $p = 0.709$; TC: 0.193, $p = 0.618$; P14: MC: $r_s = 0.220$, $p = 0.397$, n = 17 cells; TC: $r_s = 0.577$, $p = 0.175$; Figure 32).

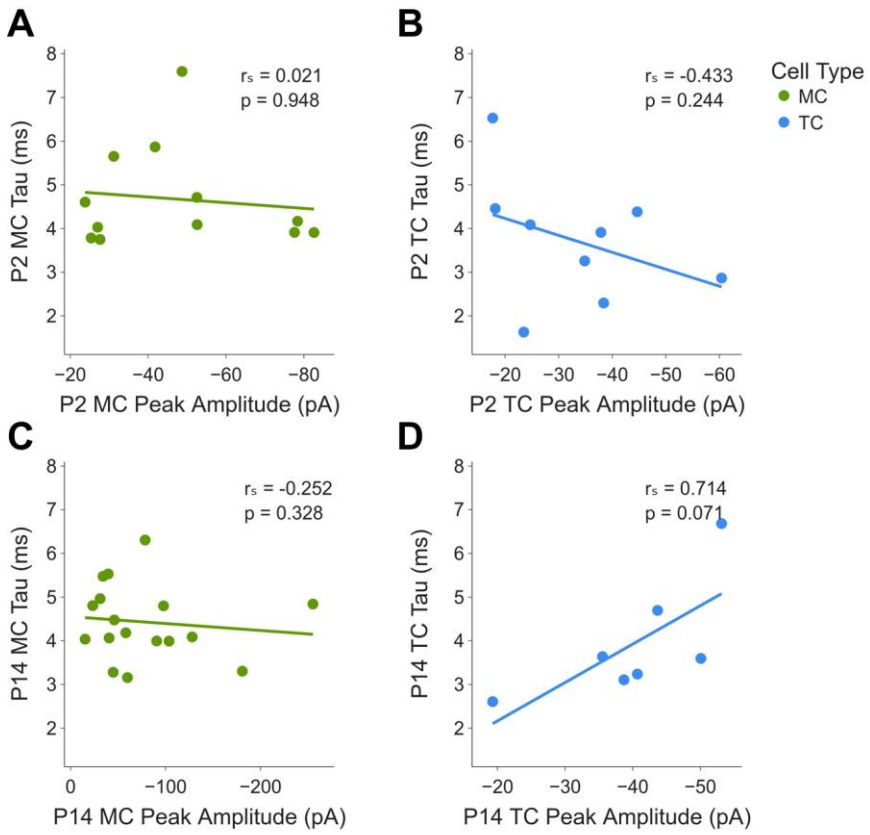

Figure 31. The peak amplitude of IPSCs is not correlated with the decay constant.

A-B. The peak amplitude of light-evoked IPSCs was not correlated with the decay constant in either MCs (**A**) or TCs (**B**) in the P2-injected cohort (Spearman rank-order tests, MC: $r_s = 0.021$, $p = 0.948$, n = 11 cells; TC: $r_s = -0.433$, $p = 0.244$, n = 9 cells). **C-D.** The peak amplitude of light-evoked IPSCs was not correlated with the decay constant in either MCs (**C**) or TCs (**D**) in the P14-injected cohort (Spearman rank-order tests, MC: $r_s = -0.252$, $p = 0.328$, n = 17 cells; TC: $r_s = 0.714$, $p = 0.071$, n = 7 cells). Symbols: individual cells.

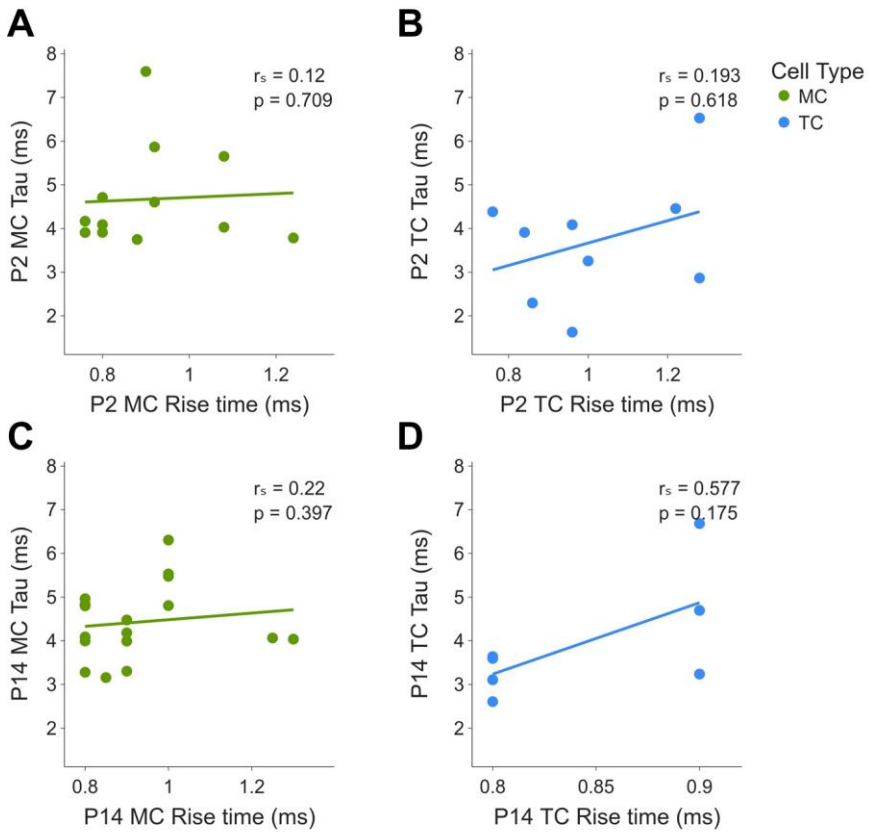

Figure 32. The rise time of IPSCs is not correlated with the decay constant.

A-B. The rise time of light-evoked IPSCs was not correlated with the decay constant in either MCs (**A**) or TCs (**B**) in the P2-injected cohort (Spearman rank-order tests, MC: $r_s = 0.120$, $p = 0.709$, n = 11 cells; TC: $r_s = 0.193$, $p = 0.618$, n = 9 cells). **C-D.** The rise time of light-evoked IPSCs was not correlated with the decay constant in either MCs (**C**) or TCs (**D**) in the P14-injected cohort (Spearman rank-order tests, MC: $r_s = 0.220$, $p = 0.397$, n = 17 cells; TC: $r_s = 0.577$, $p = 0.175$, n = 7 cells). Symbols: individual cells.

The absence of correlations in these latter comparisons suggests that the negative relationship observed between the peak amplitudes and rise times in MCs is likely not due to dendritic filtering or series resistance errors (Tran-Van-Minh et al., 2015; Zhou and Hablitz, 1997). Given that I observed a trend toward higher IPSC amplitudes in MCs compared to TCs (Figure 29A), it is not surprising that MCs would have a stronger relationship between peak amplitude and

rise time, which may result from synapses located closer to the soma (Banks et al., 1998; Pearce, 1993). The absence of significant differences between IPSC rise time and tau across light conditions and response windows, and between IPSC amplitude across Light Off conditions, suggests that the synapses recruited in each condition may share similar properties, such as size, location, number of receptors, and receptor subunits (Adlaf et al., 2017; Lagier et al., 2007).

As a control experiment, I next tested whether the initial differences observed in the mean current trace peak amplitude (Figure 17) or the correlations found above between IPSC amplitude and rise time (Figure 30) could be attributed to differences in the animals' absolute age. To address this possibility, I injected a separate cohort of animals at P2 and waited six weeks post injection before performing slice electrophysiology experiments, resulting in slices from animals that were the same age as those from the P14-injected cohort (Figure 33A). Surprisingly, the proportions of both MCs and TCs that showed light-evoked IPSCs were lower than in slices from animals injected at P2 and sacrificed four weeks later. (P14: MC responses = 19.6%, n = 10/51 cells; TC responses = 22.7%, n = 5/22 cells; Figure 33B). The few cells with light-evoked responses showed unusually large currents and frequent temporal summation (Figure 33C). Due to the presence of APV and NBQX in the recording bath solution, it is unlikely that these responses were due to recurrent excitation from activated MCs or TCs with spurious expression of ChR2 (Aroniadou-Anderjaska et al., 1999). The low probability of observing a light-evoked response in this cohort could be due to the longer time of virus expression, which may have adversely impacted GC cell health while at the same time increasing the size of photoactivated currents observed in cells that were connected to those transduced GCs that did survive. I did not further analyze the data from this cohort because of the possible technical complications.

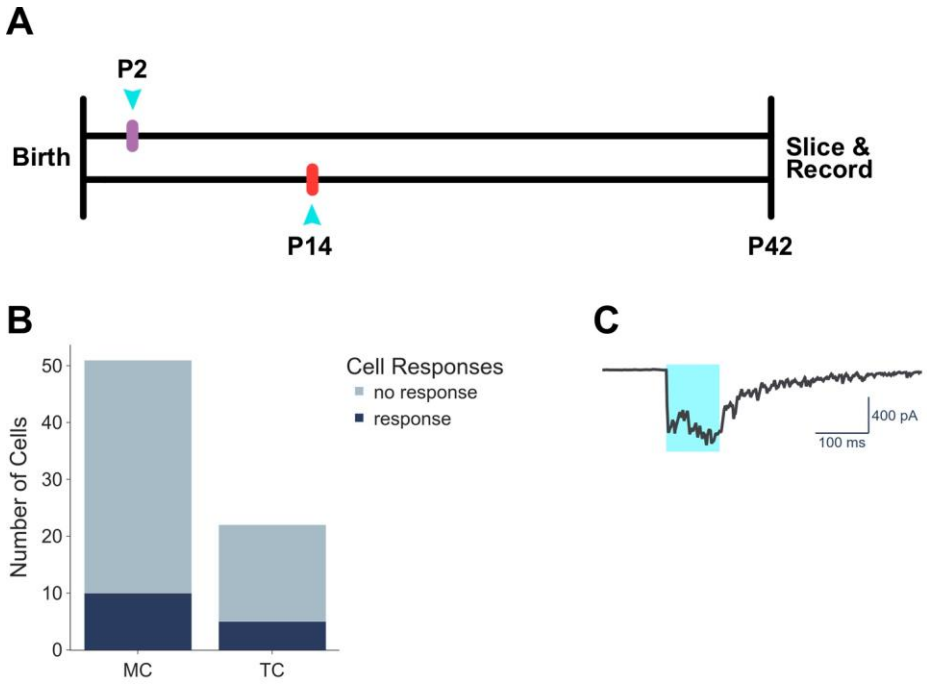

Figure 33. MCs and TCs recorded at 6 weeks post P2-transduction have a low probability of a light-evoked response.

A. Timeline of virus injection for the P2-injected, 6 wpi cohort. **B.** A low proportion of both MCs and TCs showed light-evoked IPSCs (n = 51 MCs and 22 TCs from 15 animals). **C.** Example trace of light-evoked IPSC from a MC, showing a large current and multiple overlapping peaks. Blue rectangles: 100 ms light pulse photostimulation.

3.3 Discussion

In this study, my goal was to investigate whether anatomical differences in postnatal-born GC subpopulations can lead to differences in functional connectivity of the GCs with OB principal neurons. My data show that two distinct subpopulations of early (P2-transduced) and late (P14-transduced) postnatal-born GCs can be selectively activated using virus injections and optogenetics (Figure 14), and that they display differences in functional connectivity with the

principal output neurons of the OB. In my initial analysis, I found that both P2- and P14-transduced GCs provide stronger inhibition onto the overall population of MCs compared to TCs (Figure 17).

In subsequent experiments attempting to understand the factors that contributed to this difference, I observed non-significant differences in both the probability of being connected to P2- or P14-transduced GCs and the strength of the inhibition when present. In the P2-injected cohort, both MCs and TCs showed a similar probability of being connected to transduced GCs, whereas MCs were more likely than TCs to show light-evoked IPSCs in response to activation of P14-transduced GCs, but this difference was not statistically significant (Figure 20). Both the frequency (Figure 25) and amplitude (Figure 29) of light-evoked IPSCs showed a trend of being higher in MCs compared to TCs in both cohorts, and this difference was more pronounced in the P14-injected cohort despite not reaching statistical significance. Nevertheless, the trends observed in the probability of a connection with P2- vs. P14-transduced GCs and the strength of that connection may contribute to the differences observed in the overall MC and TC populations (Figure 17). These findings provide evidence for subtle differences in the connections formed by early and late postnatal-born GCs onto MCs and TCs that may result from anatomical differences in the postnatal-born GC subpopulations.

3.3.1 Timed viral injections label different subpopulations of postnatal-born GCs

Labeling and activation of early and late postnatal-born GCs were achieved using the viral vector AAV2-hSyn-hChR2(H134R)-EYFP injected into the RMS. Other expression strategies such as lentiviral vectors, the tamoxifen approach, or the GAD65-Cre mouse line have been utilized successfully in other studies (Alonso et al., 2012; Kohwi et al., 2007; Nunez-Parra et al., 2013; Platel et al., 2019; Shani-Narkiss et al., 2020). I selected an AAV vector because it does not

infect dividing neural precursors unlike lentiviruses, which would preclude accurate birth-dating. Additionally, AAV2 and its related hybrid serotypes have been used previously to effectively transduce olfactory GCs (Gschwend et al., 2015; Muthusamy et al., 2017), show a more limited spread and higher preference for neurons compared to other serotypes (Davidson et al., 2000; Haery et al., 2019; Hammond et al., 2017), and have a reduced possibility of introducing compensatory mechanisms in development compared to using transgenic animals.

It is possible that differences in injection strategies for the P2-injected (free-hand injections) vs. P14-injected (stereotaxic surgery) cohorts may lead to differing viral expression levels. Although 1 μl of viral vector solution was used in both P2 and P14 injections, the smaller size of the mouse brain at P2 means that the RMS would be infected by a relatively larger volume of virus compared to a brain at P14. Both the higher rate of postnatal neurogenesis and the relative closeness of brain regions at P2 compared to P14 could also lead to more neuroblasts being transduced by the virus (Enwere et al., 2004; Magavi et al., 2005), resulting in an increased number of transduced cells in the OB. The analyses described in this chapter involve quantification of the size of synaptic inputs onto MCs and TCs and are directly influenced by the number of transduced cells in each slice. To eliminate possible confounds due to technique-related differences in virus expression, I only made comparisons between cell types in the same injection time point.

P2 injections occasionally resulted in nonspecific expression of ChR2-EYFP in the internal plexiform layer (IPL) and EPL, likely due to mistargeting of regions outside of the RMS during P2 injections (Muthusamy et al., 2017). Mistargeting of the AON could result in transduction of AON neurons whose feedback projections are found in the IPL and EPL (Figure 13B top, Figure 13C left). GCs receive glutamatergic input from centrifugal feedback fibers originating in the AON and PCx (Boyd et al., 2015; Markopoulos et al., 2012; Otazu et al., 2015; Rothermel and

Wachowiak, 2014) and other cortical regions (Padmanabhan et al., 2019). Additionally, GCs also receive GABAergic input from the basal forebrain, but these inputs do not target MC or TCs (Case et al., 2017; Diez et al., 2019; Hanson et al., 2020; Nunez-Parra et al., 2013).

With my experimental design, I was able to eliminate sources of synaptic input onto MCs and TCs other than inhibition from transduced GCs. First, I did not record from any slices with visible ChR2-EYFP expression outside of GCs. Second, glutamatergic transmission in all recordings was blocked by using APV and NBQX in the bath. The presence of glutamatergic blockers in the recording bath also prevents disynaptic inhibition onto MCs and TCs from AON feedback fibers (Boyd et al., 2012; Brunjes et al., 2005; Markopoulos et al., 2012). Application of gabazine in a subset of successful recordings abolished light-evoked IPSCs, confirming the events as being GABAergic (Figure 14C). The synaptic events recorded from both injection cohorts were similar. Photostimulation of both P2- and P14-transduced GCs using a 100 ms light pulse (a longer stimulus, to simulate *in vivo* odor presentation) (Labarrera et al., 2013) evoked asynchronous inhibitory events (Figure 15) that resembled IPSCs previously reported in MCs following activation of lateral inhibition or depolarization of local GC dendrites (Isaacson and Strowbridge, 1998; Kapoor and Urban, 2006; Schoppa et al., 1998). Finally, I did not observe any correlation between the $EYFP^{+}$ fluorescence intensity in a slice and the light-evoked response probability or strength of the responses recorded from that slice (Figure 21), allowing me to conclude that nonspecific transduction in the OB did not significantly impact my results.

More rigorous histological analysis of virus injections could also be performed to control for the rate of transduction in each injection cohort. Although the density of fluorescent fibers often observed in the GCL of P2-injected animals precluded this analysis, quantification of the number of transduced GC cell bodies in the GCL could provide a better estimate of the transduction

rate and viral spread in each injected animal. The rate of transduction could then be correlated with the proportion of cells that had a light-recorded response in each animal and the mean IPSC frequency of all the cells from that animal.

Although 95% of postnatal-generated neuroblasts differentiate into GCs, a small percentage do develop into PGCs residing in the GL (Belluzzi et al., 2003; Lledo and Saghatelyan, 2005). In age-matched P2- and P14-injected animals sacrificed for histology, I observed fewer than one fluorescent PGC per animal, suggesting that very small numbers of postnatal-born PGCs were transduced by my injections. This observation is supported by data showing that generation of GL interneurons decreases dramatically between E12.5 and P0, concomitant with an increase in the generation of GCL interneurons at the same time points (Batista-Brito et al., 2008). Additionally, a previous study did not report any light-evoked IPSCs in MCs after photoactivation of postnatal-born cells in the GL (Bardy et al., 2010). Thus, I do not anticipate postnatal-born PGCs to make any meaningful contribution to the light-evoked IPSCs recorded from MCs and TCs.

3.3.2 Subtle differences exist in the strength of inhibition from P2- and P14-transduced GCs onto MCs vs. TCs

The initial analysis of all recorded cells, regardless of whether they showed a light-evoked response, revealed a higher mean trace peak amplitude in MCs than in TCs (Figure 17). This measure combines both the probability of there being a connection with postnatal-born GCs and the strength of that connection, when it does exist. I next disentangled the two factors contributing to the overall difference I observed and found that the differences in neither factor were statistically significant. MCs and TCs showed a similar probability of being connected to P2-transduced GCs.

MCs were more likely than TCs to be connected to P14-transduced GCs, but the difference in proportion was not statistically significant (Figure 20).

When I restricted my analyses to only cells that showed a light-evoked response, I found that there were no statistically significant differences between the mean trace peak amplitude of MCs vs. TCs in either cohort, although the amplitude in MCs trended higher, especially in the P14-injected cohort (Figure 22). Analysis of IPSC event frequency demonstrated that in both cohorts, the peak frequency of IPSCs trended higher in MCs than in TCs, though the difference was not statistically significant (Figure 25). Previous studies have demonstrated similar increased inhibitory tone in MCs than in TCs (Arnson and Strowbridge, 2017; Geramita et al., 2016).

Comparison of individual IPSC properties also revealed similar differences as the population properties. In the MCs from both P2- and P14-injected cohorts, IPSC amplitudes were significantly larger in the 1500 ms window following photoactivation compared to either Light Off or outside response window conditions (Figures 27, 28; Tables 2, 5). The effect was more pronounced in the P14-injected cohort: the IPSC amplitude in the Light, Response Window was significantly higher than that in all three of the Light Off or outside response window conditions (Figure 28A, left; Tables 6, 7). Rise time and decay tau did not differ between light conditions, suggesting that the properties of the synapses providing light-evoked IPSCs were similar to those of synapses providing spontaneous IPSCs (Figures 27, 28). In basal conditions without light stimulation, spontaneous GABAergic release occurs at synapses between transduced GCs and MCs/TCs; with photoactivation, however, the stimulus triggers simultaneous release from multiple synapses that are also capable of spontaneous release. Given that the MC IPSC amplitude during the Light, Response Window condition was larger than the amplitude during the Light Off conditions in both P2- and P14-injected cohorts, the number or strength of the synapses formed

between transduced GCs and MCs may be such that photoactivation resulted in greater summation of IPSCs from multiple synchronized synapses (Figures 27A, 28A). And, similar to the mean current trace peak amplitude, the difference in the IPSC amplitude in MCs between light conditions was more pronounced in the P14-injected cohort compared to the P2-injected cohort.

My subsequent analysis was restricted to IPSCs in the Light condition within the response window. IPSC kinetics were similar between MCs and TCs in both cohorts, which was expected given that MCs and TCs likely receive inhibition from a similar pool of transduced GCs (Figure 29). The IPSC amplitude trended higher in MCs compared to TCs, especially in the P14-injected cohort, but the difference was not statistically significant (Figure 29A). I additionally assessed correlations between the kinetic properties of IPSCs and found that the amplitude of IPSCs was negatively correlated with the rise time in the MCs of both P2- and P14-injected cohorts (Figure 30A, C). IPSCs with fast rise times and larger amplitudes arise from synapses located closer to the soma (Banks et al., 1998; Goswami et al., 2012; Lazarus and Huang, 2011; Maccaferri et al., 2000; Pearce, 1993; Xiang et al., 2002). Although there were no differences in the IPSC kinetics between MCs and TCs, this correlation displayed in MCs suggests that a higher proportion of light-evoked IPSCs in MCs may arise from synapses closer to the soma.

Photoactivation sometimes evoked a long-lasting barrage of events (Figure 15A, bottom left) that was visible in both MCs and TCs. These events are mediated by asynchronous GABAergic release from GCs (Isaacson and Strowbridge, 1998; Kapoor and Urban, 2006; Schoppa et al., 1998). The timing of these barrages as assessed by the rise time of peak population IPSC frequency did not differ between MCs and TCs in either the P2- or P14-injected cohorts (Figure 25D).

In summary, the differences in both the probability for MCs vs. TCs to connect with P2- and P14-transduced GCs and the strength of those connections were not statistically significant and thus cannot be said to wholly account for the initial differences observed in the overall strength of inhibition onto MCs vs. TCs. Nevertheless, the trends in these two measurements suggest that they may be at least contributing factors to the overall difference, and this possibility is supported by the increased IPSC amplitudes in MCs following photostimulation and the more pronounced difference in the P14-injected cohort.

3.3.3 Differences in functional connectivity may arise from anatomical segregation of postnatal-born GCs

Overall, I observed a trend for P14-transduced GCs to form more connections with MCs than with TCs (Figure 20), and the strength of inhibition was also more pronounced in P14 MCs (Figure 28). The difference in the strength of inhibition was also statistically significant in the P2-injected cohort, but differences between MCs and TCs were more subtle (Figure 27). The preferential connection of P14-transduced GCs with MCs is supported by previous anatomical work showing that the dendrites of both MCs and deep GCs are located in the deeper EPL (Mori et al., 1983; Orona et al., 1983). If P14-transduced GCs were located deeper in the GCL compared to P2-transduced GCs given their birth dates (Lemasson et al., 2005), then their dendrites would be more likely to contact the dendrites of MCs than of TCs.

P2-transduced GCs appeared equally likely to target both MCs and TCs (Figure 20), which could be explained by dendrodendritic synapses forming all along a GC's apical dendrite as it courses up toward the GL. GC-mediated inhibition onto MCs and TCs occurs primarily outside of the GL on secondary dendrites or perisomatic sites, and MCs with truncated apical dendrites show

little decrease in the rate of sIPSCs compared to MCs with intact apical dendrites (Arnson and Strowbridge, 2017). Thus, a more superficial P2-transduced GC could make dendrodendritic synapses with MCs on its proximal apical dendrite and synapses with TCs on its distal apical dendrite.

One caveat is that I only targeted middle TCs in the middle region of EPL for recordings and did not include external TCs, superficial TCs, or internal TCs. External TCs are a population of juxtaglomerular cells that establish excitatory connections with other juxtaglomerular neurons and do not have basal dendrites (De Saint Jan et al., 2009; Hayar et al., 2004a; Hayar et al., 2004b). Superficial TCs reside at the border between the GL and the EPL and display short apical dendrites and basal lateral dendrites (Griff et al., 2008; Jones et al., 2020). Internal TCs are located in the deepest section of the EPL, often adjacent to the mitral cell layer, and have large cell bodies and physiological properties resembling those of MCs (Orona et al., 1984). By limiting my analysis to middle TCs, I hoped to limit the heterogeneity observed within cells from the same cell type and eliminate confounding variables such as differences in somatic or dendritic locations (Nagayama et al., 2014). This decision may also have biased my recordings to only a subset of middle TCs. Despite the sparsity of TC somata in the EPL, more comprehensive and systematic recordings of TCs occupying the superficial, middle, and deep portions of the EPL may reveal more pronounced differences in their connectivity with subpopulations of postnatal-born GCs.

I performed my slice recording experiments in both P2- and P14-injected cohorts at four weeks post injection; therefore, the subpopulations of transduced GCs activated by photostimulation in both cohorts should be developmentally identical. Studies have shown that postnatal-born GCs are fully mature by four weeks after birth (Carleton et al., 2003; Petreanu and Alvarez-Buylla, 2002). Dendritic development in both P14- and adult-transduced GCs is stable

four weeks after injection, showing similar spine dynamics and turnover rates (Sailor et al., 2016). Additionally, there are no differences in the dendritic morphology of P12- and adult-transduced GCs at five weeks post injection (Hardy et al., 2018). I did attempt to perform recordings in a separate cohort of P2-injected animals at six weeks post injection (Figure 21) but encountered technical difficulties; nevertheless, given that IPSC kinetics were similar between both cohorts, I concluded that the transduced-GCs in both cohorts were comparable (Figure 29).

Although the segregation of postnatal-born GC somata according to their birth date is well-established (Imayoshi et al., 2008; Lemasson et al., 2005; Orona et al., 1983; Sakamoto et al., 2014), to my knowledge, there has been no study specifically investigating the correlation of postnatal-born GC dendrite locations with their birth date. One study has identified two populations of postnatal-born GCs, with their soma and dendrites occupying either the deep or superficial EPL (Carleton et al., 2003), but the authors did not differentiate between the birth dates of the GCs. It is also likely that the anatomical segregation of postnatal-born GCs resembles a gradient rather than a stark division. In a study comparing the somatic locations of P0- vs. P42-transduced GCs, the authors found that both subpopulations occupy both the deep and superficial GCL, albeit at different proportions of the overall transduced population (P0-transduced: 20% in sGCL, 20% in dGCL; P42-transduced: 30% in sGCL, 45% in dGC) (Muthusamy et al., 2017).

In summary, I demonstrate subtle differences in the overall strength of inhibition of P2- and P14-transduced GCs with MCs vs. GCs. Though these differences are slight, they do cohere with known anatomical differences in the dendritic locations of postnatal-born GCs and of MCs and TCs, suggesting that anatomical segregation of dendrites in the EPL does result in differences in functional connectivity between subpopulations of postnatal-born GCs and OB output neurons.

3.4 Materials and Methods

3.4.1 Experimental design and animals

All animal procedures, mouse breeding, and animal housing were in compliance with guidelines established by the Institutional Animal Care and Use Committee at the University of Pittsburgh (Protocol #18103723). All animals used were C57BL/6J mice of both sexes purchased from Charles River. The adeno-associated virus AAV2-hSyn-hChR2(H134R)-EYFP (titer: 5.6e1012 iu/ml) was purchased from UNC Vector Core and used to drive expression of channelrhodopsin-2 (ChR2) and the fluorescent protein EYFP in neuroblasts migrating in the RMS. For the early postnatal-born cohort (n = 8 mice), mice were injected with AAV2-hSyn-ChR2-EYFP virus at P2, weaned at P21, then sacrificed for electrophysiology experiments between P28-33. For the late postnatal-born cohort (n = 7 mice), mice were injected with the same virus at P14, weaned at P21, then sacrificed for experiments between P42-44.

3.4.2 Neonatal AAV2 injection

Injection of neonatal pups was performed as described previously (Cheetham et al., 2015). P2 mouse pups were cryoanesthetized by placement on a wet paper towel, which was then placed on ice to avoid direct contact of the mice with ice. Anesthetization was confirmed by lack of response to toe pinch. Injections were made using a pulled glass micropipette connected via tubing to a 1 ml syringe. Negative pressure was applied using the syringe to draw up 1 µl of virus into the micropipette. The anesthetized pup was then placed on the bench surface and the head secured. The tip of the micropipette was inserted through the skull to a depth of 2 mm. Gentle positive

pressure was applied via the syringe to inject the virus into the brain. Injection site was targeted relative to the visible landmarks; injections were made halfway between lambda and the intersection of the inferior cerebral vein and the superior sagittal sinus and 0.5 mm lateral to the superior sagittal sinus for both hemispheres. Following injection, the pups were placed on a heated pad and returned to their cages once awake.

3.4.3 Stereotaxic surgery

P14 animals were anesthetized using vaporized isoflurane and checked for complete sedation via toe pinch reflex and breathing rate patterns. Animals were then placed on the stereotaxic instrument, the surgical site shaved and sterilized, and a small craniotomy performed above the injection site. Injection coordinates were (in mm): Antero-Posterior, 1.0; Medio-Lateral, ±1.0, for both right and left hemispheres, respectively, Dorso-Ventral: 2-2.5. About 500 nl virus was injected at the depths of 2.0 and 2.5 mm in each hemisphere. Depth of anesthesia was monitored throughout the surgical procedure. Following surgery, animals were returned to their cages and given standard post-op care.

3.4.4 Slice electrophysiology

Mice were deeply anesthetized with isoflurane and decapitated into ice-cold oxygenated slicing solution containing (in mM): 93 N-Methyl-D-glucamine (NMDG), 2.5 KCl, 1.2 $NaHCO_3$, 30 $NaHCO_3$, 20 HEPES, 25 glucose, 5 sodium ascorbate, 2 thiourea, 3 sodium pyruvate, 10 $MgCl_2$, and 0.5 $CaCl_2$, pH 7.4 (Ting et al., 2014). The olfactory bulbs were dissected, and coronal slices (310 μm thick) were prepared using a vibratome (Ci 5000 mz2; Campden Instruments). Slices

recovered in ACSF at 35°C for 15 min in a solution containing (in mM): 92 NaCl, 2.5 KCl, 1.2 $NaHCO_3$, 30 $NaHCO_3$, 20 HEPES, 25 glucose, 5 sodium ascorbate, 2 thiourea, 3 sodium pyruvate, 2 $MgCl_2$, and 2 $CaCl_2$, pH 7.4 (Ting et al., 2014). Slices were rested at room temperature until recording. Slices with visible ChR2-EYFP expression in cell types other than granule cells (GCs) were not used for recording.

During recording, slices were continuously superfused in Ringer solution warmed to 35°C. The recording Ringer solution contained (in mM): 125 NaCl, 25 glucose, 2.5 KCl, 25 $NaHCO_3$, 1.25 NaH_2PO_4, 1 $MgCl_2$, and 2.5 $CaCl_2$, pH 7.4. Voltage clamp recordings were made using electrodes filled with (in mM): 10 HEPES, 150 CsCl, 10 sodium phospho- creatine, 3 Mg-ATP, and 0.3 Na3GTP, 10 mM QX-314, and 0.025 Alexa Fluor 594 (Life Technologies, Carlsbad, CA). Pipettes were pulled from borosilicate capillary tubing (King Precision Glass) to a resistance of 5-8 MΩ on a P-97 Flaming/Brown Micropipette Puller (Sutter Instruments) and fire polished.

Whole-cell patch-clamp recordings were made using a Multiclamp 700A amplifier (Molecular Devices) and an ITC-18 acquisition board (Instrutech) controlled by custom software written in Igor Pro (WaveMetrics) (MIES, Allen Institute). Electrophysiological data were low-pass filtered at 4 kHz and sampled at 25 kHz for the P2 dataset and 10 kHz for the P14 dataset. MCs and TCs were identified under an IR-DIC microscope by shape and location in olfactory bulb laminae. I only targeted TCs residing in the EPL to ensure a homogeneous population of recorded TCs. Pharmacological blocking agents used were the $GABA_A$ receptor antagonist gabazine (50 µM), the NMDA receptor antagonist DL-2-amino-5-phosphonovaleric acid (APV, 20 µM), and the AMPA receptor antagonist 2,3-dihydroxy-6-nitro-7-sulfamoyl-benzo(F)quinoxaline (NBQX, 10 µM). Cells were only included for analysis if their holding current at -70 mV was less than -300 pA. Recordings were excluded from analysis if the series resistance exceeded 35 MΩ.

3.4.5 Optogenetic stimulation

At least 10 minutes elapsed between cell selection and the start of photoactivation experiments. For photoactivation of postnatal-born GCs, slices were illuminated (100 ms light pulse) by a 75 W xenon arc lamp passed through a YFP filter set and 60x water-immersion objective centered on the glomerular layer. An open field stop was used to activate all GCs expressing ChR2 in the slice. IPSCs were recorded in the presence of APV and NBQX for 5.5 s following optogenetic stimulation, for 30 Light trials per cell. The inter-trial interval was 12s. Thirty Light Off trials per cell were also collected using identical parameters as the Light trials but without optogenetic stimulation. Gabazine was applied at the end of successful recordings to confirm that the recorded photoactivated currents were GABAergic.

3.4.6 Identification of IPSCs

All data were analyzed using custom scripts written in Python and MATLAB (Mathworks). IPSCs were detected using a machine-learning optimal-filtering method (MOD) developed by members of Dr. Peter Jonas' group at the Institute of Science and Technology Austria (Zhang et al., 2021). Briefly, two trials at both the beginning and end of each set of trials for each cell were manually scored to identify all IPSCs. The algorithm was then trained to predict the manual scoring and obtain the optimal coefficients of a Wiener filter. This process generates a raw detection trace that closely matches the manual scoring trace and has a high signal-to-noise ratio. Next, the optimal detection threshold was calculated by finding the threshold that maximized Cohen's κ coefficient, and the threshold was used to convert the raw detection trace into a binary detection trace, which then determined whether a point on the trace was an event.

3.4.7 Analysis of IPSC kinetics and frequency

For each set of trials (Light and Light Off), the mean current trace was obtained by taking the average of all trials within the set. The baseline was calculated by taking the mean current values before stimulus onset. The peak of the mean trace was obtained by identifying the most negative value within 150 ms after stimulus onset, and the mean trace time to peak was defined as the amount of time elapsed from response onset (5% of peak) to time of peak.

Peristimulus time histograms (PSTHs) for IPSCs were calculated using a bin width of 10 ms and pooling the events across all trials in each set of trials. The frequency of IPSC rates for each cell was calculated by fitting firing rates in the PSTH with a Gaussian smoothing function (Olson et al., 2000). As with the mean current trace, the baseline frequency of each set of trials was calculated by taking the mean frequency value before stimulus onset. The peak frequency was obtained by finding the maximum value within 150 ms after stimulus onset, and the rise time was calculated using 20-80% of peak frequency.

The amplitude of each IPSC was obtained by finding the peak value in a window around each MOD-identified event position and subtracting the baseline value (defined as the "root" point before event onset). The rise time was defined as 20-80% peak, and a single decay exponential was fit to each event to obtain the decay constant tau. Spurious events with amplitude < 10 pA or tau > 100 ms were excluded from analysis.

3.4.8 Perfusion, immunohistochemistry, and image analysis

Mice were anesthetized with 0.4 ml ketamine (20 mg/ml)/xylazine (3.3 mg/ml) and transcardially perfused with ice-cold 1% NaCl in 0.1 M phosphate buffer (PB), followed by 4%

paraformaldehyde (PFA). The brains were then dissected, fixed overnight in PFA, then sunk in 30% sucrose. Following fixation, brains were sliced into 25 µm thick sections using a sliding microtome (Leica, SM2000R) into 12-well plates with 1 ml of 0.1 M PB solution containing 0.05% Na azide and 0.005% Tween 20. Following washing with PB, sections were labeled with Alexa Fluor 488 donkey anti-mouse antibody (Invitrogen) at 1:600 in PB containing 2% NDS and 0.05% Tween 20 with 1:40,000 Hoechst 33342 (Invitrogen) for 1 h at RT in the dark. After a final three washes in PB, sections were mounted on collagen coated slides with gelvatol for imaging and analysis. Images were collected using Eclipse 90i large area-scanning widefield microscope equipped with a Plan-Apo 10x/0.45 NA air objective and Elements software (Nikon).

Quantification of fixed electrophysiology slice sections (n = 9 for P2 dataset, n = 7 for P14 dataset) was performed by quantifying the total integrated intensity for the GCL in each section, then normalizing the intensity to the area of the GCL to obtain an integrated density/area value for each section. The integrated density/area value was plotted against the proportions of cells that had a light-evoked response recorded in each slice and the mean IPSC frequency of all the cells from that slice.

3.4.9 Statistical analyses

Electrophysiological recordings were analyzed using custom scripts written in Python and MATLAB (Mathworks). All statistical analyses were performed using Python scripts or Prism 9 (GraphPad). Fisher's exact test was used to compare proportions of responding neurons. Paired t-tests were used to determine whether a cell had a light-evoked response after stimulus onset. Two-way repeated measures ANOVA with Dunnett's multiple comparisons test was used to compare event kinetics between different response windows within the same cell type. Two-sample

Anderson-Darling tests were used to compare between MCs vs. TCs. Correlations between measurements were tested using the Spearman rank-order test.

4.0 Discussion

In this dissertation, I investigated how postnatal neurogenesis in the olfactory epithelium (OE) and olfactory bulb (OB) contribute to olfactory circuitry. First, I demonstrated that immature olfactory sensory neurons (OSNs) can make functional monosynaptic connections with superficial tufted cells (STCs) of the OB as soon as five days after terminal cell division. Analysis of the kinetic properties of these connections showed that the excitatory inputs from immature OSNs are similar to those from mature OSNs. These results from Chapter 2 suggest that immature OSNs are capable of transducing odor signals to the OB and may participate in normal olfactory processing alongside mature OSNs.

Next, I studied whether the birth date related anatomical segregation of postnatal-born granule cells (GCs) in the OB results in preferential connectivity with mitral cells (MCs) or tufted cells (TCs). By selectively activating either early or late postnatal-born GCs using optogenetics and recording inhibitory currents in MCs and TCs, I showed that subtle differences exist in the functional connectivity of early and late postnatal-born GCs. Early postnatal-born GCs show a similar probability of being connected to MC and TCs, whereas late postnatal-born GCs show a trend of being preferentially connected to MCs. Additionally, inhibition from both subgroups of postnatal-born GCs is stronger onto the overall population of MCs than TCs. Collectively, the results from Chapter 3 suggest that anatomical differences do indeed translate to functional differences in connectivity between postnatal-born GCs and the principal output neurons of the OB.

4.1 The functional connectivity of immature OSNs

The data in Chapter 2 showed that Gγ8-expressing OSN axons provide monosynaptic excitatory inputs to STCs. About 98% of Gγ8^{+} axons also express GAP43, a classical marker of OSN immaturity (Cheetham et al., 2016). The distribution of Gγ8 expression in the olfactory epithelium (OE) and its subcellular localization are similar to those of GAP43, and both markers are expressed in similar developmental stages (Tirindelli and Ryba, 1996). My initial set of experiments did not differentiate between Gγ8-expressing axons of OSNs born at different times; in order to disentangle any age-related differences between immature OSN axons, I used a methimazole (MMZ) ablation model in which only immature OSNs are present at time points shortly following MMZ treatment.

At five days after MMZ treatment, I was able to record monosynaptic excitatory currents in 1 out of 13 STCs following photoactivation of Gγ8-expressing OSN axons, suggesting that the functional connection between an immature OSN and the OB can be formed as early as five days after terminal cell division. In these experiments, I administered doxycycline-fortified chow to mice to restrict ChIEF-Citrine expression to only newly generated Gγ8-expressing OSN axons and not degenerating axons of OSNs that were ablated with MMZ. Although the axons of newly generated OSNs will have arrived into the OB by five days (Rodriguez-Gil et al., 2015), given the nature of acute slice electrophysiology experiments, the density of these axons in any given OB slice is low, resulting in a low probability of recording light-evoked EPSCs at five days post MMZ treatment. In future experiments, I could increase the number of animals recorded at different time points post MMZ treatment in order to obtain a clearer timeline for functional synapse formation by immature OSNs.

The current set of experiments involved recording light-evoked EPSCs in STCs, which are known to receive monosynaptic input from mature OSNs; STCs are relatively abundant in number and easy to identify in the glomerular layer (GL) compared to other subtypes of TCs (Sun et al., 2020). TCs are also subject to weaker lateral inhibition than MCs (Geramita et al., 2016), and given that I used multiglomerular optogenetic stimulation to activate labeled OSN axons, recording from cells receiving weaker lateral inhibition would increase the probability of observing light-evoked excitatory currents. Both MCs and TCs receive mature OSN input, although the connection is weaker in MCs compared to TCs (Bourne and Schoppa, 2017; Najac et al., 2011). Most studies characterizing TCs have focused on STCs and external tufted cells (ETCs), both of which receive strong direct OSN input (De Saint Jan et al., 2009; Gire et al., 2012; Najac et al., 2011; Sun et al., 2020). Evidence does exist, however, for stronger OSN input onto classic middle TCs compared to MCs (Burton and Urban, 2014; Gire et al., 2012). Characterizing the innervation of MCs and other TC subtypes by immature OSNs and comparing these connections with those formed by mature OSNs could provide more comprehensive insight into maturity-dependent differences in the connectivity of OSNs onto OB neurons. Additionally, whether immature OSNs also provide input to GL interneurons is unknown and would be a valuable question for future study.

Given that immature OSNs provide odor input to the OB much earlier than previously thought, they may play a role in olfaction that is complementary to mature OSNs. In normal development, immature OSNs must receive odor input and form functional synapses with OB neurons in order to survive (Watt et al., 2004). The dependence of immature OSNs on sensory input is supported by the fact that naris occlusion reduces the number of OSNs in the OE (Cavallin et al., 2010). Additionally, immature OSNs may provide odor information on a more rapid or dynamic time scale compared to information provided by mature OSNs. Immature OSNs display

a higher rate of synapse formation and elimination compared to mature OSNs, and this level of synaptic plasticity was reduced with naris occlusion (Cheetham et al., 2016). The plasticity of immature OSN synapses makes them uniquely suited to encode dynamically updated information, such as novel odor experience when the animal is adapting to new sensory environments. The ability for immature OSNs to respond to novel odor input would also be particularly valuable during both the animal's developmental stage and periods after injury or disease, when there are no mature OSNs present but odor processing is critical to the animal's survival.

4.2 Neurotransmitter release from degenerating OSN axons

While optimizing the MMZ treatment experiments, I was surprised to observe light-evoked EPSCs in OB slices at early time points when there should be no newly generated ChIEF-Citrine-expressing OSN axons present in the OB. After limiting ChIEF-Citrine expression to only newly generated OSN axons, I no longer observed any light-evoked EPSCs until five days post MMZ treatment, which was in agreement with the developmental timeframe of OSNs (Liberia et al., 2019; Rodriguez-Gil et al., 2015; Savya et al., 2019). This unexpected observation could be explained by neurotransmitter release from degenerating, ChIEF-Citrine-expressing OSN axons in recorded OB slices; a similar observation was made by Grubb et al. when they observed EPSCs in STCs following electrical stimulation of the olfactory nerve layer at seven days post MMZ treatment (Browne et al., 2022). Ablation with MMZ causes cell death in the somata of OSNs, which are found in the OE, but leaves residual degenerating axons in the OB. There has been no characterization of these degenerating axons beyond noting their presence (Blanco-Hernández et al., 2012; Kikuta et al., 2015; Tsai and Barnea, 2014). Understanding the physiological properties

of neurotransmitter release from degenerating synapses and axons may provide additional insight into circuit changes during neurodegeneration or spinal injury (Gillingwater and Ribchester, 2001; Neukomm and Freeman, 2014; Pemberton et al., 2020).

It is tempting to speculate on the functional significance of neurotransmitter release mediated by degenerating axons, especially following injury to the olfactory system. Release from degenerating axons may act as guiding signals for axonal targeting of new OSNs to maintain or re-establish glomerular targeting patterns. Of all the OE ablation techniques, MMZ treatment exhibits the best regenerated glomerular map (Rodriguez-Gil et al., 2015), followed by other chemical ablation methods (Cheung et al., 2014; John and Key, 2003), then surgical transection (Christensen et al., 2001; Costanzo, 2000). Treatment with dichlobenil, an olfactory toxicant, ablates the OE and results in axonal mistargeting that persists at four months after ablation (John and Key, 2003; Vedin et al., 2004). Ablation using other chemical methods such as intranasal zinc sulfate administration and methyl bromide also results in alteration or loss of the glomerular map (Burd, 1993; Schwob et al., 1995). Conventional surgical transection techniques cause damage to the outer layers of the OB and to the cribriform plate (Costanzo, 2000; Kobayashi and Costanzo, 2009), resulting in extensive injury that disrupts the structures provided by support cells and glia involved in axonal guidance (John and Key, 2003).

Unlike the ablation methods described above, MMZ treatment spares the lamina propria of the OE, a region responsible for early fasciculation and organization of OSN axon bundles for axonal targeting (Blanco-Hernández et al., 2012). The presence of both residual degenerating axons in the OB, combined with an intact lamina propria, may contribute to improved regeneration of the glomerular map by allowing newly generated OSN axons to use degenerating axons for guidance and re-innervation of previously targeted glomeruli.

Despite the sparsity of responses I observed in MMZ-treated animals that were previously given doxycycline-fortified chow, it is also possible that MMZ ablation and deafferentation could result in an overall increased gain in OB activity. A previous study reported increased gain in odor responses following sensory deprivation with nose plugs (Barber and Coppola, 2015). Additionally, sensory deprivation using a variety of techniques such as zinc sulfate treatment, naris occlusion, and deafferentation leads to changes in GluR1 expression levels in the GL, external plexiform layer (EPL), and mitral cell layer (MCL) (Hamilton and Coppola, 2003; Hamilton et al., 2008; Tyler et al., 2007). Modulation of AMPA receptor expression could act as a form of gain control in response to changes in sensory input. It would be interesting to measure the intrinsic properties of MCs and TCs after MMZ treatment to see whether odor deprivation could cause changes in the intrinsic excitability of OB output neurons.

4.3 Differences between subtypes of GCs

To my knowledge, the results presented in Chapter 3 are the first to specifically investigate differences in the functional connections between early and late postnatal-born GCs and MCs vs. TCs. Our lab has previously shown that, in response to activation of a single glomerulus, a higher proportion of superficial GCs are recruited and show larger EPSC amplitudes compared to deep GCs. Superficial GCs have a more hyperpolarized action potential (AP) threshold and higher firing rates in response to step current injections, which may explain the differences observed in the study (Geramita et al., 2016).

Accordingly, I also attempted to record from postnatal-born GCs transduced at P2 and P14 and compare both the intrinsic properties of and feedforward excitation onto early vs. late

postnatal-born GCs, but technical difficulties prevented me from obtaining any meaningful data. However, a previous study has noted that the distribution of presynaptic $GABA_BR1$ in postnatal-born synapses is different in GCs born at P6 vs. P60, and that presynaptic $GABA_BR1$ regulates GABA release from P60 GCs but not P6 GCs. The authors also recorded light-evoked IPSCs in MCs following activation of either GC subgroup and found that the amplitude of light-evoked IPSCs was not significantly different following activation of P6 vs. P60 GCs (Valley et al., 2013).

Characterizing the strength of excitation from MCs vs. TCs onto early and late postnatal-born GCs would complement my current data, but current markers for labeling MCs vs. TCs may not be selective enough for this purpose. PCdh21 and Tbx21 label both MCs and TCs and have been used to optogenetically activate both populations (Faedo et al., 2002; Haddad et al., 2013; Mitsui et al., 2011; Wachowiak et al., 2013). Markers selective for MCs are limited: in some transgenic lines, Thy1 is somewhat selectively expressed in MCs (Arenkiel et al., 2007; Chen et al., 2012; Dana et al., 2014; Nishizumi et al., 2019), though a recent study has also identified the Lbhd2 gene to be specifically expressed in MCs (Koldaeva et al., 2021). Candidates for TC-specific markers are more promising: CCK appears to be preferentially expressed in TCs over MCs (Cheetham et al., 2015; Seroogy et al., 1985), but most applications rely on anatomical segregation and involve comparisons of STCs and MCs (Economo et al., 2016; Short and Wachowiak, 2019). A subset of STCs also express vasopressin (Lukas et al., 2019). Ongoing advances in bulk and single-nucleus RNA sequencing have identified additional molecular markers that could be used to selectively label MCs and all TC subtypes (Zeppilli et al., 2021). Expressing a channelrhodopsin in MCs or TCs labeled by these markers would allow selective optogenetic activation of the cell types and enable direct comparison of their excitatory inputs onto subpopulations of GCs.

A logical follow-up to characterizing the synapses between postnatal-born GCs and MCs and TCs would be to compare whether the GC subpopulations differentially modulate MC and TC output. I briefly attempted to address this question by injecting step currents in MCs and TCs to evoke spike trains while optogenetically activating P2 or P14 GCs on interleaving trials, but I did not observe any difference in spiking activity and encountered additional technical problems, so I abandoned this direction. Lledo and colleagues previously expressed ChR2 in a single population of adult-born GCs and demonstrated a clear reduction in MC output during photoactivation of GCs. Interestingly, they also noted a dramatic increase in synapse formation between four to six weeks after virus injection into the rostral migratory stream (RMS) (Bardy et al., 2010). It is possible that I did not observe any reduction in MC and TC spiking activity in my limited experiments because the number of synapses present at four weeks post injection was not sufficient to produce a noticeable effect.

Another possible difference among postnatal-born GCs is their biochemical identity; different biochemical subpopulations of GCs correspond to different birth windows and are implicated in odor discrimination (Batista-Brito et al., 2008). Calretinin$^-$ GCs are superficial in the granule cell layer (GCL), and pharmacogenetic inhibition leads to impaired olfactory discrimination (Hardy et al., 2018); although they represent a small proportion of prenatally-generated GCs, they are the most numerous biochemical subgroup out of all postnatally-generated GCs (Batista-Brito et al., 2008). CaMKIIα^+ GCs are found in all depths of the GCL and required for odor discrimination (Malvaut et al., 2017). 5T4$^+$ GCs are located even more superficially than Calretinin$^+$ GCs in the GCL and can sometimes be found in the MCL; they form synapses with ETCs and MCs, and mice with genetic knockout of 5T4 show impairments in odor discrimination (Imamura et al., 2006; Takahashi et al., 2016). In agreement with the superficial location of their

somata, a slightly higher proportion of $5T4^+$ GCs are generated prenatally, but they also continue to be generated throughout the animal's life (Batista-Brito et al., 2008). I was interested in whether my P2 and P14 viral injections transduced biochemically distinct subpopulations of GCs, but the antibodies I used failed to provide accurate staining.

This dissertation focuses on differences between P2 vs. P14-transduced GCs, but it would also be interesting to compare subgroups of GCs born at time points that are farther apart. Although the experiments may be technically challenging given the age of the mice at time of recording, I could perform viral injections in mice at P30 or P60 and compare the transduced GCs with GCs labeled at P2 and P14. A previous study compared P0 vs. P60 adult-born GCs and showed that increasingly complex olfactory learning tasks recruited additional numbers of P60 adult-born GCs, and the P60 GCs displayed increased spine plasticity all along their apical dendrites; these changes were limited in P0 GCs and only occurred after increasing the complexity of the olfactory tasks (Forest et al., 2020). *In utero* electroporation (Sánchez-González et al., 2020) or embryonic injections of AAV vectors (Togashi et al., 2020) could also be used to label prenatally-generated GCs with high specificity, allowing for comparisons between prenatal and postnatal-born GCs.

4.4 The dendritic properties of GCs

I initially expected early postnatal-born GCs to preferentially connect with TCs for two reasons: 1) early postnatal-born GCs occupy the superficial layers of the GCL (Lemasson et al., 2005) and the dendritic arbors of superficial GCs are found in the superficial EPL, and 2) the dendrites of TCs are mostly found in the superficial EPL (Mori et al., 1983; Orona et al., 1984). My data from Chapter 3, however, show that early postnatal-born (P2-transduced) GCs show an

equal probability of being connected to MCs and TCs, whereas late postnatal-born (P14-transduced) GCs show a trend of being preferentially connected with MCs.

This observation is supported by anatomical work showing the existence of not only GCs with dendritic spines either in the superficial or deep EPL, but also of GCs with widespread distribution of gemmules from the MCL to superficial EPL (Geramita et al., 2016; Mori, 1987; Mori et al., 1983; Shepherd et al., 2007). The depths of the somata of these GCs have not been characterized, but it is possible that their somata occupy the intermediate EPL, or that my P2 injections transduced GCs from this population. GCs with gemmules along the entire length of their dendrites would be able to form synapses with both MCs and TCs, and evidence exists for GCs that synapse with both MCs and TCs (Arnson and Strowbridge, 2017). Differential functional organization of spines along the dendrite could also lead to differential inhibition onto subsets of MCs and TCs (Woolf et al., 1991). Axodendritic synapses are found on the proximal apical and basal dendrites of GCs, where GCs receive excitatory inputs from the axon collaterals of MCs, TCs, and feedback projection fibers; there is no evidence for GC-mediated GABAergic release from these sites (Mori, 1987). Thus, GABAergic release from the proximal apical and basal dendrites of GCs is unlikely to mediate the light-evoked IPSCs shown in my data.

Additionally, it is also possible that the somata of early vs. late postnatal-born GCs are found at a spectrum of depths in the EPL instead of only occupying the superficial or deep regions. A more graded difference in either the distribution of gemmules or GC somata within the EPL between P2- and P14-transduced GCs would result in the subtle differences in connectivity that I observed in my data. Comparison of time points that are farther apart, such as GCs transduced at P2 vs. P60, may reveal more distinct anatomical differences.

4.5 Implications for olfactory circuitry

A glomerular column, simplified for our purposes, consists of the MCs and TCs whose apical dendrites innervate a particular glomerulus and the GCs receiving excitation from those MCs and TCs (Burton and Urban, 2014; Egger, 2008; Kim et al., 2011; Schoppa et al., 1998; Willhite et al., 2006). Modeling studies suggest that APs generated by MCs during olfactory experience and learning propagate down the lateral dendrites of MCs, where they contact GCs (Migliore et al., 2007). The synaptic activity strengthens MC-GC synapses located along those contacting dendrites and contributes to the formation of a glomerular column. GC dendrites extend in a range of around 25-100 μm and are capable of contacting 3-5 glomeruli (Arnson and Strowbridge, 2017; Kim et al., 2011; Orona et al., 1983; Price and Powell, 1970b). A GC that belongs to one glomerulus can enable lateral inhibition of MCs and TCs that belong to another glomerulus (Chatterjee et al., 2016; Egger and Kuner, 2021). Lateral inhibition mediated by GCs is involved in the decorrelation of odor-evoked responses in MCs and TCs, which is critical in the patterning of glomerular maps and odor discrimination (Arevian et al., 2008; Gschwend et al., 2015; Urban and Sakmann, 2002; Yokoi et al., 1995).

Inhibition from GCs also modulates gamma and beta oscillations in the local field potentials of the OB, which have been shown to reflect synchronized neural activity during olfactory processing, memory, and learning (Lagier et al., 2007; Martin and Ravel, 2014; Schoppa, 2006). MC-to-GC synapses that are proximal on the lateral dendrite of the MC play a large role in MC synchrony, whereas distal MC-to-GC synapses are negligible, as expected. Distant MCs can be synchronized if they share GCs via their lateral dendrites (McTavis et al., 2012). It is possible that TCs are also more strongly modulated by more proximal synapses with GCs.

Spatially distinct inhibitory connections that are dependent on the birth date of the GC could promote the formation of glomerular columns that are also birth date-dependent. A given glomerular column contains both early and late postnatal-born GCs (Willhite et al., 2006), which may preferentially mediate lateral inhibition with MCs or TCs. For example, the survival of superficial early postnatal-born GCs is more sensitive to odor exposure, and superficial 5T4-expressing GCs show sensory input-dependent dendritic plasticity (Lemasson et al., 2005; Yoshihara et al., 2012). Early postnatal odorant exposure increases the strength of lateral inhibition onto TCs but not MCs, which could be due to the putative preference for superficial, early postnatal-born GCs to connect with TCs (Geramita and Urban, 2016). Different glomerular columns could be recruited in different olfactory behaviors (Bear et al., 2016), and stronger lateral inhibition of the TCs or MCs in each column bears consequences for how odor signals are represented and transformed before they are sent to higher cortical areas for further processing (Fukunaga et al., 2012; Kikuta et al., 2013; Nagayama et al., 2010; Nagayama et al., 2004).

4.6 Contributions of adult neurogenesis

The healthy brain must maintain a balance between stability and plasticity. New neurons must integrate without disrupting existing functions, but at the same time, the brain should also be able to adapt to changes in the environment, learn new information, and repair injuries. A central question is whether new neurons generated via adult neurogenesis bring unique contributions to the circuitry. In this dissertation, I show that immature OSNs make functional connections with the OB, suggesting that they may provide an additional layer of plasticity along with mature OSNs. Additionally, I demonstrate that the functional connectivity of postnatally-generated GCs with OB

output neurons show subtle differences depending on whether the GCs were born in the early vs. late postnatal period. Differences in functional connectivity lead to differential inhibition of MCs vs. TCs, which have wide implications for olfactory processing.

If adult-born neurons are eliminated in response to environmental or behavioral states, this suggests that adult neurogenesis is also a means of shaping the sensory system to better represent the odor environment, rather than simply replenishing neurons via turnover. Two previous studies of postnatal-born GCs from the Lledo group support this hypothesis. In agreement with previous work demonstrating that the bulk of GC turnover occurs in late postnatal-born GCs (Lemasson et al., 2005), Lledo and colleagues showed that olfactory learning altered turnover only in deep GCs, which are composed of mostly late postnatal-born GCs (Mouret et al., 2008). Perhaps the type of olfactory learning assessed by the authors preferentially involved late postnatal-born GCs and specifically activated MC-GC synapses. MCs and TCs experience lateral inhibition at different firing rates and perform odor discriminations at different concentration ranges (Geramita et al., 2016), so it is possible for different olfactory tasks and behaviors to preferentially employ GC inhibition of MCs or TCs.

Another study from the Lledo group found that increased adult neurogenesis following olfactory learning was not uniformly distributed across the GCL, but GCL depths were not analyzed (Alonso et al., 2006). The difference in the location of GC changes observed in this study compared to the Mouret et al., 2008 study could be explained by the learning paradigms used: the 2008 study used a go/no-go odor discrimination task, whereas Alonso et al., 2006 used a buried food task. Despite these variations in experimental design, both studies showed that different postnatal-born GC subpopulations are sensitive to changes induced by olfactory tasks. Postnatal-born neurons may represent a pool of neurons with enhanced synaptic plasticity and

responsiveness to olfactory learning and act as the primary mediators in neural representations of a changing environment.

4.7 Plasticity in adult-born olfactory neurons

In the OE, the continuous replacement of OSNs allows an animal to constantly adapt its olfactory receptors (ORs) to its environment. The fact that immature OSNs form functional synapses with OB neurons (as shown in Chapter 2) adds another level of plasticity to an already highly plastic system. The genetic profiles of OSNs are sensitive to the animal's odor environment, and transcriptional changes influence the response properties of OSN odor-evoked responses (Tsukahara et al., 2021).

In the OB, postnatal-born GCs show uniquely plastic properties in both the immature and mature stages (Hardy and Saghatelyan, 2017; Livneh et al., 2014). During synaptic development in adult-born GCs, odor deprivation reduces glutamatergic input at the distal apical and basal dendrite but increases glutamatergic synapses in the proximal apical dendrite. After synaptic development is complete, however, odor deprivation increases synapses in the proximal apical dendrite and not the basal and distal dendrite. This difference in dendritic domain suggests that the proximal apical dendrite may have synaptic plasticity that persists longer than that in the basal and apical dendrite (Kelsch et al., 2009). Unlike the somatosensory and visual systems that show a refinement of excitatory connections during maturation (Gordon and Stryker, 1996; Iwasato et al., 1997), the sensory maps of GC odor-evoked activity are broadened as the GCs mature, and these changes are accompanied by increased excitatory inputs onto the GCs. Sensory experience accelerates these features of maturation. Interestingly, sensory deprivation via naris occlusion

modifies the sensory maps and synaptic connections of immature but not mature GCs (Quast et al., 2017).

Even in maturity, the apical dendrites of all GCs remain plastic throughout life (Sailor et al., 2016). After the dendritic morphology of adult-born GCs stabilizes in development, their spines remain dynamic as the animal ages (Mizrahi, 2007). The persistence of spine plasticity is not observed in either cortical interneurons or MCs and TCs (Lee et al., 2005; Mizrahi and Katz, 2003; Trachtenberg et al., 2002). Odor enrichment, learning, and sensory deprivation can all change the spine dynamics and turnover of mature adult-born GCs (Dahlen et al., 2011; Livneh and Mizrahi, 2012). Reward-associated olfactory learning increases spine density in the proximal apical and basal dendrites of adult-born GCs, where they receive cortical feedback projections (Lepousez et al., 2014). Implicit and explicit olfactory learning have opposite effects on spine density in adult-born GCs and sIPSC amplitudes recorded in MCs; the authors theorized that decreased inhibition in MCs could enhance the neural representation of only the conditioned odor (Mandairon et al., 2018). This possibility is supported by a study showing that odor associative learning increases the strength of excitation from MCs onto GCs within odor-activated regions and sharpens the GC-mediated inhibition back onto the MCs (Huang et al., 2016).

During olfactory learning, spine density increases on the apical dendrites of adult-born GCs along with the strength of excitatory odor responses, but these changes do not occur in resident GCs (Wu et al., 2020). The spines of mature adult-born GCs can relocate in response to local synaptic input from MCs (Breton-Provencher et al., 2016). A recent *in vivo* calcium imaging study found that mature adult-born olfactory cells (including both PGCs and GCs) have higher levels of spontaneous activity compared to resident cells. Compared to resident cells, fewer mature adult-born cells respond reliably to odor stimulation, and their response amplitudes are smaller than

those of resident cells. Mature adult-born cells, unlike resident cells, are also strongly modulated by serotonergic inputs (Fomin-Thunemann et al., 2020). Collectively, these data show that adult-born GCs appear to be more sensitive to sensory experience compared to resident or prenatally-generated GCs and support the possibility that adult-born neurons perform additional functions beyond replenishing dying neurons.

4.8 External and internal states affecting neurogenesis

Both environmental factors and the animal's internal state can influence neurogenesis in behaviorally relevant ways (Lledo and Valley, 2016). As discussed previously, neurogenesis in the OE and OB is sensitive to sensory input. Increased activation of OSNs or odor activity increases the survival of newly generated OSNs (Santoro and Dulac, 2012; Watt et al., 2004). Conversely, reducing sensory input using naris occlusion decreases the number of OSNs present in the OE (Cavallin et al., 2010). In the OB, an enriched odor environment and olfactory learning promote GC neurogenesis (Alonso et al., 2006; Kamimura et al., 2022; Lemasson et al., 2005), whereas naris occlusion decreases the generation and survival of GCs (Saghatelyan et al., 2005). Neurogenesis in both the OE and OB also decreases with age (Daynac et al., 2016; Enwere et al., 2004; Kondo et al., 2010; Loo et al., 1996; Magavi et al., 2005); perhaps neurogenesis naturally declines later in the animal's life because learning and adaptation are no longer as critical to survival as earlier in life, or the neurogenic potential of stem cells diminishes with age (Child et al., 2018).

Aside from sensory experience and aging, there are additional studies linking neurogenesis to behaviors that guide survival. Mice show increased apoptosis among adult-born GCs during

feeding and post-feeding time windows; this effect was not observed in hippocampal GCs, which is expected given that feeding is a behavior mediated by olfaction (Yokoyama et al., 2011). The authors proposed that a subset of adult-born GCs is recruited by the mice's food-finding and eating behavior. After eating, the activated GCs survive, and the adult-born GCs that were not recruited or activated undergo apoptosis. This hypothesis is supported by the fact that blocking apoptosis in adult-born GCs impaired response times in spontaneous odor exploration and odor discrimination (Mouret et al., 2009).

A previous study has also found that pregnancy stimulates the production of adult-born GCs via prolactin, suggesting that newly generated neurons may be involved in maternal behavior and bonding with offspring (Shingo et al., 2003). A subsequent study using lactating mice reported that adult-born GCs show more stable dendritic spine numbers and a lower spine density, suggesting increased dendritic integration of adult-born GCs following giving birth (Kopel et al., 2012).The studies cited above are but a few examples linking adult neurogenesis in the olfactory system to behaviors that are essential to survival; they demonstrate that adult neurogenesis is intertwined with plasticity and environmental adaptation. It would be interesting to investigate whether there is any coupling between OE neurogenesis and OB neurogenesis and whether manipulating one can affect the other.

4.9 Shared similarities with hippocampal neurogenesis

Hippocampal adult neurogenesis in the dentate gyrus is also sensitive to the environment and sensory experience. An early study in chickadees found that the birds show increased neurogenesis in the hippocampus during the fall, when birds are storing food for the winter (Barnea

and Nottebohm, 1994). The rate of neurogenesis was lower in captive birds compared to free-ranging birds. Increased recruitment of new hippocampal neurons may be critical in the formation of new spatial memories used in food storage, which is more important for free-range birds than captive birds. Additionally, mice raised in an enriched environment with littermates, novel objects, and running wheels show increased hippocampal neurogenesis (Kempermann et al., 1997).

Changes in the environment also affect the maturation and integration of adult-born dentate gyrus GCs (Kirschen et al., 2017; Piatti et al., 2011). Presynaptic connections to dentate gyrus GCs can be modified in an enriched environment, and a degree of plasticity persists beyond the critical window when most of the changes occur (Bergami et al., 2015). Just like in the OB, hippocampal neurogenesis is sensitive to the internal or physiological state of the animal: stress, maternal separation, depression, pregnancy, hormones, and aging all reduce dentate gyrus neurogenesis (Gould et al., 1997; Kuhn et al., 1996; Mirescu et al., 2004; Montero-Pedrazuela et al., 2006; Snyder et al., 2011; Tanapat et al., 1999).

Adult-born dentate GCs are involved in a variety of functions, including memory retrieval (Gu et al., 2012) and memory clearance (Akers et al., 2014; Epp et al., 2016). Similarly to OB GCs, dentate gyrus GCs mediate pattern separation, which facilitates discriminating between similar events or locations (Clelland et al., 2009; Deng et al., 2013; Toda et al., 2018). The role of adult neurogenesis in other hippocampal-dependent tasks such as initial memory acquisition, Morris water maze navigation, and fear conditioning is more disputed (Toda et al., 2018). Nevertheless, robust evidence exists for hippocampal adult neurogenesis involvement in aging and disease. Hippocampal neurogenesis declines with age (Spalding et al., 2013), and a recent study suggested that age-associated cognitive decline could be prevented or slowed by restarting hippocampal adult neurogenesis (McAvoy et al., 2016). Hippocampal neurogenesis in both

humans and mouse models is also impaired in Alzheimer's disease, Parkinson's disease, depression, and epilepsy (Crews et al., 2010; Hattiangady et al., 2004; Li et al., 2008; Lucassen et al., 2010; Winner et al., 2012).

Changes in hippocampal adult neurogenesis have farther-reaching implications in behavior compared to neurogenesis in the OB simply because of the hippocampus' involvement in a diverse range of functions. Insights obtained from studying adult neurogenesis in the OB, however, may illuminate the mechanisms regulating the generation and integration of new hippocampal neurons.

4.10 Conclusion

Adult neurogenesis is an essential feature of the healthy rodent brain, allowing it to replenish neurons during normal turnover and to adapt to the animal's external environment. In this dissertation, I utilize the well-characterized circuitry of the OB to study the contribution of neurogenesis in the olfactory system. I show that immature OSNs make monosynaptic connections to neurons in the OB, providing evidence that immature OSNs play a previously unappreciated role in odor processing. I also show that birth date related differences in the functional connectivity of postnatal-born GCs lead to differential inhibitory inputs onto MCs and TCs. Collectively, these data suggest that adult neurogenesis plays a unique role in olfactory processing and challenge the notion that the sole function of new neurons is to replace old dying neurons.

Bibliography

Ache, B. W., & Young, J. M. (2005). Olfaction: Diverse Species, Conserved Principles. *Neuron, 48*(3), 417-430. doi:10.1016/j.neuron.2005.10.022

Adam, Y., Livneh, Y., Miyamichi, K., Groysman, M., Luo, L., & Mizrahi, A. (2014). Functional transformations of odor inputs in the mouse olfactory bulb. *Frontiers in Neural Circuits, 8*, 129. doi:10.3389/fncir.2014.00129

Adipietro, K. A., Mainland, J. D., & Matsunami, H. (2012). Functional Evolution of Mammalian Odorant Receptors. *PLOS Genetics, 8*(7), e1002821. doi:10.1371/JOURNAL.PGEN.1002821

Adlaf, E. W., Vaden, R. J., Niver, A. J., Manuel, A. F., Onyilo, V. C., Araujo, M. T., . . . Overstreet-Wadiche, L. (2017). Adult-born neurons modify excitatory synaptic transmission to existing neurons. *eLife, 6*, e19886. doi:10.7554/eLife.19886

Akers, K. G., Martinez-Canabal, A., Restivo, L., Yiu, A. P., De Cristofaro, A., Hsiang, H.-L., . . . Frankland, P. W. (2014). Hippocampal Neurogenesis Regulates Forgetting During Adulthood and Infancy. *Science, 344*(6184), 598-602. doi:10.1126/science.1248903

Alonso, M., Lepousez, G., Wagner, S., Bardy, C., Gabellec, M.-M., Torquet, N., & Lledo, P.-M. (2012). Activation of adult-born neurons facilitates learning and memory. *Nature Neuroscience, 15*(6), 897-904. doi:10.1038/nn.3108

Alonso, M., Viollet, C., Gabellec, M.-M., Meas-Yedid, V., Olivo-Marin, J.-C., & Lledo, P.-M. (2006). Olfactory Discrimination Learning Increases the Survival of Adult-Born Neurons in the Olfactory Bulb. *Journal of Neuroscience, 26*(41), 10508-10513. doi:10.1523/JNEUROSCI.2633-06.2006

Altman, J. (1969). Autoradiographic and histological studies of postnatal neurogenesis. IV. Cell proliferation and migration in the anterior forebrain, with special reference to persisting neurogenesis in the olfactory bulb. *Journal of Comparative Neurology, 137*(4), 433-457. doi:10.1002/CNE.901370404

Altman, J., & Das, G. D. (1965). Autoradiographic and histological evidence of postnatal hippocampal neurogenesis in rats. *J Comp Neurol, 124*(3), 319-335.

Alvarez-Buylla, A., García-Verdugo, J. M., & Tramontin, A. D. (2001). A unified hypothesis on the lineage of neural stem cells. *Nature Reviews Neuroscience 2001 2:4, 2*(4), 287-293. doi:10.1038/35067582

Alvarez-Buylla, A., & Lim, D. A. (2004). For the Long Run: Maintaining Germinal Niches in the Adult Brain. *Neuron, 41*(5), 683-686. doi:10.1016/S0896-6273(04)00111-4

Antal, M., Eyre, M., Finklea, B., & Nusser, Z. (2006). External tufted cells in the main olfactory bulb form two distinct subpopulations. *European Journal of Neuroscience, 24*(4), 1124-1136. doi:10.1111/J.1460-9568.2006.04988.X

Arenkiel, B. R., Peca, J., Davison, I. G., Feliciano, C., Deisseroth, K., Augustine, G. J., . . . Feng, G. (2007). In Vivo Light-Induced Activation of Neural Circuitry in Transgenic Mice Expressing Channelrhodopsin-2. *Neuron, 54*(2), 205-218. doi:10.1016/j.neuron.2007.03.005

Arevian, A. C., Kapoor, V., & Urban, N. N. (2008). Activity-dependent gating of lateral inhibition in the mouse olfactory bulb. *Nature Neuroscience, 11*(1), 80-87. doi:10.1038/nn2030

Arnson, H. A., & Strowbridge, B. W. (2017). Spatial Structure of Synchronized Inhibition in the Olfactory Bulb. *Journal of Neuroscience, 37*(43), 10468-10480. doi:10.1523/JNEUROSCI.1004-17.2017

Aroniadou-Anderjaska, V., Ennis, M., & Shipley, M. T. (1999). Dendrodendritic Recurrent Excitation in Mitral Cells of the Rat Olfactory Bulb. *Journal of Neurophysiology, 82*(1), 489-494. doi:10.1152/jn.1999.82.1.489

Balu, R., Pressler, R. T., & Strowbridge, B. W. (2007). Multiple modes of synaptic excitation of olfactory bulb granule cells. *J Neurosci, 27*(21), 5621-5632. doi:10.1523/jneurosci.4630-06.2007

Banks, M. I., Li, T. B., & Pearce, R. A. (1998). The Synaptic Basis of GABAA,slow. *The Journal of Neuroscience, 18*(4), 1305. doi:10.1523/JNEUROSCI.18-04-01305.1998

Barber, C. N., & Coppola, D. M. (2015). Compensatory plasticity in the olfactory epithelium: age, timing, and reversibility. *Journal of Neurophysiology, 114*(3), 2023-2032. doi:10.1152/jn.00076.2015

Bardy, C., Alonso, M., Bouthour, W., & Lledo, P. M. (2010). How, When, and Where New Inhibitory Neurons Release Neurotransmitters in the Adult Olfactory Bulb. *Journal of Neuroscience, 30*(50), 17023-17034. doi:10.1523/JNEUROSCI.4543-10.2010

Barnea, A., & Nottebohm, F. (1994). Seasonal recruitment of hippocampal neurons in adult free-ranging black-capped chickadees. *Proceedings of the National Academy of Sciences of the United States of America, 91*(23), 11217-11221.

Batista-Brito, R., Close, J., Machold, R., & Fishell, G. (2008). The Distinct Temporal Origins of Olfactory Bulb Interneuron Subtypes. *Journal of Neuroscience, 28*(15), 3966-3975. doi:10.1523/JNEUROSCI.5625-07.2008

Bear, D. M., Lassance, J.-M., Hoekstra, H. E., & Datta, S. R. (2016). The Evolving Neural and Genetic Architecture of Vertebrate Olfaction. *Current Biology, 26*(20), R1039-R1049. doi:10.1016/j.cub.2016.09.011

Belluscio, L., Lodovichi, C., Feinstein, P., Mombaerts, P., & Katz, L. C. (2002). Odorant receptors instruct functional circuitry in the mouse olfactory bulb. *Nature 2002 419:6904, 419*(6904), 296-300. doi:10.1038/NATURE01001

Belluzzi, O., Benedusi, M., Ackman, J., & LoTurco, J. J. (2003). Electrophysiological Differentiation of New Neurons in the Olfactory Bulb. *Journal of Neuroscience, 23*(32), 10411-10418. doi:10.1523/JNEUROSCI.23-32-10411.2003

Benda, J. (2021). Neural adaptation. *Current Biology, 31*(3), R110-R116. doi:10.1016/j.cub.2020.11.054

Bergami, M., Masserdotti, G., Temprana, S. G., Motori, E., Eriksson, T. M., Göbel, J., . . . Berninger, B. (2015). A Critical Period for Experience-Dependent Remodeling of Adult-Born Neuron Connectivity. *Neuron, 85*(4), 710-717. doi:10.1016/j.neuron.2015.01.001

Bergman, U., Östergren, A., Gustafson, A. L., & Brittebo, E. (2002). Differential effects of olfactory toxicants on olfactory regeneration. *Archives of Toxicology, 76*(2), 104-112. doi:10.1007/s00204-002-0321-2

Bergstr¨om, U., Bergstr¨om, B., Giovanetti, A., Piras, E., & Brittebo, E. B. (2003). Methimazole-Induced Damage in the Olfactory Mucosa: Effects on Ultrastructure and Glutathione Levels. *Toxicologic Pathology, 31*, 379-387. doi:10.1080/01926230390201101

Blanco-Hernández, E., Valle-Leija, P., Zomosa-Signoret, V., Drucker-Colín, R., & Vidaltamayo, R. (2012). Odor Memory Stability after Reinnervation of the Olfactory Bulb. *PLOS ONE, 7*(10), e46338. doi:10.1371/JOURNAL.PONE.0046338

Boesveldt, S., & Parma, V. (2021). The importance of the olfactory system in human well-being, through nutrition and social behavior. *Cell and Tissue Research, 383*(1), 559-567. doi:10.1007/s00441-020-03367-7

Bourne, J. N., & Schoppa, N. E. (2017). Three-dimensional synaptic analyses of mitral cell and external tufted cell dendrites in rat olfactory bulb glomeruli. *Journal of Comparative Neurology, 525*(3), 592-609. doi:10.1002/cne.24089

Boyd, A. M., Kato, H. K., Komiyama, T., & Isaacson, J. S. (2015). Broadcasting of cortical activity to the olfactory bulb. *Cell Rep, 10*(7), 1032-1039. doi:10.1016/j.celrep.2015.01.047

Boyd, A. M., Sturgill, J. F., Poo, C., & Isaacson, J. S. (2012). Cortical Feedback Control of Olfactory Bulb Circuits. *Neuron, 76*(6), 1161-1174. doi:10.1016/J.NEURON.2012.10.020/ATTACHMENT/D1F5716A-297E-4E83-B8D8-D1F37EC6665F/MMC1.PDF

Bressel, O. C., Khan, M., & Mombaerts, P. (2016). Linear correlation between the number of olfactory sensory neurons expressing a given mouse odorant receptor gene and the total volume of the corresponding glomeruli in the olfactory bulb. *Journal of Comparative Neurology, 524*(1), 199-209. doi:10.1002/cne.23835

Breton-Provencher, V., Bakhshetyan, K., Hardy, D., Bammann, R. R., Cavarretta, F., Snapyan, M., . . . Saghatelyan, A. (2016). Principal cell activity induces spine relocation of adult-born interneurons in the olfactory bulb. *Nature Communications, 7*, 12659. doi:10.1038/ncomms12659

Breton-Provencher, V., Lemasson, M., Peralta 3rd, M. R., & Saghatelyan, A. (2009). Interneurons produced in adulthood are required for the normal functioning of the olfactory bulb network and for the execution of selected olfactory behaviors. *J Neurosci, 29*(48), 15245-15257. doi:10.1523/jneurosci.3606-09.2009

Browne, L. P., Crespo, A., & Grubb, M. S. (2022). *Rapid presynaptic maturation in naturally regenerating axons*. Retrieved from

Brunjes, P. C., Illig, K. R., & Meyer, E. A. (2005). A field guide to the anterior olfactory nucleus (cortex). *Brain Research Reviews, 50*(2), 305-335. doi:10.1016/j.brainresrev.2005.08.005

Buck, L., & Axel, R. (1991). A Novel Multigene Family May Encode Odorant Receptors: A Molecular Basis for Odor Recognition. *Cell, 65*, 175-187.

Buck, L. B. (1996). Information coding in the vertebrate olfactory system. *Annual Review of Neuroscience, 19*, 517-544. doi:10.1146/ANNUREV.NE.19.030196.002505

Burd, G. D. (1993). Morphological study of the effects of intranasal zinc sulfate irrigation on the mouse olfactory epithelium and olfactory bulb. *Microscopy Research and Technique, 24*(3), 195-213. doi:10.1002/jemt.1070240302

Burton, S. D. (2017). Inhibitory circuits of the mammalian main olfactory bulb. *Journal of Neurophysiology, 118*(4), 2034-2051. doi:10.1152/JN.00109.2017/ASSET/IMAGES/LARGE/Z9K0091743140002.JPEG

Burton, S. D., & Urban, N. N. (2014). Greater excitability and firing irregularity of tufted cells underlies distinct afferent-evoked activity of olfactory bulb mitral and tufted cells. *J Physiol, 592*(10), 2097-2118. doi:10.1113/jphysiol.2013.269886

Burton, S. D., & Urban, N. N. (2015). Rapid Feedforward Inhibition and Asynchronous Excitation Regulate Granule Cell Activity in the Mammalian Main Olfactory Bulb. *Journal of Neuroscience, 35*(42), 14103-14122. doi:10.1523/JNEUROSCI.0746-15.2015

Burton, S. D., & Urban, N. N. (2021). Cell and circuit origins of fast network oscillations in the mammalian main olfactory bulb. *eLife, 10*, e74213. doi:10.7554/eLife.74213

Bushdid, C., Magnasco, M. O., Vosshall, L. B., & Keller, A. (2014). Humans Can Discriminate More than 1 Trillion Olfactory Stimuli. *Science, 343*(6177), 1370-1372. doi:10.1126/science.1249168

Butowt, R., & von Bartheld, C. S. (2021). Anosmia in COVID-19: Underlying Mechanisms and Assessment of an Olfactory Route to Brain Infection. *The Neuroscientist, 27*(6), 582-603. doi:10.1177/1073858420956905

Bywalez, W. G., Patirniche, D., Rupprecht, V., Stemmler, M., Herz, A. V. M., Pálfi, D., . . . Egger, V. (2015). Local Postsynaptic Voltage-Gated Sodium Channel Activation in Dendritic Spines of Olfactory Bulb Granule Cells. *Neuron, 85*(3), 590-601. doi:10.1016/j.neuron.2014.12.051

Cadiou, H., Aoudé, I., Tazir, B., Molinas, A., Fenech, C., Meunier, N., & Grosmaitre, X. (2014). Postnatal Odorant Exposure Induces Peripheral Olfactory Plasticity at the Cellular Level. *Journal of Neuroscience, 34*(14), 4857-4870. doi:10.1523/JNEUROSCI.0688-13.2014

Caggiano, M., Kauer, J. S., & Hunter, D. D. (1994). Globose Basal Cells Are Neuronal Progenitors in the Olfactory Epithelium: A lineage Analysis Using a Replication-Incompetent Retrovirus. *Neuron, 13*, 339-352.

Cajal, S. R. Y. (1913). *Degeneration & Regeneration of the Nervous System*: Oxford University Press.

Capaldi, E. D., Hunter, M. J., & Privitera, G. J. (2004). Odor of Taste Stimuli in Conditioned "Taste" Aversion Learning. *Behavioral Neuroscience, 118*(6), 1400-1408. doi:10.1037/0735-7044.118.6.1400

Carleton, A., Petreanu, L. T., Lansford, R., Alvarez-Buylla, A., & Lledo, P.-M. (2003). Becoming a new neuron in the adult olfactory bulb. *Nature Neuroscience, 6*(5), 507-518. doi:10.1038/nn1048

Carlson, G. C., Shipley, M. T., & Keller, A. (2000). Long-Lasting Depolarizations in Mitral Cells of the Rat Olfactory Bulb. *The Journal of Neuroscience, 20*, 2011-2021.

Case, D. T., Burton, S. D., Gedeon, J. Y., Williams, S. P. G., Urban, N. N., & Seal, R. P. (2017). Layer- and cell type-selective co-transmission by a basal forebrain cholinergic projection to the olfactory bulb. *Nature Communications 2017 8:1, 8*(1), 1-9. doi:10.1038/s41467-017-00765-4

Cavallin, M. A., Powell, K., Biju, K. C., & Fadool, D. A. (2010). State-dependent sculpting of olfactory sensory neurons is attributed to sensory enrichment, odor deprivation, and aging. *Neuroscience Letters, 483*(2), 90-95. doi:10.1016/J.NEULET.2010.07.059

Chatterjee, M., Perez de los Cobos Pallares, F., Loebel, A., Lukas, M., & Egger, V. (2016). Sniff-Like Patterned Input Results in Long-Term Plasticity at the Rat Olfactory Bulb Mitral and Tufted Cell to Granule Cell Synapse. *Neural Plasticity, 2016*, e9124986. doi:10.1155/2016/9124986

Cheetham, C. E. J., Grier, B. D., & Belluscio, L. (2015). Bulk regional viral injection in neonatal mice enables structural and functional interrogation of defined neuronal populations throughout targeted brain areas. *Frontiers in Neural Circuits, 9*, 72. doi:10.3389/fncir.2015.00072

Cheetham, C. E. J., Park, U., & Belluscio, L. (2016). Rapid and continuous activity-dependent plasticity of olfactory sensory input. *Nature Communications 2016 7:1, 7*(1), 1-11. doi:10.1038/ncomms10729

Chen, Q., Cichon, J., Wang, W., Qiu, L., Lee, S.-J. R., Campbell, N. R., . . . Feng, G. (2012). Imaging Neural Activity Using Thy1-GCaMP Transgenic Mice. *Neuron, 76*(2), 297-308. doi:10.1016/j.neuron.2012.07.011

Cheung, M. C., Jang, W., Schwob, J. E., & Wachowiak, M. (2014). Functional recovery of odor representations in regenerated sensory inputs to the olfactory bulb. *Frontiers in Neural Circuits, 7*, 207. doi:10.3389/fncir.2013.00207

Child, K. M., Herrick, D. B., Schwob, J. E., Holbrook, E. H., & Jang, W. (2018). The Neuroregenerative Capacity of Olfactory Stem Cells Is Not Limitless: Implications for Aging. *Journal of Neuroscience, 38*(31), 6806-6824. doi:10.1523/JNEUROSCI.3261-17.2018

Christensen, M. D., Holbrook, E. H., Costanzo, R. M., & Schwob, J. E. (2001). Rhinotopy is Disrupted During the Re-innervation of the Olfactory Bulb that Follows Transection of the Olfactory Nerve. *Chemical Senses, 26*(4), 359-369. doi:10.1093/chemse/26.4.359

Christie, J. M., Schoppa, N. E., & Westbrook, G. L. (2001). Tufted Cell Dendrodendritic Inhibition in the Olfactory Bulb Is Dependent on NMDA Receptor Activity. *Journal of Neurophysiology, 85*(1), 169-173. doi:10.1152/jn.2001.85.1.169

Clelland, C. D., Choi, M., Romberg, C., Clemenson, G. D., Fragniere, A., Tyers, P., . . . Bussey, T. J. (2009). A Functional Role for Adult Hippocampal Neurogenesis in Spatial Pattern Separation. *Science, 325*(5937), 210-213. doi:10.1126/science.1173215

Connelly, T., Yu, Y., Grosmaitre, X., Wang, J., Santarelli, L. C., Savigner, A., . . . Carlson, J. R. (2015). G protein-coupled odorant receptors underlie mechanosensitivity in mammalian olfactory sensory neurons. *Proceedings of the National Academy of Sciences of the United States of America, 112*(2), 590-595. doi:10.1073/PNAS.1418515112/SUPPL_FILE/PNAS.201418515SI.PDF

Coopersmith, R., & Leon, M. (1984). Enhanced Neural Response to Familiar Olfactory Cues. *Science, 225*(4664), 849-851. doi:10.1126/science.6474157

Costanzo, R. M. (2000). Rewiring the Olfactory Bulb: Changes in Odor Maps following Recovery from Nerve Transection. *Chemical Senses, 25*(2), 199-205. doi:10.1093/chemse/25.2.199

Crews, L., Adame, A., Patrick, C., DeLaney, A., Pham, E., Rockenstein, E., . . . Masliah, E. (2010). Increased BMP6 Levels in the Brains of Alzheimer's Disease Patients and APP Transgenic Mice Are Accompanied by Impaired Neurogenesis. *Journal of Neuroscience, 30*(37), 12252-12262. doi:10.1523/JNEUROSCI.1305-10.2010

Dahlen, J. E., Jimenez, D. A., Gerkin, R. C., & Urban, N. N. (2011). Morphological analysis of activity-reduced adult-born neurons in the mouse olfactory bulb. *Frontiers in Neuroscience, 0*(MAY), 1-8. doi:10.3389/FNINS.2011.00066/BIBTEX

Dana, H., Chen, T.-W., Hu, A., Shields, B. C., Guo, C., Looger, L. L., . . . Svoboda, K. (2014). Thy1-GCaMP6 Transgenic Mice for Neuronal Population Imaging In Vivo. *PLOS ONE, 9*(9), e108697. doi:10.1371/journal.pone.0108697

Davidson, B. L., Stein, C. S., Heth, J. A., Martins, I., Kotin, R. M., Derksen, T. A., . . . Chiorini, J. A. (2000). Recombinant adeno-associated virus type 2, 4, and 5 vectors: Transduction of variant cell types and regions in the mammalian central nervous system. *Proceedings of the National Academy of Sciences, 97*(7), 3428-3432. doi:10.1073/pnas.97.7.3428

Daynac, M., Morizur, L., Chicheportiche, A., Mouthon, M. A., & Boussin, F. D. (2016). Age-related neurogenesis decline in the subventricular zone is associated with specific cell cycle regulation changes in activated neural stem cells. *Scientific Reports 2016 6:1, 6*(1), 1-10. doi:10.1038/srep21505

De Saint Jan, D., Hirnet, D., Westbrook, G. L., & Charpak, S. (2009). External Tufted Cells Drive the Output of Olfactory Bulb Glomeruli. *Journal of Neuroscience, 29*(7), 2043-2052. doi:10.1523/JNEUROSCI.5317-08.2009

Deng, W., Mayford, M., & Gage, F. H. (2013). Selection of distinct populations of dentate granule cells in response to inputs as a mechanism for pattern separation in mice. *eLife, 2*, e00312. doi:10.7554/eLife.00312

Dhawale, A. K., Hagiwara, A., Bhalla, U. S., Murthy, V. N., & Albeanu, D. F. (2010). Non-redundant odor coding by sister mitral cells revealed by light addressable glomeruli in the mouse. *Nature Neuroscience 2010 13:11, 13*(11), 1404-1412. doi:10.1038/NN.2673

Diez, A. S., Najac, M., & Jan, D. D. S. (2019). Basal forebrain GABAergic innervation of olfactory bulb periglomerular interneurons. *The Journal of Physiology, 597*(9), 2547-2563. doi:10.1113/JP277811

Durante, M. A., Kurtenbach, S., Sargi, Z. B., Harbour, J. W., Choi, R., Kurtenbach, S., . . . Goldstein, B. J. (2020). Single-cell analysis of olfactory neurogenesis and differentiation in adult humans. *Nature Neuroscience, 23*(3), 323-326. doi:10.1038/s41593-020-0587-9

Economo, M. N., Hansen, K. R., & Wachowiak, M. (2016). Control of Mitral/Tufted Cell Output by Selective Inhibition among Olfactory Bulb Glomeruli. *Neuron, 91*(2), 397-411. doi:10.1016/j.neuron.2016.06.001

Eerdunfu, Ihara, N., Ligao, B., Ikegaya, Y., & Takeuchi, H. (2017). Differential timing of neurogenesis underlies dorsal-ventral topographic projection of olfactory sensory neurons. *Neural Development, 12*(1), 2. doi:10.1186/s13064-017-0079-0

Egger, V. (2008). Synaptic sodium spikes trigger long-lasting depolarizations and slow calcium entry in rat olfactory bulb granule cells. *European Journal of Neuroscience, 27*(8), 2066-2075. doi:10.1111/J.1460-9568.2008.06170.X

Egger, V., & Kuner, T. (2021). Olfactory bulb granule cells: specialized to link coactive glomerular columns for percept generation and discrimination of odors. *Cell and Tissue Research, 383*(1), 495-506. doi:10.1007/S00441-020-03402-7/FIGURES/2

Egger, V., Svoboda, K., & Mainen, Z. F. (2005). Dendrodendritic Synaptic Signals in Olfactory Bulb Granule Cells: Local Spine Boost and Global Low-Threshold Spike. *The Journal of Neuroscience, 25*, 3521-3530.

Egger, V., & Urban, N. N. (2006). Dynamic connectivity in the mitral cell–granule cell microcircuit. *Seminars in Cell & Developmental Biology, 17*(4), 424-432. doi:10.1016/j.semcdb.2006.04.006

Enwere, E., Shingo, T., Gregg, C., Fujikawa, H., Ohta, S., & Weiss, S. (2004). Aging Results in Reduced Epidermal Growth Factor Receptor Signaling, Diminished Olfactory Neurogenesis, and Deficits in Fine Olfactory Discrimination. *Journal of Neuroscience, 24*(38), 8354-8365. doi:10.1523/JNEUROSCI.2751-04.2004

Epp, J. R., Silva Mera, R., Köhler, S., Josselyn, S. A., & Frankland, P. W. (2016). Neurogenesis-mediated forgetting minimizes proactive interference. *Nature Communications, 7*(1), 10838. doi:10.1038/ncomms10838

Ezeh, P. I., Wellis, D. P., & Scott, J. W. (1993). Organization of inhibition in the rat olfactory bulb external plexiform layer. *Journal of Neurophysiology, 70*(1), 263-274.

Faedo, A., Ficara, F., Ghiani, M., Aiuti, A., Rubenstein, J. L. R., & Bulfone, A. (2002). Developmental expression of the T-box transcription factor T-bet/Tbx21 during mouse embryogenesis. *Mechanisms of Development, 116*(1), 157-160. doi:10.1016/S0925-4773(02)00114-4

Falk, N., Lösl, M., Schröder, N., & Gießl, A. (2015). Specialized Cilia in Mammalian Sensory Systems. *Cells 2015, Vol. 4, Pages 500-519, 4*(3), 500-519. doi:10.3390/CELLS4030500

Fomin-Thunemann, N., Kovalchuk, Y., Fink, S., Alsema, A., Mojtahedi, N., Zirdum, E., & Garaschuk, O. (2020). Unique Functional Properties of Mature Adult-Born Neurons in the Mouse Olfactory Bulb. *Stem Cell Reports, 15*(6), 1333-1346. doi:10.1016/j.stemcr.2020.10.010

Forest, J., Chalençon, L., Midroit, M., Terrier, C., Caillé, I., Sacquet, J., . . . Mandairon, N. (2020). Role of Adult-Born Versus Preexisting Neurons Born at P0 in Olfactory Perception in a Complex Olfactory Environment in Mice. *Cerebral Cortex, 30*(2), 534-549. doi:10.1093/cercor/bhz105

Fukunaga, I., Berning, M., Kollo, M., Schmaltz, A., & Schaefer, A. T. (2012). Two distinct channels of olfactory bulb output. *Neuron, 75*(2), 320-329. doi:10.1016/j.neuron.2012.05.017

Geramita, M., & Urban, N. N. (2016). Postnatal Odor Exposure Increases the Strength of Interglomerular Lateral Inhibition onto Olfactory Bulb Tufted Cells. *Journal of Neuroscience, 36*(49), 12321-12327. doi:10.1523/JNEUROSCI.1991-16.2016

Geramita, M. A., Burton, S. D., & Urban, N. N. (2016). Distinct lateral inhibitory circuits drive parallel processing of sensory information in the mammalian olfactory bulb. *eLife, 5*, e16039. doi:10.7554/eLife.16039

Gerkin, R. C., & Castro, J. B. (2015). The number of olfactory stimuli that humans can discriminate is still unknown. *eLife, 4*, e08127. doi:10.7554/eLife.08127

Gillingwater, T. H., & Ribchester, R. R. (2001). Compartmental neurodegeneration and synaptic plasticity in the Wlds mutant mouse. *The Journal of Physiology, 534*(Pt 3), 627. doi:10.1111/J.1469-7793.2001.00627.X

Gire, D. H., Franks, K. M., Zak, J. D., Tanaka, K. F., Whitesell, J. D., Mulligan, A. A., . . . Schoppa, N. E. (2012). Mitral cells in the olfactory bulb are mainly excited through a multistep signaling path. *J Neurosci, 32*(9), 2964-2975. doi:10.1523/jneurosci.5580-11.2012

Glusman, G., Yanai, I., Rubin, I., & Lancet, D. (2001). The Complete Human Olfactory Subgenome. *Genome Research, 11*(5), 685-702. doi:10.1101/gr.171001

Godfrey, P. A., Malnic, B., & Buck, L. B. (2004). The mouse olfactory receptor gene family. *Proceedings of the National Academy of Sciences, 101*(7), 2156-2161. doi:10.1073/pnas.0308051100

Gordon, J. A., & Stryker, M. P. (1996). Experience-Dependent Plasticity of Binocular Responses in the Primary Visual Cortex of the Mouse. *The Journal of Neuroscience, 16*(10), 3274. doi:10.1523/JNEUROSCI.16-10-03274.1996

Goswami, S. P., Bucurenciu, I., & Jonas, P. (2012). Miniature IPSCs in Hippocampal Granule Cells Are Triggered by Voltage-Gated Ca2+ Channels via Microdomain Coupling. *Journal of Neuroscience, 32*(41), 14294-14304. doi:10.1523/JNEUROSCI.6104-11.2012

Gould, E. (2007). How widespread is adult neurogenesis in mammals? *Nature Reviews Neuroscience, 8*(6), 481-488. doi:10.1038/nrn2147

Gould, E., McEwen, B. S., Tanapat, P., Galea, L. A. M., & Fuchs, E. (1997). Neurogenesis in the Dentate Gyrus of the Adult Tree Shrew Is Regulated by Psychosocial Stress and NMDA Receptor Activation. *The Journal of Neuroscience, 17*(7), 2492. doi:10.1523/JNEUROSCI.17-07-02492.1997

Gracia-Llanes, F. J., Crespo, C., Blasco-Ibáñez, J. M., Nacher, J., Varea, E., Rovira-Esteban, L., & Martínez-Guijarro, F. J. (2010). GABAergic basal forebrain afferents innervate

selectively GABAergic targets in the main olfactory bulb. *Neuroscience, 170*(3), 913-922. doi:10.1016/j.neuroscience.2010.07.046

Graziadei, P. P. C., & Graziadei, G. A. M. (1979). Neurogenesis and neuron regeneration in the olfactory system of mammals. I. Morphological aspects of differentiation and structural organization of the olfactory sensory neurons. *Journal of neurocytology, 8*(1), 1-18. doi:10.1007/BF01206454

Graziadei, P. P. C., Levine, R. R., Graziadei, G. A. M., Harding, Donlan, J., Chen, K., & Wright, H. (1978). Regeneration of olfactory axons and synapse formation in the forebrain after bulbectomy in neonatal mice. *Proceedings of the National Academy of Sciences of the United States of America, 75*(10), 5230-5234. doi:10.1073/PNAS.75.10.5230

Grelat, A., Benoit, L., Wagner, S., Moigneu, C., Lledo, P.-M., & Alonso, M. (2018). Adult-born neurons boost odor–reward association. *Proceedings of the National Academy of Sciences, 115*(10), 2514-2519. doi:10.1073/pnas.1716400115

Griff, E. R., Mafhouz, M., & Chaput, M. A. (2008). Comparison of Identified Mitral and Tufted Cells in Freely Breathing Rats: II. Odor-Evoked Responses. *Chemical Senses, 33*(9), 793-802. doi:10.1093/CHEMSE/BJN040

Gschwend, O., Abraham, N. M., Lagier, S., Begnaud, F., Rodriguez, I., & Carleton, A. (2015). Neuronal pattern separation in the olfactory bulb improves odor discrimination learning. *Nat Neurosci, 18*(10), 1474-1482. doi:10.1038/nn.4089

Gu, Y., Arruda-Carvalho, M., Wang, J., Janoschka, S. R., Josselyn, S. A., Frankland, P. W., & Ge, S. (2012). Optical controlling reveals time-dependent roles for adult-born dentate granule cells. *Nature Neuroscience, 15*(12), 1700-1706. doi:10.1038/nn.3260

Haddad, R., Lanjuin, A., Madisen, L., Zeng, H., Murthy, V. N., & Uchida, N. (2013). Olfactory cortical neurons read out a relative time code in the olfactory bulb. *Nature Neuroscience, 16*(7), 949-957. doi:10.1038/nn.3407

Haery, L., Deverman, B. E., Matho, K. S., Cetin, A., Woodard, K., Cepko, C., . . . Fan, M. (2019). Adeno-Associated Virus Technologies and Methods for Targeted Neuronal Manipulation. *Frontiers in Neuroanatomy, 13*, 93. doi:10.3389/FNANA.2019.00093/BIBTEX

Halabisky, B., & Strowbridge, B. W. (2003). γ-Frequency Excitatory Input to Granule Cells Facilitates Dendrodendritic Inhibition in the Rat Olfactory Bulb. *Journal of Neurophysiology, 90*(2), 644-654. doi:10.1152/jn.00212.2003

Hamilton, K. A., & Coppola, D. M. (2003). Distribution of GluR1 is altered in the olfactory bulb following neonatal naris occlusion. *Journal of Neurobiology, 54*(2), 326-336. doi:10.1002/neu.10182

Hamilton, K. A., Parrish-Aungst, S., Margolis, F. L., Erdélyi, F., Szabó, G., & Puche, A. C. (2008). Sensory Deafferentation Transsynaptically Alters Neuronal GluR1 Expression in the

External Plexiform Layer of the Adult Mouse Main Olfactory Bulb. *Chemical Senses, 33*(2), 201-210. doi:10.1093/chemse/bjm079

Hammond, S. L., Leek, A. N., Richman, E. H., & Tjalkens, R. B. (2017). Cellular selectivity of AAV serotypes for gene delivery in neurons and astrocytes by neonatal intracerebroventricular injection. *PLOS ONE, 12*(12). doi:10.1371/JOURNAL.PONE.0188830

Hanchate, N. K., Kondoh, K., Lu, Z., Kuang, D., Ye, X., Qiu, X., . . . Buck, L. B. (2015). Single-cell transcriptomics reveals receptor transformations during olfactory neurogenesis. *Science, 350*(6265), 1251-1255. doi:10.1126/SCIENCE.AAD2456/SUPPL_FILE/AAD2456-HANCHATE-SM.PDF

Hanson, E., Swanson, J., & Arenkiel, B. R. (2020). GABAergic Input From the Basal Forebrain Promotes the Survival of Adult-Born Neurons in the Mouse Olfactory Bulb. *Frontiers in Neural Circuits, 14*, 17. doi:10.3389/FNCIR.2020.00017/BIBTEX

Hardy, D., Malvaut, S., Breton-Provencher, V., & Saghatelyan, A. (2018). The role of calretinin-expressing granule cells in olfactory bulb functions and odor behavior. *Scientific Reports 2018 8:1, 8*(1), 1-17. doi:10.1038/s41598-018-27692-8

Hardy, D., & Saghatelyan, A. (2017). Different forms of structural plasticity in the adult olfactory bulb. *Neurogenesis, 4*(1), e1301850. doi:10.1080/23262133.2017.1301850

Hattiangady, B., Rao, M. S., & Shetty, A. K. (2004). Chronic temporal lobe epilepsy is associated with severely declined dentate neurogenesis in the adult hippocampus. *Neurobiology of Disease, 17*(3), 473-490. doi:10.1016/j.nbd.2004.08.008

Hayar, A., Karnup, S., Ennis, M., & Shipley, M. T. (2004a). External Tufted Cells: A Major Excitatory Element That Coordinates Glomerular Activity. *Journal of Neuroscience, 24*(30), 6676-6685. doi:10.1523/JNEUROSCI.1367-04.2004

Hayar, A., Karnup, S., Shipley, M. T., & Ennis, M. (2004b). Olfactory Bulb Glomeruli: External Tufted Cells Intrinsically Burst at Theta Frequency and Are Entrained by Patterned Olfactory Input. *Journal of Neuroscience, 24*(5), 1190-1199. doi:10.1523/JNEUROSCI.4714-03.2004

Hayar, A., Shipley, M. T., & Ennis, M. (2005). Olfactory Bulb External Tufted Cells Are Synchronized by Multiple Intraglomerular Mechanisms. *The Journal of Neuroscience, 25*, 8197-8208.

He, W., Boesveldt, S., de Graaf, C., & de Wijk, R. (2014). Dynamics of autonomic nervous system responses and facial expressions to odors. *Frontiers in Psychology, 5*.

Holl, A. M. (2018). Survival of mature mouse olfactory sensory neurons labeled genetically perinatally. *Molecular and Cellular Neuroscience, 88*, 258-269. doi:10.1016/J.MCN.2018.02.005

Huang, J. S., Kunkhyen, T., Liu, B., Muggleton, R. J., Avon, J. T., & Cheetham, C. E. J. (2021). Immature olfactory sensory neurons provide behaviorally useful sensory input to the olfactory bulb. *bioRxiv*.

Huang, L., Ung, K., Garcia, I., Quast, K. B., Cordiner, K., Saggau, P., & Arenkiel, B. R. (2016). Task Learning Promotes Plasticity of Interneuron Connectivity Maps in the Olfactory Bulb. *Journal of Neuroscience, 36*(34), 8856-8871. doi:10.1523/JNEUROSCI.0794-16.2016

Ibarra-Soria, X., Nakahara, T. S., Lilue, J., Jiang, Y., Trimmer, C., Souza, M. A. A., . . . Logan, D. W. (2017). Variation in olfactory neuron repertoires is genetically controlled and environmentally modulated. *eLife, 6*. doi:10.7554/ELIFE.21476

Igarashi, K. M., Ieki, N., An, M., Yamaguchi, Y., Nagayama, S., Kobayakawa, K., . . . Mori, K. (2012). Parallel mitral and tufted cell pathways route distinct odor information to different targets in the olfactory cortex. *J Neurosci, 32*(23), 7970-7985. doi:10.1523/jneurosci.0154-12.2012

Imamura, F., Nagao, H., Naritsuka, H., Murata, Y., Taniguchi, H., & Mori, K. (2006). A leucine-rich repeat membrane protein, 5T4, is expressed by a subtype of granule cells with dendritic arbors in specific strata of the mouse olfactory bulb. *Journal of Comparative Neurology, 495*(6), 754-768. doi:10.1002/CNE.20896

Imayoshi, I., Sakamoto, M., Ohtsuka, T., Takao, K., Miyakawa, T., Yamaguchi, M., . . . Kageyama, R. (2008). Roles of continuous neurogenesis in the structural and functional integrity of the adult forebrain. *Nature Neuroscience, 11*(10), 1153-1161. doi:10.1038/nn.2185

Isaacson, J. S. (2001). Mechanisms governing dendritic γ-aminobutyric acid (GABA) release in the rat olfactory bulb. *Proceedings of the National Academy of Sciences, 98*(1), 337-342. doi:10.1073/pnas.98.1.337

Isaacson, J. S., & Strowbridge, B. W. (1998). Olfactory reciprocal synapses: dendritic signaling in the CNS. *Neuron, 20*(4), 749-761.

Iwai, N., Zhou, Z., Roop, D. R., & Behringer, R. R. (2008). Horizontal Basal Cells Are Multipotent Progenitors in Normal and Injured Adult Olfactory Epithelium. *Stem Cells, 26*(5), 1298-1306. doi:10.1634/STEMCELLS.2007-0891

Iwasato, T., Erzurumlu, R. S., Huerta, P. T., Chen, D. F., Sasaoka, T., Ulupinar, E., & Tonegawa, S. (1997). NMDA Receptor-Dependent Refinement of Somatotopic Maps. *Neuron, 19*(6), 1201-1210. doi:10.1016/S0896-6273(00)80412-2

Iwema, C. L., & Schwob, J. E. (2003). Odorant receptor expression as a function of neuronal maturity in the adult rodent olfactory system. *Journal of Comparative Neurology, 459*(3), 209-222. doi:10.1002/CNE.10583

John, J. A. S., & Key, B. (2003). Axon Mis-targeting in the Olfactory Bulb During Regeneration of Olfactory Neuroepithelium. *Chemical Senses, 28*(9), 773-779. doi:10.1093/chemse/bjg068

Jones, S., Zylberberg, J., & Schoppa, N. (2020). Cellular and Synaptic Mechanisms That Differentiate Mitral Cells and Superficial Tufted Cells Into Parallel Output Channels in the Olfactory Bulb. *Frontiers in Cellular Neuroscience, 14*, 443. doi:10.3389/FNCEL.2020.614377/BIBTEX

Joussain, P., Rouby, C., & BENSAFI, M. (2014). A pleasant familiar odor influences perceived stress and peripheral nervous system activity during normal aging. *Frontiers in Psychology, 5*. doi:10.3389/fpsyg.2014.00113

Kamimura, S., Masaoka, Y., Yoshikawa, A., Kamijo, S., Ohtaki, H., Koiwa, N., . . . Izumizaki, M. (2022). New granule cells in the olfactory bulb are associated with high respiratory input in an enriched odor environment. *Neuroscience Research*. doi:10.1016/J.NEURES.2022.05.007

Kaplan, M. S., McNelly, N. A., & Hinds, J. W. (1985). Population dynamics of adult-formed granule neurons of the rat olfactory bulb. *Journal of Comparative Neurology, 239*(1), 117-125. doi:10.1002/CNE.902390110

Kapoor, V., & Urban, N. N. (2006). Glomerulus-Specific, Long-Latency Activity in the Olfactory Bulb Granule Cell Network. *Journal of Neuroscience, 26*(45), 11709-11719. doi:10.1523/JNEUROSCI.3371-06.2006

Kato, A., & Touhara, K. (2009). Mammalian olfactory receptors: pharmacology, G protein coupling and desensitization. *Cellular and Molecular Life Sciences 2009 66:23*, *66*(23), 3743-3753. doi:10.1007/S00018-009-0111-6

Kelsch, W., Lin, C. W., Mosley, C. P., & Lois, C. (2009). A Critical Period for Activity-Dependent Synaptic Development during Olfactory Bulb Adult Neurogenesis. *Journal of Neuroscience, 29*(38), 11852-11858. doi:10.1523/JNEUROSCI.2406-09.2009

Kempermann, G., Kuhn, H. G., & Gage, F. H. (1997). More hippocampal neurons in adult mice living in an enriched environment. *Nature, 386*(6624), 493-495. doi:10.1038/386493a0

Kikuta, S., Fletcher, M. L., Homma, R., Yamasoba, T., & Nagayama, S. (2013). Odorant response properties of individual neurons in an olfactory glomerular module. *Neuron, 77*(6), 1122-1135. doi:10.1016/j.neuron.2013.01.022

Kikuta, S., Sakamoto, T., Nagayama, S., Kanaya, K., Kinoshita, M., Kondo, K., . . . Yamasoba, T. (2015). Sensory Deprivation Disrupts Homeostatic Regeneration of Newly Generated Olfactory Sensory Neurons after Injury in Adult Mice. *Journal of Neuroscience, 35*(6), 2657-2673. doi:10.1523/JNEUROSCI.2484-14.2015

Kim, D., Phillips, M., Chang, A., Patel, H., Nguyen, K., & Willhite, D. (2011). Lateral Connectivity in the Olfactory Bulb is Sparse and Segregated. *Frontiers in Neural Circuits, 5*.

Kirschen, G. W., Shen, J., Tian, M., Schroeder, B., Wang, J., Man, G., . . . Ge, S. (2017). Active Dentate Granule Cells Encode Experience to Promote the Addition of Adult-Born Hippocampal Neurons. *Journal of Neuroscience, 37*(18), 4661-4678. doi:10.1523/JNEUROSCI.3417-16.2017

Kiyokage, E., Pan, Y. Z., Shao, Z., Kobayashi, K., Szabo, G., Yanagawa, Y., . . . Shipley, M. T. (2010). Molecular Identity of Periglomerular and Short Axon Cells. *Journal of Neuroscience, 30*(3), 1185-1196. doi:10.1523/JNEUROSCI.3497-09.2010

Kobayashi, M., & Costanzo, R. M. (2009). Olfactory Nerve Recovery Following Mild and Severe Injury and the Efficacy of Dexamethasone Treatment. *Chemical Senses, 34*(7), 573-580. doi:10.1093/chemse/bjp038

Kohwi, M., Petryniak, M. A., Long, J. E., Ekker, M., Obata, K., Yanagawa, Y., . . . Alvarez-Buylla, A. (2007). A Subpopulation of Olfactory Bulb GABAergic Interneurons Is Derived from Emx1- and Dlx5/6-Expressing Progenitors. *Journal of Neuroscience, 27*(26), 6878-6891. doi:10.1523/JNEUROSCI.0254-07.2007

Koldaeva, A., Zhang, C., Huang, Y.-P., Reinert, J. K., Mizuno, S., Sugiyama, F., . . . Fukunaga, I. (2021). Generation and Characterization of a Cell Type-Specific, Inducible Cre-Driver Line to Study Olfactory Processing. *Journal of Neuroscience, 41*(30), 6449-6467. doi:10.1523/JNEUROSCI.3076-20.2021

Kondo, K., Suzukawa, K., Sakamoto, T., Watanabe, K., Kanaya, K., Ushio, M., . . . Yamasoba, T. (2010). Age-related changes in cell dynamics of the postnatal mouse olfactory neuroepithelium: Cell proliferation, neuronal differentiation, and cell death. *Journal of Comparative Neurology, 518*(11), 1962-1975. doi:10.1002/CNE.22316

Kopel, H., Schechtman, E., Groysman, M., & Mizrahi, A. (2012). Enhanced Synaptic Integration of Adult-Born Neurons in the Olfactory Bulb of Lactating Mothers. *Journal of Neuroscience, 32*(22), 7519-7527. doi:10.1523/JNEUROSCI.6354-11.2012

Kuhn, H. G., Dickinson-Anson, H., & Gage, F. H. (1996). Neurogenesis in the Dentate Gyrus of the Adult Rat: Age-Related Decrease of Neuronal Progenitor Proliferation. *The Journal of Neuroscience, 76*(6), 2027-2033.

Labarrera, C., London, M., & Angelo, K. (2013). Tonic inhibition sets the state of excitability in olfactory bulb granule cells. *The Journal of Physiology, 591*(7), 1841-1850. doi:10.1113/JPHYSIOL.2012.241851

Lage-Rupprecht, V., Zhou, L., Bianchini, G., Aghvami, S. S., Mueller, M., Rózsa, B., . . . Egger, V. (2020). Presynaptic nmdars cooperate with local spikes toward gaba release from the reciprocal olfactory bulb granule cell spine. *eLife, 9*, 1-27. doi:10.7554/ELIFE.63737

Lagier, S., Panzanelli, P., Russo, R. E., Nissant, A., Bathellier, B., Sassoè-Pognetto, M., . . . Lledo, P. M. (2007). GABAergic inhibition at dendrodendritic synapses tunes γ oscillations in the olfactory bulb. *Proceedings of the National Academy of Sciences of the United States of America, 104*(17), 7259-7264. doi:10.1073/PNAS.0701846104/SUPPL_FILE/01846FIG13.PDF

Lazarus, M. S., & Huang, Z. J. (2011). Distinct maturation profiles of perisomatic and dendritic targeting GABAergic interneurons in the mouse primary visual cortex during the critical period of ocular dominance plasticity. *Journal of Neurophysiology, 106*(2), 775-787. doi:10.1152/JN.00729.2010/ASSET/IMAGES/LARGE/Z9K0081108810009.JPEG

Lee, W.-C. A., Huang, H., Feng, G., Sanes, J. R., Brown, E. N., So, P. T., & Nedivi, E. (2005). Dynamic Remodeling of Dendritic Arbors in GABAergic Interneurons of Adult Visual Cortex. *PLOS Biology, 4*(2), e29. doi:10.1371/journal.pbio.0040029

Lemasson, M., Saghatelyan, A., Olivo-Marin, J.-C., & Lledo, P.-M. (2005). Neonatal and Adult Neurogenesis Provide Two Distinct Populations of Newborn Neurons to the Mouse Olfactory Bulb. *Journal of Neuroscience, 25*(29), 6816-6825. doi:10.1523/JNEUROSCI.1114-05.2005

Lepousez, G., Nissant, A., Bryant, A. K., Gheusi, G., Greer, C. A., & Lledo, P.-M. (2014). Olfactory learning promotes input-specific synaptic plasticity in adult-born neurons. *Proceedings of the National Academy of Sciences, 111*(38), 13984-13989. doi:10.1073/pnas.1404991111

Levy, F., Keller, M., & Poindron, P. (2004). Olfactory regulation of maternal behavior in mammals. *Hormones and Behavior, 46*, 284-302. doi:10.1016/j.yhbeh.2004.02.005

Li, B., Yamamori, H., Tatebayashi, Y., Shafit-Zagardo, B., Tanimukai, H., Chen, S., . . . Grundke-Iqbal, I. (2008). Failure of Neuronal Maturation in Alzheimer Disease Dentate Gyrus. *Journal of Neuropathology & Experimental Neurology, 67*(1), 78-84. doi:10.1097/nen.0b013e318160c5db

Li, W. L., Chu, M. W., Wu, A., Suzuki, Y., Imayoshi, I., & Komiyama, T. (2018). Adult-born neurons facilitate olfactory bulb pattern separation during task engagement. *eLife, 7*. doi:10.7554/ELIFE.33006

Liberia, T., Martin-Lopez, E., Meller, S. J., & Greer, C. A. (2019). Sequential Maturation of Olfactory Sensory Neurons in the Mature Olfactory Epithelium. *eNeuro, 6*(5). doi:10.1523/ENEURO.0266-19.2019

Lin, C. W., Sim, S., Ainsworth, A., Okada, M., Kelsch, W., & Lois, C. (2010). Genetically Increased Cell-Intrinsic Excitability Enhances Neuronal Integration into Adult Brain Circuits. *Neuron, 65*(1), 32-39. doi:10.1016/J.NEURON.2009.12.001/ATTACHMENT/6E429F6F-5682-4504-8F27-768D8355B19A/MMC1.PDF

Liu, S., Aungst, J. L., Puche, A. C., & Shipley, M. T. (2012). Serotonin modulates the population activity profile of olfactory bulb external tufted cells. *Journal of Neurophysiology, 107*(1), 473-483. doi:10.1152/JN.00741.2011/ASSET/IMAGES/LARGE/Z9K0021211260007.JPEG

Liu, S., Plachez, C., Shao, Z., Puche, A., & Shipley, M. T. (2013). Olfactory Bulb Short Axon Cell Release of GABA and Dopamine Produces a Temporally Biphasic Inhibition–Excitation Response in External Tufted Cells. *Journal of Neuroscience, 33*(7), 2916-2926. doi:10.1523/JNEUROSCI.3607-12.2013

Liu, S., Puche, A. C., & Shipley, M. T. (2016). The Interglomerular Circuit Potently Inhibits Olfactory Bulb Output Neurons by Both Direct and Indirect Pathways. *The Journal of Neuroscience, 36*, 9604-9617.

Liu, S., & Shipley, M. T. (2008). Multiple Conductances Cooperatively Regulate Spontaneous Bursting in Mouse Olfactory Bulb External Tufted Cells. *The Journal of Neuroscience, 28*, 1625-1639.

Livneh, Y., Adam, Y., & Mizrahi, A. (2014). Odor Processing by Adult-Born Neurons. *Neuron, 81*(5), 1097-1110. doi:10.1016/j.neuron.2014.01.007

Livneh, Y., & Mizrahi, A. (2012). Experience-dependent plasticity of mature adult-born neurons. *Nature Neuroscience, 15*(1), 26-28. doi:10.1038/nn.2980

Lledo, P.-M., Alonso, M., & Grubb, M. S. (2006). Adult neurogenesis and functional plasticity in neuronal circuits. *Nature Reviews Neuroscience, 7*(3), 179-193. doi:10.1038/nrn1867

Lledo, P.-M., & Valley, M. (2016). Adult Olfactory Bulb Neurogenesis. *Cold Spring Harbor Perspectives in Biology, 8*(8). doi:10.1101/cshperspect.a018945

Lledo, P. M., & Saghatelyan, A. (2005). Integrating new neurons into the adult olfactory bulb: joining the network, life-death decisions, and the effects of sensory experience. *Trends Neurosci, 28*(5), 248-254. doi:10.1016/j.tins.2005.03.005

Loo, A. T., Youngentob, S. L., Kent, P. F., & Schwob, J. E. (1996). The aging olfactory epithelium: Neurogenesis, response to damage, and odorant-induced activity. *International Journal of Developmental Neuroscience, 14*(7-8), 881-900. doi:10.1016/S0736-5748(96)00046-9

Lübke, K. T., & Pause, B. M. (2015). Always follow your nose: The functional significance of social chemosignals in human reproduction and survival. *Hormones and Behavior, 68*, 134-144. doi:10.1016/j.yhbeh.2014.10.001

Lucassen, P. J., Stumpel, M. W., Wang, Q., & Aronica, E. (2010). Decreased numbers of progenitor cells but no response to antidepressant drugs in the hippocampus of elderly depressed patients. *Neuropharmacology, 58*(6), 940-949. doi:10.1016/j.neuropharm.2010.01.012

Lukas, M., Suyama, H., & Egger, V. (2019). Vasopressin Cells in the Rodent Olfactory Bulb Resemble Non-Bursting Superficial Tufted Cells and Are Primarily Inhibited upon Olfactory Nerve Stimulation. *eNeuro, 6*(4). doi:10.1523/ENEURO.0431-18.2019

Lundström, J. N., & Olsson, M. J. (2010). Chapter One - Functional Neuronal Processing of Human Body Odors. In G. Litwack (Ed.), *Vitamins & Hormones* (Vol. 83, pp. 1-23): Academic Press.

Maccaferri, G., David, J., Roberts, B., Szucs, P., Cottingham, C. A., & Somogyi, P. (2000). Cell surface domain specific postsynaptic currents evoked by identified GABAergic neurones in rat hippocampus in vitro. *The Journal of Physiology, 524*(1), 91-116. doi:10.1111/J.1469-7793.2000.T01-3-00091.X

Magavi, S. S. P., Mitchell, B. D., Szentirmai, O., Carter, B. S., & Macklis, J. D. (2005). Adult-Born and Preexisting Olfactory Granule Neurons Undergo Distinct Experience-Dependent Modifications of their Olfactory Responses In Vivo. *The Journal of Neuroscience, 25*(46), 10729. doi:10.1523/JNEUROSCI.2250-05.2005

Malnic, B., Godfrey, P. A., & Buck, L. B. (2004). The human olfactory receptor gene family. *Proceedings of the National Academy of Sciences, 101*(8), 2584-2589. doi:10.1073/pnas.0307882100

Malnic, B., Hirono, J., Sato, T., & Buck, L. B. (1999). Combinatorial Receptor Codes for Odors. *Cell, 96*(5), 713-723. doi:10.1016/S0092-8674(00)80581-4

Malvaut, S., Gribaudo, S., Hardy, D., David, L. S., Daroles, L., Labrecque, S., . . . Saghatelyan, A. (2017). CaMKIIα Expression Defines Two Functionally Distinct Populations of Granule Cells Involved in Different Types of Odor Behavior. *Current Biology, 27*(21), 3315-3329.e3316. doi:10.1016/j.cub.2017.09.058

Mandairon, N., Kuczewski, N., Kermen, F., Forest, J., Midroit, M., Richard, M., . . . Didier, A. (2018). Opposite regulation of inhibition by adult-born granule cells during implicit versus explicit olfactory learning. *eLife, 7*, e34976. doi:10.7554/eLife.34976

Marcucci, F., Maier-Balough, E., Zou, D. J., & Firestein, S. (2011). Exuberant growth and synapse formation of olfactory sensory neuron axonal arborizations. *Journal of Comparative Neurology, 519*(18), 3713-3726. doi:10.1002/CNE.22684

Margrie, T. W., Sakmann, B., & Urban, N. N. (2001). Action potential propagation in mitral cell lateral dendrites is decremental and controls recurrent and lateral inhibition in the mammalian olfactory bulb. *Proceedings of the National Academy of Sciences, 98*(1), 319-324. doi:10.1073/pnas.98.1.319

Markopoulos, F., Rokni, D., Gire, D. H., & Murthy, V. N. (2012). Functional Properties of Cortical Feedback Projections to the Olfactory Bulb. *Neuron, 76*(6), 1175-1188. doi:10.1016/J.NEURON.2012.10.028/ATTACHMENT/D8EE3549-7D8B-4846-A559-5ED6C5E37190/MMC1.PDF

Martelli, C., & Storace, D. A. (2021). Stimulus Driven Functional Transformations in the Early Olfactory System. *Frontiers in Cellular Neuroscience, 15*.

Martin, C., & Ravel, N. (2014). Beta and gamma oscillatory activities associated with olfactory memory tasks: different rhythms for different functional networks? *Frontiers in Behavioral Neuroscience, 8*.

McAvoy, K. M., Scobie, K. N., Berger, S., Russo, C., Guo, N., Decharatanachart, P., . . . Sahay, A. (2016). Modulating Neuronal Competition Dynamics in the Dentate Gyrus to Rejuvenate Aging Memory Circuits. *Neuron, 91*(6), 1356-1373. doi:10.1016/j.neuron.2016.08.009

McGann, J. P. (2013). Presynaptic Inhibition of Olfactory Sensory Neurons: New Mechanisms and Potential Functions. *Chemical Senses, 38*(6), 459-474. doi:10.1093/CHEMSE/BJT018

McGann, J. P. (2017). Poor human olfaction is a 19th-century myth. *Science, 356*(6338), eaam7263. doi:10.1126/science.aam7263

McIntyre, J. C., Titlow, W. B., & McClintock, T. S. (2010). Axon growth and guidance genes identify nascent, immature, and mature olfactory sensory neurons. *Journal of Neuroscience Research, 88*(15), 3243-3256. doi:10.1002/JNR.22497

McTavis, T. S., Migliore, M., Shepherd, G. M., & Hines, M. L. (2012). Mitral cell spike synchrony modulated by dendrodendritic synapse location. *Frontiers in Computational Neuroscience, 0*(JANUARY 2012), 3. doi:10.3389/FNCOM.2012.00003/BIBTEX

Migliore, M., Inzirillo, C., & Shepherd, G. (2007). Learning mechanism for column formation in the olfactory bulb. *Frontiers in Integrative Neuroscience, 1*.

Milinski, M., Croy, I., Hummel, T., & Boehm, T. (2013). Major histocompatibility complex peptide ligands as olfactory cues in human body odour assessment. *Proceedings of the Royal Society B: Biological Sciences, 280*(1755), 20122889. doi:10.1098/rspb.2012.2889

Ming, G. l., & Song, H. (2011). Adult Neurogenesis in the Mammalian Brain: Significant Answers and Significant Questions. *Neuron, 70*(4), 687-702. doi:10.1016/J.NEURON.2011.05.001

Miragall, F., & Graziadei, G. A. M. (1982). Experimental studies on the olfactory marker protein. II. Appearance of the olfactory marker protein during differentiation of the olfactory sensory neurons of mouse: an immunohistochemical and autoradiographic study. *Brain Research, 239*, 245-250.

Mirescu, C., Peters, J. D., & Gould, E. (2004). Early life experience alters response of adult neurogenesis to stress. *Nature Neuroscience, 7*(8), 841-846. doi:10.1038/nn1290

Mitsui, S., Igarashi, K. M., Mori, K., & Yoshihara, Y. (2011). Genetic visualization of the secondary olfactory pathway in Tbx21 transgenic mice. *Neural Systems & Circuits, 1*(1), 5. doi:10.1186/2042-1001-1-5

Mizrahi, A. (2007). Dendritic development and plasticity of adult-born neurons in the mouse olfactory bulb. *Nature Neuroscience 2007 10:4*, *10*(4), 444-452. doi:10.1038/NN1875

Mizrahi, A., & Katz, L. C. (2003). Dendritic stability in the adult olfactory bulb. *Nature Neuroscience*, *6*(11), 1201-1207. doi:10.1038/nn1133

Mombaerts, P. (1996). Targeting olfaction. *Current Opinion in Neurobiology*, *6*(4), 481-486. doi:10.1016/S0959-4388(96)80053-5

Mombaerts, P., Wang, F., Dulac, C., Chao, S. K., Nemes, A., Mendelsohn, M., . . . Axel, R. (1996). Visualizing an Olfactory Sensory Map. *Cell*, *87*(4), 675-686. doi:10.1016/S0092-8674(00)81387-2

Montero-Pedrazuela, A., Venero, C., Lavado-Autric, R., Fernández-Lamo, I., García-Verdugo, J. M., Bernal, J., & Guadaño-Ferraz, A. (2006). Modulation of adult hippocampal neurogenesis by thyroid hormones: implications in depressive-like behavior. *Molecular Psychiatry*, *11*(4), 361-371. doi:10.1038/sj.mp.4001802

Moreno, M. M., Linster, C., Escanilla, O., Sacquet, J., Didier, A., & Mandairon, N. (2009). Olfactory perceptual learning requires adult neurogenesis. *Proceedings of the National Academy of Sciences*, *106*(42), 17980-17985. doi:10.1073/pnas.0907063106

Mori, K. (1987). Membrane and synaptic properties of identified neurons in the olfactory bulb. *Progress in Neurobiology*, *29*(3), 275-320. doi:10.1016/0301-0082(87)90024-4

Mori, K., Kishi, K., & Ojima, H. (1983). Distribution of dendrites of mitral, displaced mitral, tufted, and granule cells in the rabbit olfactory bulb. *The Journal of Comparative Neurology*, *219*(3), 339-355. doi:10.1002/cne.902190308

Mouret, A., Gheusi, G., Gabellec, M.-M., Chaumont, F. d., Olivo-Marin, J.-C., & Lledo, P.-M. (2008). Learning and Survival of Newly Generated Neurons: When Time Matters. *Journal of Neuroscience*, *28*(45), 11511-11516. doi:10.1523/JNEUROSCI.2954-08.2008

Mouret, A., Lepousez, G., Gras, J., Gabellec, M. M., & Lledo, P. M. (2009). Turnover of Newborn Olfactory Bulb Neurons Optimizes Olfaction. *Journal of Neuroscience*, *29*(39), 12302-12314. doi:10.1523/JNEUROSCI.3383-09.2009

Murdoch, B., & Roskams, A. J. (2007). Olfactory epithelium progenitors: Insights from transgenic mice and in vitro biology. *Journal of Molecular Histology*, *38*(6), 581-599. doi:10.1007/S10735-007-9141-2/FIGURES/6

Murphy, G. J., Glickfeld, L. L., Balsen, Z., & Isaacson, J. S. (2004). Sensory Neuron Signaling to the Brain: Properties of Transmitter Release from Olfactory Nerve Terminals. *Journal of Neuroscience*, *24*(12), 3023-3030. doi:10.1523/JNEUROSCI.5745-03.2004

Muthusamy, N., Zhang, X., Johnson, C. A., Yadav, P. N., & Ghashghaei, H. T. (2017). Developmentally defined forebrain circuits regulate appetitive and aversive olfactory learning. *Nature Neuroscience*, *20*(1), 20-23. doi:10.1038/nn.4452

Nagayama, S., Enerva, A., Fletcher, M. L., Masurkar, A. V., Igarashi, K. M., Mori, K., & Chen, W. R. (2010). Differential axonal projection of mitral and tufted cells in the mouse main olfactory system. *Frontiers in Neural Circuits, 4*(SEP), 120. doi:10.3389/FNCIR.2010.00120/BIBTEX

Nagayama, S., Homma, R., & Imamura, F. (2014). Neuronal organization of olfactory bulb circuits. *Front Neural Circuits, 8*, 98. doi:10.3389/fncir.2014.00098

Nagayama, S., Takahashi, Y. K., Yoshihara, Y., & Mori, K. (2004). Mitral and tufted cells differ in the decoding manner of odor maps in the rat olfactory bulb. *J Neurophysiol, 91*(6), 2532-2540. doi:10.1152/jn.01266.2003

Najac, M., Jan, D. D. S., Reguero, L., Grandes, P., & Charpak, S. (2011). Monosynaptic and Polysynaptic Feed-Forward Inputs to Mitral Cells from Olfactory Sensory Neurons. *Journal of Neuroscience, 31*(24), 8722-8729. doi:10.1523/JNEUROSCI.0527-11.2011

Nei, M., Niimura, Y., & Nozawa, M. (2008). The evolution of animal chemosensory receptor gene repertoires: roles of chance and necessity. *Nature Reviews Genetics 2008 9:12, 9*(12), 951-963. doi:10.1038/NRG2480

Neukomm, L. J., & Freeman, M. R. (2014). Diverse cellular and molecular modes of axon degeneration. *Trends in cell biology, 24*(9), 515. doi:10.1016/J.TCB.2014.04.003

Neuland, C., Bitter, T., Marschner, H., Gudziol, H., & Guntinas-Lichius, O. (2011). Health-related and specific olfaction-related quality of life in patients with chronic functional anosmia or severe hyposmia. *The Laryngoscope, 121*(4), 867-872. doi:10.1002/lary.21387

Nguyen, M. Q., Zhou, Z., Marks, C. A., Ryba, N. J. P., & Belluscio, L. (2007). Prominent Roles for Odorant Receptor Coding Sequences in Allelic Exclusion. *Cell, 131*(5), 1009-1017. doi:10.1016/j.cell.2007.10.050

Nickell, M. D., Breheny, P., Stromberg, A. J., & Mcclintock, T. S. (2012). Genomics of mature and immature olfactory sensory neurons. *Journal of Comparative Neurology, 520*(12), 2608-2629. doi:10.1002/CNE.23052

Nishizumi, H., Miyashita, A., Inoue, N., Inokuchi, K., Aoki, M., & Sakano, H. (2019). Primary dendrites of mitral cells synapse unto neighboring glomeruli independent of their odorant receptor identity. *Communications Biology, 2*(1), 1-12. doi:10.1038/s42003-018-0252-y

Nunez-Parra, A., Maurer, R. K., Krahe, K., Smith, R. S., & Araneda, R. C. (2013). Disruption of centrifugal inhibition to olfactory bulb granule cells impairs olfactory discrimination. *Proceedings of the National Academy of Sciences of the United States of America, 110*(36), 14777-14782. doi:10.1073/PNAS.1310686110/SUPPL_FILE/PNAS.201310686SI.PDF

Olson, C. R., Gettner, S. N., Ventura, V., Carta, R., & Kass, R. E. (2000). Neuronal Activity in Macaque Supplementary Eye Field During Planning of Saccades in Response to Pattern and Spatial Cues. *Journal of Neurophysiology, 84*(3), 1369-1384. doi:10.1152/jn.2000.84.3.1369

Orona, E., Rainer, E. C., & Scott, J. W. (1984). Dendritic and axonal organization of mitral and tufted cells in the rat olfactory bulb. *Journal of Comparative Neurology, 226*(3), 346-356. doi:10.1002/CNE.902260305

Orona, E., Scott, J. W., & Rainer, E. C. (1983). Different granule cell populations innervate superficial and deep regions of the external plexiform layer in rat olfactory bulb. *Journal of Comparative Neurology, 217*(2), 227-237. doi:10.1002/cne.902170209

Otazu, Gonzalo H., Chae, H., Davis, Martin B., & Albeanu, Dinu F. (2015). Cortical Feedback Decorrelates Olfactory Bulb Output in Awake Mice. *Neuron, 86*(6), 1461-1477. doi:10.1016/j.neuron.2015.05.023

Padmanabhan, K., Osakada, F., Tarabrina, A., Kizer, E., Callaway, E. M., Gage, F. H., & Sejnowski, T. J. (2019). Centrifugal inputs to the main olfactory bulb revealed through whole brain circuit-mapping. *Frontiers in Neuroanatomy, 12*, 115. doi:10.3389/FNANA.2018.00115/BIBTEX

Pankevich, D. E., Baum, M. J., & Cherry, J. A. (2004). Olfactory Sex Discrimination Persists, Whereas the Preference for Urinary Odorants from Estrous Females Disappears in Male Mice after Vomeronasal Organ Removal. *The Journal of Neuroscience, 24*, 9451-9457.

Paredes, M. F., Sorrells, S. F., Garcia-Verdugo, J. M., & Alvarez-Buylla, A. (2016). Brain Size and Limits to Adult Neurogenesis. *The Journal of Comparative Neurology, 524*(3), 646-664. doi:10.1002/cne.23896

Parrish-Aungst, S., Shipley, M. T., Erdelyi, F., Szabo, G., & Puche, A. C. (2007). Quantitative analysis of neuronal diversity in the mouse olfactory bulb. *J Comp Neurol, 501*(6), 825-836. doi:10.1002/cne.21205

Pause, B. M. (2012). Processing of Body Odor Signals by the Human Brain. *Chemosensory Perception, 5*(1), 55-63. doi:10.1007/s12078-011-9108-2

Pearce, R. A. (1993). Physiological evidence for two distinct GABAA responses in rat hippocampus. *Neuron, 10*(2), 189-200. doi:10.1016/0896-6273(93)90310-N

Pemberton, J. M., Pogmore, J. P., & Andrews, D. W. (2020). Neuronal cell life, death, and axonal degeneration as regulated by the BCL-2 family proteins. *Cell Death & Differentiation 2020 28:1, 28*(1), 108-122. doi:10.1038/s41418-020-00654-2

Petreanu, L., & Alvarez-Buylla, A. (2002). Maturation and death of adult-born olfactory bulb granule neurons: role of olfaction. *J Neurosci, 22*(14), 6106-6113. doi:20026588

Piatti, V. C., Davies-Sala, M. G., Espósito, M. S., Mongiat, L. A., Trinchero, M. F., & Schinder, A. F. (2011). The Timing for Neuronal Maturation in the Adult Hippocampus Is Modulated by Local Network Activity. *Journal of Neuroscience, 31*(21), 7715-7728. doi:10.1523/JNEUROSCI.1380-11.2011

Pinching, A. J., & Powell, T. P. S. (1971a). THE NEURON TYPES OF THE GLOMERULAR LAYER OF THE OLFACTORY BULB. *J. Cell Sci, 9*, 305-345.

Pinching, A. J., & Powell, T. P. S. (1971b). THE NEUROPIL OF THE GLOMERULI OF THE OLFACTORY BULB. *J. Cell Sci, 9*, 347.

Platel, J.-C., Angelova, A., Bugeon, S., Wallace, J., Ganay, T., Chudotvorova, I., . . . Cremer, H. (2019, 2019-07-11). Neuronal integration in the adult mouse olfactory bulb is a non-selective addition process. *eLife*.

Pressler, R. T., & Strowbridge, B. W. (2020). Activation of Granule Cell Interneurons by Two Divergent Local Circuit Pathways in the Rat Olfactory Bulb. *Journal of Neuroscience, 40*(50), 9701-9714. doi:10.1523/JNEUROSCI.0989-20.2020

Price, J. L., & Powell, T. P. S. (1970a). THE MITRAL AND SHORT AXON CELLS OF THE OLFACTORY BULB. *J. Cell Sci, 7*, 631-651.

Price, J. L., & Powell, T. P. S. (1970b). THE MORPHOLOGY OF THE GRANULE CELLS OF THE OLFACTORY BULB. *J. Cell Sci, 7*, 91-123.

Quast, K. B., Ung, K., Froudarakis, E., Huang, L., Herman, I., Addison, A. P., . . . Arenkiel, B. R. (2017). Developmental broadening of inhibitory sensory maps. *Nat Neurosci, 20*(2), 189-199. doi:10.1038/nn.4467

Ressler, K. J., Sullivan, S. L., & Buck, L. B. (1994). Information coding in the olfactory system: Evidence for a stereotyped and highly organized epitope map in the olfactory bulb. *Cell, 79*(7), 1245-1255. doi:10.1016/0092-8674(94)90015-9

Richard, M. B., Taylor, S. R., & Greer, C. A. (2010). Age-induced disruption of selective olfactory bulb synaptic circuits. *Proceedings of the National Academy of Sciences of the United States of America, 107*(35), 15613-15618. doi:10.1073/PNAS.1007931107/SUPPL_FILE/PNAS.201007931SI.PDF

Roberts, T., & Roiser, J. P. (2010). In the nose of the beholder: are olfactory influences on human mate choice driven by variation in immune system genes or sex hormone levels? *Experimental Biology and Medicine, 235*(11), 1277-1281. doi:10.1258/ebm.2010.010112

Rodriguez-Gil, D. J., Bartel, D. L., Jaspers, A. W., Mobley, A. S., Imamura, F., & Greer, C. A. (2015). Odorant receptors regulate the final glomerular coalescence of olfactory sensory neuron axons. *Proceedings of the National Academy of Sciences of the United States of America, 112*(18), 5821-5826. doi:10.1073/PNAS.1417955112/SUPPL_FILE/PNAS.201417955SI.PDF

Rothermel, M., & Wachowiak, M. (2014). Functional imaging of cortical feedback projections to the olfactory bulb. *Frontiers in Neural Circuits, 8*(JULY), 73. doi:10.3389/FNCIR.2014.00073/BIBTEX

Royet, J. P., Souchier, C., Jourdan, F., & Ploye, H. (1988). Morphometric study of the glomerular population in the mouse olfactory bulb: numerical density and size distribution along the rostrocaudal axis. *J Comp Neurol, 270*(4), 559-568. doi:10.1002/cne.902700409

Rubin, B. D., & Katz, L. C. (1999). Optical Imaging of Odorant Representations in the Mammalian Olfactory Bulb. *Neuron, 23*(3), 499-511. doi:10.1016/S0896-6273(00)80803-X

Ryba, N. J., & Tirindelli, R. (1995). A Novel GTP-binding Protein γ-Subunit, Gγ8, Is Expressed during Neurogenesis in the Olfactory and Vomeronasal Neuroepithelia (∗). *Journal of Biological Chemistry, 270*(12), 6757-6767.

Saghatelyan, A., Roux, P., Migliore, M., Rochefort, C., Desmaisons, D., Charneau, P., . . . Lledo, P.-M. (2005). Activity-dependent adjustments of the inhibitory network in the olfactory bulb following early postnatal deprivation. *Neuron, 46*(1), 103-116. doi:10.1016/j.neuron.2005.02.016

Sailor, K. A., Valley, M. T., Wiechert, M. T., Riecke, H., Sun, G. J., Adams, W., . . . Lledo, P.-M. (2016). Persistent Structural Plasticity Optimizes Sensory Information Processing in the Olfactory Bulb. *Neuron, 91*(2), 384-396. doi:10.1016/j.neuron.2016.06.004

Sakamoto, M., Ieki, N., Miyoshi, G., Mochimaru, D., Miyachi, H., Imura, T., . . . Imayoshi, I. (2014). Continuous Postnatal Neurogenesis Contributes to Formation of the Olfactory Bulb Neural Circuits and Flexible Olfactory Associative Learning. *Journal of Neuroscience, 34*(17), 5788-5799. doi:10.1523/JNEUROSCI.0674-14.2014

Sakamoto, T., Kondo, K., Kashio, A., Suzukawa, K., & Yamasoba, T. (2007). Methimazole-induced cell death in rat olfactory receptor neurons occurs via apoptosis triggered through mitochondrial cytochrome c-mediated caspase-3 activation pathway. *Journal of Neuroscience Research, 85*(3), 548-557. doi:10.1002/JNR.21155

Sánchez-González, R., Figueres-Oñate, M., Ojalvo-Sanz, A. C., & López-Mascaraque, L. (2020). Cell Progeny in the Olfactory Bulb after Targeting Specific Progenitors with Different UbC-StarTrack Approaches. *Genes, 11*(3), 305. doi:10.3390/genes11030305

Santoro, S. W., & Dulac, C. (2012). The activity-dependent histone variant H2BE modulates the life span of olfactory neurons. *eLife, 2012*(1). doi:10.7554/ELIFE.00070

Sarafoleanu, C., Mella, C., Georgescu, M., & Perederco, C. (2009). The importance of the olfactory sense in the human behavior and evolution. *Journal of Medicine and Life, 2*(2), 196-198.

Savya, S. P., Kunkhyen, T., & Cheetham, C. E. J. (2019). Low survival rate of young adult-born olfactory sensory neurons in the undamaged mouse olfactory epithelium. *Journal of Bioenergetics and Biomembranes, 51*(1), 41-51. doi:10.1007/S10863-018-9774-8/FIGURES/5

Schindelin, J., Arganda-Carreras, I., Frise, E., Kaynig, V., Longair, M., Pietzsch, T., . . . Cardona, A. (2012). Fiji: an open-source platform for biological-image analysis. *Nature Methods, 9*(7), 676-682. doi:10.1038/nmeth.2019

Schoppa, N. E. (2006). Synchronization of Olfactory Bulb Mitral Cells by Precisely Timed Inhibitory Inputs. *Neuron, 49*(2), 271-283. doi:10.1016/j.neuron.2005.11.038

Schoppa, N. E., Kinzie, J. M., Sahara, Y., Segerson, T. P., & Westbrook, G. L. (1998). Dendrodendritic Inhibition in the Olfactory Bulb Is Driven by NMDA Receptors. *Journal of Neuroscience, 18*(17), 6790-6802. doi:10.1523/JNEUROSCI.18-17-06790.1998

Schoppa, N. E., & Westbrook, G. L. (1999). Regulation of synaptic timing in the olfactory bulb by an A-type potassium current. *Nature Neuroscience 1999 2:12, 2*(12), 1106-1113. doi:10.1038/16033

Schoppa, N. E., & Westbrook, G. L. (2001). Glomerulus-Specific Synchronization of Mitral Cells in the Olfactory Bulb. *Neuron, 31*(4), 639-651. doi:10.1016/S0896-6273(01)00389-0

Schwob, J. E. (2002). Neural regeneration and the peripheral olfactory system. *The Anatomical Record, 269*(1), 33-49. doi:10.1002/AR.10047

Schwob, J. E., Youngentob, S. L., & Mezza, R. C. (1995). Reconstitution of the rat olfactory epithelium after methyl bromide-induced lesion. *Journal of Comparative Neurology, 359*(1), 15-37. doi:10.1002/cne.903590103

Secundo, L., Snitz, K., Weissler, K., Pinchover, L., Shoenfeld, Y., Loewenthal, R., . . . Sobel, N. (2015). Individual olfactory perception reveals meaningful nonolfactory genetic information. *Proceedings of the National Academy of Sciences, 112*(28), 8750-8755. doi:10.1073/pnas.1424826112

Serizawa, S., Ishii, T., Nakatani, H., Tsuboi, A., Nagawa, F., Asano, M., . . . Sakano, H. (2000). Mutually exclusive expression of odorant receptor transgenes. *Nature Neuroscience 2000 3:7, 3*(7), 687-693. doi:10.1038/76641

Seroogy, K. B., Brecha, N., & Gall, C. (1985). Distribution of cholecystokinin-like immunoreactivity in the rat main olfactory bulb. *Journal of Comparative Neurology, 239*(4), 373-383. doi:https://doi.org/10.1002/cne.902390403

Shani-Narkiss, H., Vinograd, A., Landau, I. D., Tasaka, G., Yayon, N., Terletsky, S., . . . Mizrahi, A. (2020). Young adult-born neurons improve odor coding by mitral cells. *Nature Communications, 11*(1), 5867. doi:10.1038/s41467-020-19472-8

Shao, Z., Puche, A. C., Kiyokage, E., Szabo, G., & Shipley, M. T. (2009). Two GABAergic intraglomerular circuits differentially regulate tonic and phasic presynaptic inhibition of olfactory nerve terminals. *Journal of Neurophysiology, 101*(4), 1988-2001. doi:10.1152/JN.91116.2008/ASSET/IMAGES/LARGE/Z9K0040994100007.JPEG

Shepherd, G. M. (2004a). The Human Sense of Smell: Are We Better Than We Think? *PLOS Biology, 2*(5), e146. doi:10.1371/journal.pbio.0020146

Shepherd, G. M. (2004b). The Synaptic Organization of the Brain. *The Synaptic Organization of the Brain*, 1-736. doi:10.1093/ACPROF:OSO/9780195159561.001.1

Shepherd, G. M., Chen, W. R., Willhite, D., Migliore, M., & Greer, C. A. (2007). The olfactory granule cell: From classical enigma to central role in olfactory processing. *Brain Research Reviews, 55*(2), 373-382. doi:10.1016/j.brainresrev.2007.03.005

Shingo, T., Gregg, C., Enwere, E., Fujikawa, H., Hassam, R., Geary, C., . . . Weiss, S. (2003). Pregnancy-Stimulated Neurogenesis in the Adult Female Forebrain Mediated by Prolactin. *Science, 299*(5603), 117-120. doi:10.1126/science.1076647

Short, S. M., & Wachowiak, M. (2019). Temporal dynamics of inhalation-linked activity across defined subpopulations of mouse olfactory bulb neurons imaged in vivo. *eNeuro*, ENEURO.0189-0119.2019. doi:10.1523/ENEURO.0189-19.2019

Smeets, M., & Dijksterhuis, G. (2014). Smelly primes – when olfactory primes do or do not work. *Frontiers in Psychology, 5*.

Snyder, J. S., Soumier, A., Brewer, M., Pickel, J., & Cameron, H. A. (2011). Adult hippocampal neurogenesis buffers stress responses and depressive behaviour. *Nature, 476*(7361), 458-461. doi:10.1038/nature10287

Soucy, E. R., Albeanu, D. F., Fantana, A. L., Murthy, V. N., & Meister, M. (2009). Precision and diversity in an odor map on the olfactory bulb. *Nature Neuroscience, 12*(2), 210-220. doi:10.1038/nn.2262

Spalding, K. L., Bergmann, O., Alkass, K., Bernard, S., Salehpour, M., Huttner, H. B., . . . Frisén, J. (2013). Dynamics of Hippocampal Neurogenesis in Adult Humans. *Cell, 153*(6), 1219-1227. doi:10.1016/j.cell.2013.05.002

Stroh, O., Freichel, M., Kretz, O., Birnbaumer, L., Hartmann, J., & Egger, V. (2012). NMDA Receptor-Dependent Synaptic Activation of TRPC Channels in Olfactory Bulb Granule Cells. *Journal of Neuroscience, 32*(17), 5737-5746. doi:10.1523/JNEUROSCI.3753-11.2012

Sun, X., Liu, X., Starr, E. R., & Liu, S. (2020). CCKergic Tufted Cells Differentially Drive Two Anatomically Segregated Inhibitory Circuits in the Mouse Olfactory Bulb. *Journal of Neuroscience, 40*(32), 6189-6206. doi:10.1523/JNEUROSCI.0769-20.2020

Takahashi, H., Ogawa, Y., Yoshihara, S.-i., Asahina, R., Kinoshita, M., Kitano, T., . . . Tsuboi, A. (2016). A Subtype of Olfactory Bulb Interneurons Is Required for Odor Detection and Discrimination Behaviors. *The Journal of Neuroscience, 36*(31), 8210. doi:10.1523/JNEUROSCI.2783-15.2016

Tan, L., Li, Q., & Xie, X. S. (2015). Olfactory sensory neurons transiently express multiple olfactory receptors during development. *Molecular Systems Biology, 11*(12), 844. doi:10.15252/MSB.20156639

Tanapat, P., Hastings, N. B., Reeves, A. J., & Gould, E. (1999). Estrogen Stimulates a Transient Increase in the Number of New Neurons in the Dentate Gyrus of the Adult Female Rat. *Journal of Neuroscience, 19*(14), 5792-5801. doi:10.1523/JNEUROSCI.19-14-05792.1999

Tesileanu, T., Cocco, S., Monasson, R., & Balasubramanian, V. (2019). Adaptation of olfactory receptor abundances for efficient coding. *eLife, 8*. doi:10.7554/ELIFE.39279

Ting, J. T., Daigle, T. L., Chen, Q., & Feng, G. (2014). Acute brain slice methods for adult and aging animals: Application of targeted patch clamp analysis and optogenetics. *Methods in Molecular Biology, 1183*, 221-242. doi:10.1007/978-1-4939-1096-0_14/FIGURES/7

Tirindelli, R., & Ryba, N. J. P. (1996). The G-protein γ-subunit Gy8 is Expressed in the Developing Axons of Olfactory and Vomeronasal Neurons. *European Journal of Neuroscience, 8*(11), 2388-2398. doi:10.1111/J.1460-9568.1996.TB01202.X

Toda, T., Parylak, S. L., Linker, S. B., & Gage, F. H. (2018). The role of adult hippocampal neurogenesis in brain health and disease. *Molecular Psychiatry 2018 24:1, 24*(1), 67-87. doi:10.1038/S41380-018-0036-2

Togashi, K., Tsuji, M., Takeuchi, S., Nakahama, R., Koizumi, H., & Emoto, K. (2020). Adeno-Associated Virus-Mediated Single-Cell Labeling of Mitral Cells in the Mouse Olfactory Bulb: Insights into the Developmental Dynamics of Dendrite Remodeling. *Frontiers in Cellular Neuroscience, 14*.

Trachtenberg, J. T., Chen, B. E., Knott, G. W., Feng, G., Sanes, J. R., Welker, E., & Svoboda, K. (2002). Long-term in vivo imaging of experience-dependent synaptic plasticity in adult cortex. *Nature, 420*(6917), 788-794. doi:10.1038/nature01273

Tran-Van-Minh, A., Cazé, R. D., Abrahamsson, T., Cathala, L., Gutkin, B. S., & DiGregorio, D. A. (2015). Contribution of sublinear and supralinear dendritic integration to neuronal computations. *Frontiers in Cellular Neuroscience, 9*, 67. doi:10.3389/FNCEL.2015.00067/BIBTEX

Tsai, L., & Barnea, G. (2014). A Critical Period Defined by Axon-Targeting Mechanisms in the Murine Olfactory Bulb. *Science, 344*(6180), 197-200. doi:10.1126/science.1248806

Tsukahara, T., Brann, D. H., Pashkovski, S. L., Guitchounts, G., Bozza, T., & Datta, S. R. (2021). A transcriptional rheostat couples past activity to future sensory responses. *Cell, 184*(26), 6326-6343.e6332. doi:10.1016/J.CELL.2021.11.022/ATTACHMENT/7B2C1591-AF79-4DEF-8266-56B347729F67/MMC5.CSV

Tyler, W. J., Petzold, G. C., Pal, S. K., & Murthy, V. N. (2007). Experience-Dependent Modification of Primary Sensory Synapses in the Mammalian Olfactory Bulb. *Journal of Neuroscience, 27*(35), 9427-9438. doi:10.1523/JNEUROSCI.0664-07.2007

Urban, N. N., & Sakmann, B. (2002). Reciprocal intraglomerular excitation and intra- and interglomerular lateral inhibition between mouse olfactory bulb mitral cells. *J Physiol, 542*(Pt 2), 355-367.

Vaaga, C. E., & Westbrook, G. L. (2016). Parallel processing of afferent olfactory sensory information. *The Journal of Physiology, 594*(22), 6715-6732. doi:https://doi.org/10.1113/JP272755

Vaaga, C. E., Yorgason, J. T., Williams, J. T., & Westbrook, G. L. (2017). Presynaptic gain control by endogenous cotransmission of dopamine and GABA in the olfactory bulb. *Journal of Neurophysiology, 117*(3), 1163-1170. doi:10.1152/jn.00694.2016

Valley, M. T., Henderson, L. G., Inverso, S. A., & Lledo, P.-M. (2013). Adult Neurogenesis Produces Neurons with Unique GABAergic Synapses in the Olfactory Bulb. *Journal of Neuroscience, 33*(37), 14660-14665. doi:10.1523/JNEUROSCI.2845-13.2013

Vassar, R., Chao, S. K., Sitcheran, R., Nuiiez, M., Vosshall, L. B., & Axel, R. (1994). Topographic Organization of Sensory Projection to the Olfactory Bulb. *Cell, 79*, 951-991.

Vedin, V., Slotnick, B., & Berghard, A. (2004). Zonal ablation of the olfactory sensory neuroepithelium of the mouse: effects on odorant detection. *The European Journal of Neuroscience, 20*(7), 1858-1864. doi:10.1111/j.1460-9568.2004.03634.x

Verhaagen, J., Oestreicher, A. B., Gispen, W. H., & Margolisi, F. L. (1989). The Expression of the Growth Associated Protein B50/GAP43 in the Olfactory System of Neonatal and Adult Rats. *The Journal of Neuroscience*(2), 683-691.

Villar, P. S., Hu, R., & Araneda, R. C. (2021). Long-Range GABAergic Inhibition Modulates Spatiotemporal Dynamics of the Output Neurons in the Olfactory Bulb. *The Journal of neuroscience : the official journal of the Society for Neuroscience, 41*(16), 3610-3621. doi:10.1523/JNEUROSCI.1498-20.2021

Wachowiak, M., Economo, M. N., Díaz-Quesada, M., Brunert, D., Wesson, D. W., White, J. A., & Rothermel, M. (2013). Optical Dissection of Odor Information Processing In Vivo Using GCaMPs Expressed in Specified Cell Types of the Olfactory Bulb. *Journal of Neuroscience, 33*(12), 5285-5300. doi:10.1523/JNEUROSCI.4824-12.2013

Watt, W. C., Sakano, H., Lee, Z. Y., Reusch, J. E., Trinh, K., & Storm, D. R. (2004). Odorant Stimulation Enhances Survival of Olfactory Sensory Neurons via MAPK and CREB. *Neuron, 41*(6), 955-967. doi:10.1016/S0896-6273(04)00075-3

Wienisch, M., & Murthy, V. N. (2016). Population imaging at subcellular resolution supports specific and local inhibition by granule cells in the olfactory bulb. *Scientific Reports, 6*(1), 29308. doi:10.1038/srep29308

Willhite, D. C., Nguyen, K. T., Masurkar, A. V., Greer, C. A., Shepherd, G. M., & Chen, W. R. (2006). Viral tracing identifies distributed columnar organization in the olfactory bulb. *Proceedings of the National Academy of Sciences, 103*(33), 12592-12597. doi:10.1073/pnas.0602032103

Winner, B., Cooper-Kuhn, C. M., Aigner, R., Winkler, J., & Kuhn, H. G. (2002). Long-term survival and cell death of newly generated neurons in the adult rat olfactory bulb. *European Journal of Neuroscience, 16*(9), 1681-1689. doi:10.1046/J.1460-9568.2002.02238.X

Winner, B., Regensburger, M., Schreglmann, S., Boyer, L., Prots, I., Rockenstein, E., . . . Gage, F. H. (2012). Role of α-Synuclein in Adult Neurogenesis and Neuronal Maturation in the Dentate Gyrus. *The Journal of Neuroscience, 32*(47), 16906. doi:10.1523/JNEUROSCI.2723-12.2012

Woolf, B., Shepherd, M., & Greeriv, A. (1991). Local Information Processing in Dendritic Trees: Subsets Spines in Granule Cells of the Mammalian Olfactory Bulb. 18.

Wu, A., Yu, B., Chen, Q., Matthews, G. A., Lu, C., Campbell, E., . . . Komiyama, T. (2020). Context-dependent plasticity of adult-born neurons regulated by cortical feedback. *Science Advances, 6*(42), 8319-8335. doi:10.1126/SCIADV.ABC8319/SUPPL_FILE/ABC8319_SM.PDF

Xiang, Z., Huguenard, J. R., & Prince, D. A. (2002). Synaptic inhibition of pyramidal cells evoked by different interneuronal subtypes in layer V of rat visual cortex. *Journal of Neurophysiology, 88*(2), 740-750. doi:10.1152/JN.2002.88.2.740/ASSET/IMAGES/LARGE/9K0822496008.JPEG

Yamaguchi, M., & Mori, K. (2005). Critical period for sensory experience-dependent survival of newly generated granule cells in the adult mouse olfactory bulb. *Proceedings of the National Academy of Sciences of the United States of America, 102*(27), 9697-9702. doi:10.1073/PNAS.0406082102/ASSET/3E7C0884-DB1B-4C94-B230-B40B4ED31506/ASSETS/GRAPHIC/ZPQ0280587910005.JPEG

Yang, M., & Crawley, J. N. (2009). Simple Behavioral Assessment of Mouse Olfaction. *Current Protocols in Neuroscience, 48*(1), 8.24.21-28.24.12. doi:10.1002/0471142301.ns0824s48

Yokoi, M., Mori, K., & Nakanishi, S. (1995). Refinement of odor molecule tuning by dendrodendritic synaptic inhibition in the olfactory bulb. *Proceedings of the National Academy of Sciences, 92*(8), 3371-3375. doi:10.1073/pnas.92.8.3371

Yokoyama, T. K., Mochimaru, D., Murata, K., Manabe, H., Kobayakawa, K., Kobayakawa, R., . . . Yamaguchi, M. (2011). Elimination of Adult-Born Neurons in the Olfactory Bulb Is Promoted during the Postprandial Period. *Neuron, 71*(5), 883-897. doi:10.1016/j.neuron.2011.05.046

Yoshihara, S.-i., Takahashi, H., Nishimura, N., Naritsuka, H., Shirao, T., Hirai, H., . . . Tsuboi, A. (2012). 5T4 Glycoprotein Regulates the Sensory Input-Dependent Development of a

Specific Subtype of Newborn Interneurons in the Mouse Olfactory Bulb. *Journal of Neuroscience, 32*(6), 2217-2226. doi:10.1523/JNEUROSCI.5907-11.2012

Young, J. M., Friedman, C., Williams, E. M., Ross, J. A., Tonnes-Priddy, L., & Trask, B. J. (2002). Different evolutionary processes shaped the mouse and human olfactory receptor gene families. *Human Molecular Genetics, 11*(5), 535-546. doi:10.1093/hmg/11.5.535

Yu, C. R., Power, J., Barnea, G., O'Donnell, S., Brown, H. E. V., Osborne, J., . . . Gogos, J. A. (2004). Spontaneous Neural Activity Is Required for the Establishment and Maintenance of the Olfactory Sensory Map. *Neuron, 42*(4), 553-566. doi:10.1016/S0896-6273(04)00224-7

Zapiec, B., & Mombaerts, P. (2015). Multiplex assessment of the positions of odorant receptor-specific glomeruli in the mouse olfactory bulb by serial two-photon tomography. *Proceedings of the National Academy of Sciences of the United States of America, 112*(43), E5873-E5882. doi:10.1073/PNAS.1512135112/SUPPL_FILE/PNAS.1512135112.SM01.MOV

Zeppilli, S., Ackels, T., Attey, R., Klimpert, N., Ritola, K. D., Boeing, S., . . . Fleischmann, A. (2021). Molecular characterization of projection neuron subtypes in the mouse olfactory bulb. *eLife, 10*, e65445. doi:10.7554/eLife.65445

Zhang, X., & Firestein, S. (2002). The olfactory receptor gene superfamily of the mouse. *Nature Neuroscience, 5*(2), 124-133. doi:10.1038/nn800

Zhang, X., Schlögl, A., Vandael, D., & Jonas, P. (2021). MOD: A novel machine-learning optimal-filtering method for accurate and efficient detection of subthreshold synaptic events in vivo. *Journal of Neuroscience Methods, 357*, 109125. doi:10.1016/J.JNEUMETH.2021.109125

Zhou, F. M., & Hablitz, J. J. (1997). Rapid kinetics and inward rectification of miniature EPSCs in layer I neurons of rat neocortex. *Journal of Neurophysiology, 77*(5), 2416-2426. doi:10.1152/JN.1997.77.5.2416/ASSET/IMAGES/LARGE/JNP.MY08F7.JPEG